



LIBRARY Michigan State University

This is to certify that the

dissertation entitled

Atomic Diffusion and Step Dynamics On Vicinal Surfaces

presented by

Branislav D. Blagojevic

has been accepted towards fulfillment of the requirements for

Ph.D. degree in Physics

Date July 16, 1999

MSU is an Affirmative Action/Equal Opportunity Institution

O-12771

PLACE IN RETURN BOX to remove this checkout from your record. TO AVOID FINES return on or before date due. MAY BE RECALLED with earlier due date if requested.

DATE DUE	DATE DUE	DATE DUE

1/98 c/CIRC/DateDue.p65-p.14

ATOMIC DIFFUSION AND STEP DYNAMICS ON VICINAL SURFACES

By

Branislav D. Blagojevic

A DISSERTATION

Submitted to
Michigan State University
in partial fulfillment of the requirements
for the degree of

DOCTOR OF PHILOSOPHY

Department of Physics and Astronomy

ABSTRACT

ATOMIC DIFFUSION AND STEP DYNAMICS ON VICINAL SURFACES

By

Branislav D. Blagojevic

Steps are the most fundamental extended defects on crystal surfaces. Their dynamics mediate the annealing of crystal surfaces, the growth of single crystals and many other surface processes. Step dynamics are in turn mediated by atom motion, usually either attachment and detachment from a vapor, diffusion across terraces or facets, or by diffusion along step edges. The high resolution provided by Scanning Tunneling Microscopy (STM) and Reflection Electron Microscopy (REM) is providing atomic scale images of stochastic step fluctuations. Understanding of this data requires a quantitative analysis of step fluctuations in terms of the atomic processes producing them. Such theory, in combination with high quality step fluctuation data, provides a unique method for determining the dominant modes of atomic mass transport across surfaces, and for estimating the energy barriers which impede the various types of atomic processes. A complementary probe of atomic diffusion processes is the study of the decay of specially prepared surface gratings, which in the small slope limit are described by a closely related theory. Here, a comprehensive formalism, based on atomic diffusion, for treating step fluctuations and the decay of surface gratings is presented.

ACKNOWLEDGMENTS

I would like to thank my advisor, Prof. Phil Duxbury, for his knowledgeable, relaxed and professional guidance.

I would also like to thank professors Wolfgang Bauer, Norman Birge, Mark Dykman, and Daniel Stump for their time and effort while serving in my Ph.D. committee.

I thank Prof. Julius Kovacs, Janet King, Stephanie Holland, and Debbie Simmons for their assistance.

TABLE OF CONTENTS

LIST OF TABLES	vi
LIST OF FIGURES	vii
CHAPTER 1	
INTRODUCTION	1
1.1 Research in Surface Physics	
1.2 Basic Concepts in Surface Physics	
1.3 Vicinal Surfaces	
1.4 Overview of Chapters	
CHAPTER 2	
AN OVERVIEW	13
2.1 Average Height and Fluctuation Width	
2.2 Scaling Concepts	
2.3 Correlation Length	
2.4 Analysis of Simulation and Experimental Data	
2.5 Fluctuation Equation and Symmetry Principles	
2.6 Step-Edge Diffusion	
2.7 Attachment-Detachment	
CHAPTER 3	
AN ISOLATED STEP	30
3.1 Description of the Model	
3.2 Step-Edge Diffusion	
3.3 Attachment-Detachment Model	
3.4 Terrace Diffusion	
3.5 Anomalous Diffusion	
OHA DTED 4	
CHAPTER 4 ARRAY OF STEPS	50
4.1 Introduction	
4.2. The Model	
4.3 Analysis of Various Time Regimes	
4.4. Terrace Diffusion	/3
CHAPTER 5	00
SURFACE EVOLUTION DUE TO STEP INTERACTIONS	
5.1 Introduction	88
5.2 Chemical Potential of Interacting Steps	
5.3 Continuum Limit, The Entropic Repulsion	92

CHAPTER 6	
MONTE-CARLO SIMULATIONS AND NUMERICAL ANALYSIS	
6.3 Integration of Stochastic Equations	106
5.4 Method for Checking Probabilities	
CHAPTER 7	
VLSI DESIGN	113
7.1 Introduction	113
7.2 MOS Transistors	113
7.3 Design Steps	
7.4 Simulation	120
CHAPTER 8	
CONCLUSION	122
APPENDICES	124
Appendix A: Calculation of Equilibrium	
Appendix B: Solution of Langevin Equation	128
Appendix C: Random Walk Probabilities	131
Appendix D: Overview of Other Models	136
BIBLIOGRAPHY	141

LIST OF TABLES

Table 4.1 Limiting behaviors for $G(0,t)$	85
Table 4.2 Limiting behaviors for $C_{k\neq 0}(0,t)$	86
Table 4.3 Equations for limiting timescales	87

LIST OF FIGURES

Figure 1.1 SIM image showing the	steps on a surface near Si(001)3
Figure 1.2 A scanning tunneling mi surface	croscope image of the phase separation of a vicinal Si
Figure 1.3 Two step trains and an is	solated step as viewed by REM5
Figure 1.4 A STM derivative-mode	image of a Si(001) vicinal surface miscut 0.3°
Figure 1.5 Sample configurations o	f the surfaces in Monte-Carlo
	8
Figure 2.1 Isolated step edge	14
Figure 2.2 Fluctuation width vs. tim	ne16
Figure 2.3 A typical trajectory of a	random walker17
Figure 2.4 Saturation width for diff	erent system sizes18
	lved in rescaling the time dependent fluctuation21
	ible local geometries
Figure 2.7 Monte Carlo simulation	of an isolated step evolving through step-edge
	raged over space and time35
Figure 2.9 Monte Carlo simulation	of an isolated step evolving through attachment
	dth for Au(110) at 556K
	iffusion kernel42
-	step edge49
<u> </u>	51
Figure 3.4 The correlation function	in terrace diffusion case52
Figure 3.5 The fluctuation exponen	t β is plotted vs. α 57
U	vicinal surface60
•	se relaxation times in the terrace diffusion case75
U	ction in the terrace diffusion limit
Figure 4.4 The step-step correlation	n function in the terrace diffusion T3 limit80
	in89
	95
	of the train vs. time97
<u>-</u>	napes98
Figure 5.5 Evolution of the profile	99
Figure 6.1 A snap-shot of the step s	shape in the equilibrium102
	lo simulation for the terrace diffusion with perfect
-	103

Figure 6.3 Isolated step Monte-Carlo simulation for weak sticking terrace diffusion	104
Figure 6.4 The simulation of terrace diffusion with perfect sticking	105
Figure 6.5 The fluctuation width of an isolated step obtained doing numerical	
integration	107
Figure 6.6 The distance between steps in 2-step train obtained doing numerical	
integration	108
Figure 6.7 The probability that an atom is at the site (i, j)	111
Figure 6.8 The matrix method	112
Figure 7.1 A 3-dimensional view of the (a) PMOS; and (b) NMOS	114
Figure 7.2 The schematic symbols for the (a) NMOS; and (b) PMOS	115
Figure 7.3 An inverter	116

Chapter 1

Introduction

1.1 Research in Surface Physics

There has been a large amount of work on the equilibrium properties and the dynamics of crystal surfaces and interfaces [22,28,37,44]. To gain comprehension of surface phenomena, it is critical to understand the complexity arising from the termination of a crystal by a surface.

The manifestations of this complexity can be studied from two different aspects. Firstly, the atomic arrangement in the surface region. Two particularly interesting effects may take place due to the presence of a surface: (1) the distance between the surface plane and those parallel to the surface deviate from their bulk values; (2) some lateral structural change such as formation of steps, islands, and ripples on the surface may also occur. Secondly, dynamic properties, for instance vibrations and diffusions, which are of considerable importance to the elucidation of surface phenomena and understanding of experimental results.

1.2 Basic Concepts in Surface Physics

To understand complex surface problems, one must address several fundamental problems: atomic and electronic structure, diffusion along surfaces or across interfaces, the energy and chemistry of surface regions and the response to external forces. Existing techniques for investigating surfaces have reached maturity and are increasingly being applied to systems of practical relevance. Here, four important ideas are briefly discussed.

Scaling concepts: One of the modern concepts used to study various roughening processes on surfaces is scaling [37]. It has a surprising power of prediction and simple manipulations that enable connection of apparently independent quantities and exponents. As will be shown later, many measurable quantities obey simple scaling relations. For example, for a large number of systems it is found that the interface width, w, increases as a power of time, $w(t) \sim t^{\beta}$. The width eventually saturates at a value that increases as a power law of the system size, $w(L) \sim L^{\alpha}$.

Experiments: In many branches of physics, experiments are the driving force that leads to new problems for theoretical investigation. Sometimes, the reverse occurs. For example, the roughening process was an unwanted experimental artifact that one attempted to minimize. It was only recently that a number of experimentalists became interested in it, and now they are taking the lead showing that there are more mechanisms leading to roughening than theoretically anticipated [3,5,35]. Thanks to the innovation and widening

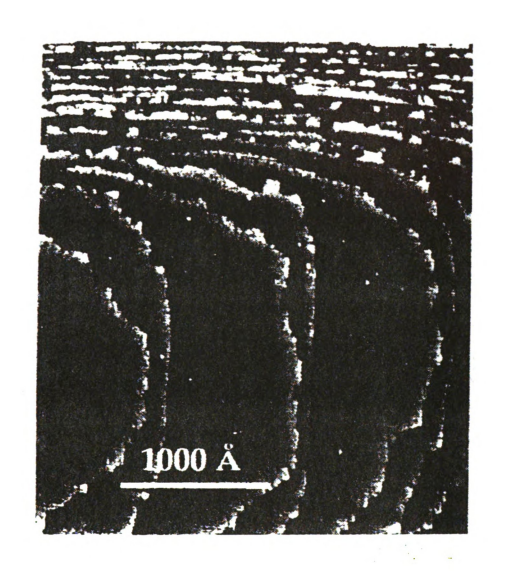


Figure 1.1 STM image showing the steps on a surface near Si(001) [35].

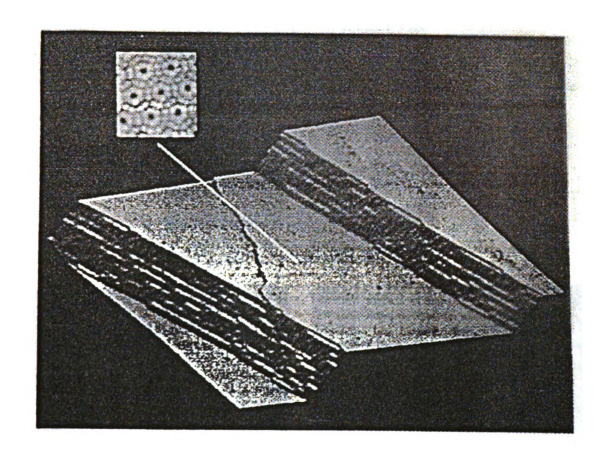


Figure 1.2 A scanning tunneling microscope image of the phase separation of a vicinal Si surface [6].

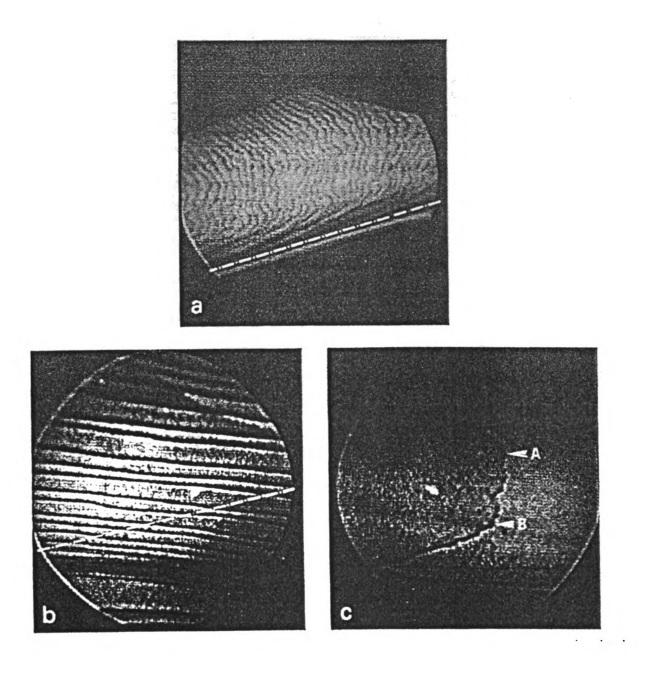


Figure 1.3 Two step trains and an isolated step as viewed by REM [5].

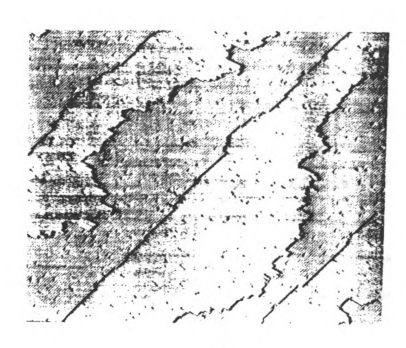


Figure 1.4 A STM derivative-mode image of a Si(001) vicinal surface miscut 0.3° towards (100). The surface steps down from left to right [3].

applications of reflection electron microscopy (REM) and scanning tunneling microscopy (STM), surface research has clearly shifted its interest from the macroscopic to the nanometer scale (see Figures 1.1-1.4).

Discrete models: Theoretical discrete modeling provided a substantial fraction of the driving force behind early investigations of interface and surface morphology. Besides, many phenomena can be modeled successfully using elementary computer algorithms [8,16,23,31]. Computer simulation is adding a new dimension to scientific investigation, establishing a role of equal importance with the traditional approaches of theory and experiment. Moreover, simulation studies represent an essential link between theory and experiments, and can allow us to separate the essential ingredients determining the morphology from the unnecessary details. As the speed and accuracy of arithmetic computers improve tremendously, it is feasible and advantageous to carry out quantitative investigation through detailed computer simulation (see Figure 1.5).

Continuum equations: A very successful tool for understanding the behavior of the various surface relaxation processes is stochastic differential equations [37]. Such equations typically describe the interface at large length scales, which means that short length scale "details" are neglected and focus is only on the asymptotic coarse-grained properties. If there already is a discrete model for the system, then it should be possible to derive the corresponding continuum equation directly from this model. There is an alternative method for deriving such equations: exploiting symmetry principles. Every interface fluctuation process obeys some simple symmetries. For example, the laws of

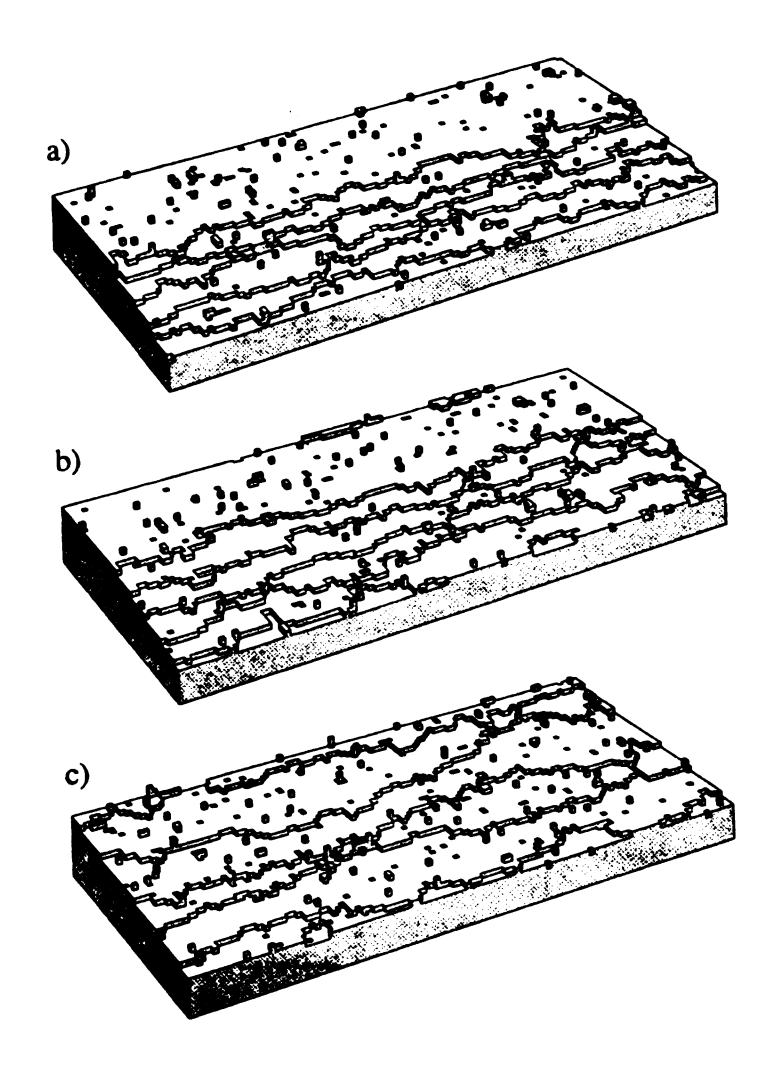


Figure 1.5 Sample configurations of the surfaces used to study step motion. (a) The initial configuration of 5 steps separated by 6 lattice constants. (b) The surface after 10⁶ Monte Carlo steps per site. (c) The final configuration after 3 x 10⁶ MCS/site [16].

physics are independent of where one defines the zero height of the interface, so the continuum equation must have this same invariance. In most cases the scaling properties of the system and the continuum equations are unambiguously determined by the symmetries of the system. Once an equation is obtained one must find its predictions, determining, e.g., the scaling exponents and scaling functions. If the relaxation process is described by a sufficiently simple equation, it can be solved exactly. However, for many equations no exact solutions exist, so one must apply various approximations to uncover the scaling behavior.

1.3 Vicinal Surfaces

The work presented here is focused on special surfaces, called *vicinal surfaces*. Vicinal surfaces have pronounced steps and terraces between them (see Figures 1.1-1.5). Steps are the most fundamental extended defects on crystal surfaces. Their dynamics mediate the annealing of crystal surfaces, the growth of single crystals and many other surface processes. Step dynamics are in turn mediated by atom motion, usually either attachment and detachment from a vapor, diffusion across terraces or facets, or by diffusion along step edges. The high resolution provided by Scanning Tunneling Microscopy (STM) and Reflection Electron Microscopy (REM) is providing atomic scale images of stochastic step fluctuations. Understanding of this data requires a quantitative analysis of step fluctuations in terms of the atomic processes producing them. Such theory, in combination with high quality step fluctuation data, provides a unique method for determining the dominant modes of atomic mass transport across surfaces, and for

estimating the energy barriers which impede the various types of atomic processes. A complementary probe of atomic diffusion processes is the study of the decay of specially prepared surface gratings, which in the small slope limit are described by a closely related theory.

The equilibrium structure [1-6] and dynamics [7-20] of steps on vicinal surfaces are now routinely probed and modeled with atomic precision. Traditionally, the relaxation of these structures is treated using linear relaxation theory [21-23]. However as realized even in those early seminal papers, the linear theory usually needs significant modification below roughening [24-33] where steps are well defined. Actually, when the steps are well defined, their (capillary) fluctuations are usually treated linearly, and the non-linear evolution is though the center-of-mass motion of the steps. In Chapters 3-5, a complimentary formalism based on atomic diffusion is presented, the atomic diffusion processes which lead to the various limiting behaviors treated by previous workers [8-17] are explicitly shown. It also predicts when "non-universal" behavior can occur, and it provides a formalism which describes the crossover between the various limits.

1.4 Overview of Chapters

This dissertation is arranged as follows. In Chapter 2, an overview of the general approach to treating step-edge fluctuations is given. It starts by defining the average step height and fluctuation width. Then, scaling concepts are introduced. It is shown that the fluctuation width of an initially flat step increases with time as a power law until it

reaches a saturation width. The concept of correlation and correlation length is also introduced. Correlation between the parts of the fluctuating step plays an important role in describing the mechanisms that lead to saturation. Also, five methods of extracting the scaling parameters from computer simulation, in order to compare them with experimental and analytical results, are described. A general continuum stochastic equation that describes step fluctuations and which satisfies symmetry principles is derived. Finally, two previously introduced models, step-edge diffusion and attachment-detachment, are analyzed. Analytical, simulation and experimental results for those two models are given.

In Chapter 3, a complimentary formalism to treat the isolated step fluctuations is introduced. It is based on atomic diffusion through a Langevin (rate) theory. The different atomic mechanisms are mathematically described by different diffusion kernels. This allows one to smoothly interpolate between the step-edge diffusion limit and the attachment-detachment limit.

In Chapter 4, the same method is expanded to an array of steps. Step-step interaction terms in the step free energy are ignored. There are diffusion kernels between steps as well as a diffusion kernel to the same step. This enables one to analyze the correlation between the fluctuation along the same step as well as mutual correlation between any two steps on the surface.

In Chapter 5, the formalism is extended to include step-step interaction terms. That leads to the spreading of a step array (train) and is related to the relaxation of the whole surface.

In Chapter 6, the methods for Monte-Carlo simulation of atomic diffusion and numerical integration of stochastic differential equations are summarized. The results obtained by those two methods are then compared to analytical results.

In Chapter 7, an overview of VLSI electrical design is given. It describes the computational modeling experience gained while doing practical training in industry (a final part of Ph.D. program).

Chapter 8 contains brief conclusion.

There are four appendices. Appendix A derives saturation width for two cases of boundary conditions at the ends of the step: pinned and periodic. Appendix B summarizes the calculation of correlation functions from the linear Langevin equation. Appendix C derives diffusion kernels used in the model. Appendix D summarizes recent analytical work of two other research groups and compares the approach presented here with theirs.

Chapter 2

An Overview

2.1 Average Height and Fluctuation Width

Consider a single isolated step at the surface (see Figure 2.1 (a) or (b)). The length of the step is L. The surface is defined with the axis x (along step edge) and height h(x,t) describing the position of the step edge at time t. x has discrete values I to L. The step edge fluctuates due to the atoms detaching from the step edge and attaching to the step edge on both sides. In order to describe step fluctuations quantitatively, two functions are introduced:

(i) The average height of the step, $\langle h(t) \rangle$, defined by

$$\langle h(t) \rangle \equiv \frac{1}{L} \sum_{x=1}^{L} h(x,t)$$
 (2.1)

If the flux of atoms detaching equals the flux that is reattaching, then $\langle h(t) \rangle$ is constant in time.

(ii) The fluctuation width, w(t), which characterizes the roughness of the step edge, is defined by the rms fluctuation in the height,

$$w^{2}(t) = \frac{1}{L} \sum_{t=1}^{L} \left[h(x,t) - \left\langle h(t) \right\rangle \right]^{2} = \left\langle h^{2}(t) \right\rangle - \left\langle h(t) \right\rangle^{2}$$
 (2.2)

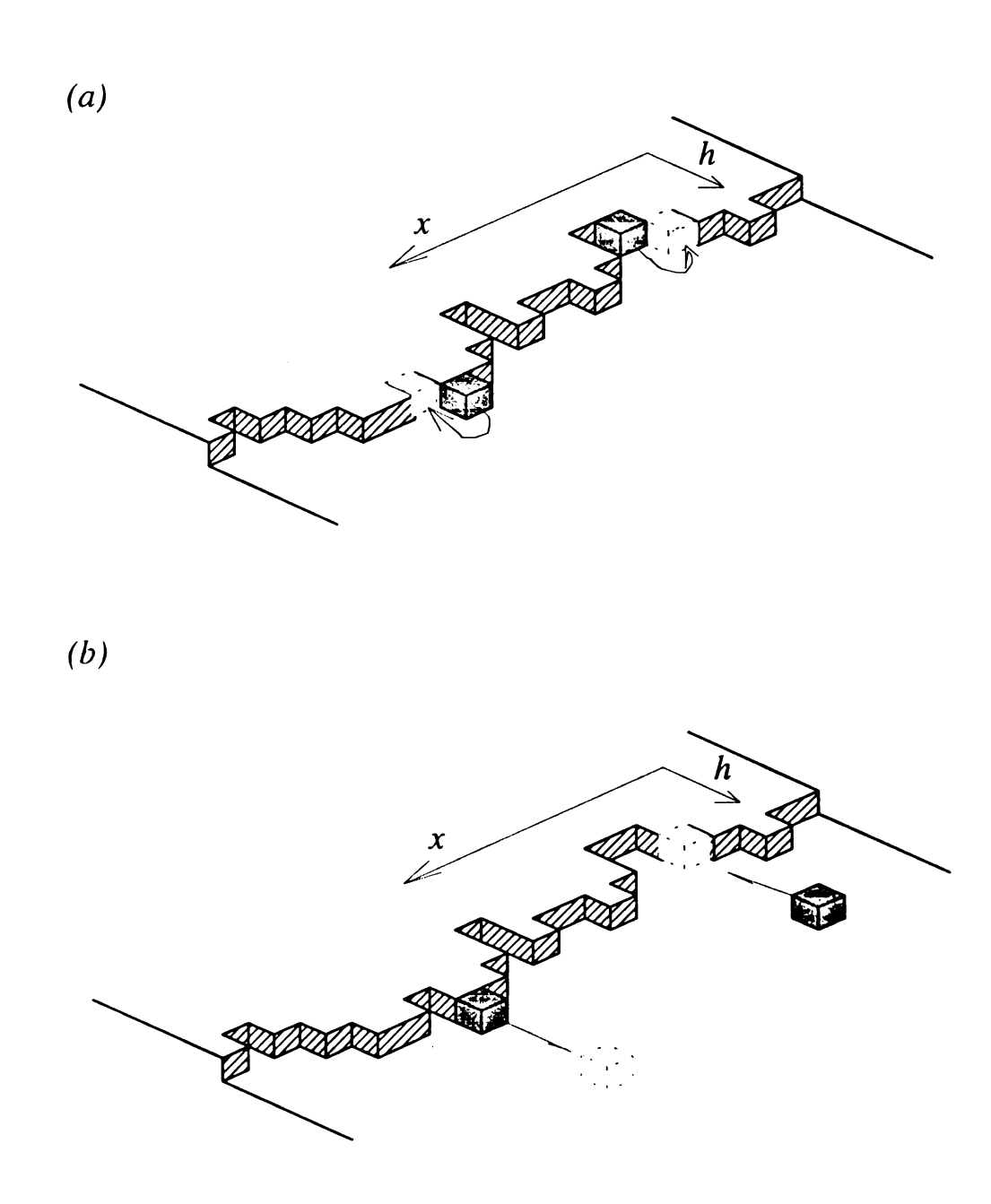


Figure 2.1 Isolated step edge. Two mechanisms for atomic processes which mediate step fluctuations. a) Step-edge diffusion; b) Attachment-detachment.

To monitor the roughening process quantitatively, one measures the fluctuation width as a function of time. By definition, the step edge at time zero is simply a straight line, with zero width. As detachment and attachment occur, the step edge gradually roughens.

2.2 Scaling Concepts

A typical plot of the time evolution of the width has two regions separated by a "crossover" time t_{sat} (see Figure 2.2).

(i) Initially, the width increases as a power of time,

$$w(t) \sim t^{\mu} \tag{2.3}$$

The exponent β , called the *fluctuation exponent*, characterizes the time-dependent dynamics of the roughening process. The driving force for the increase of the step edge fluctuation is its tendency to increase entropy - the larger the fluctuation, the larger the entropy of the system. If one imagines each step edge as a one dimensional random walker along the h-axis, it would give the fluctuating line with exponent $\beta = 1/2$ (see Figure 2.3). But, sites of the step edge are not completely free to move perpendicularly to x because the motion of each site is constrained by attachment to its neighboring sites. Thus, the exponent β is always less that $\frac{1}{2}$. Its value depends on the specific processes that drives the step-edge fluctuations and that will be discussed later in this chapter.

(ii) The power-law increase in width does not continue indefinitely, but is followed by a saturation regime (the horizontal region of Figure 2.4) during which the width reaches a

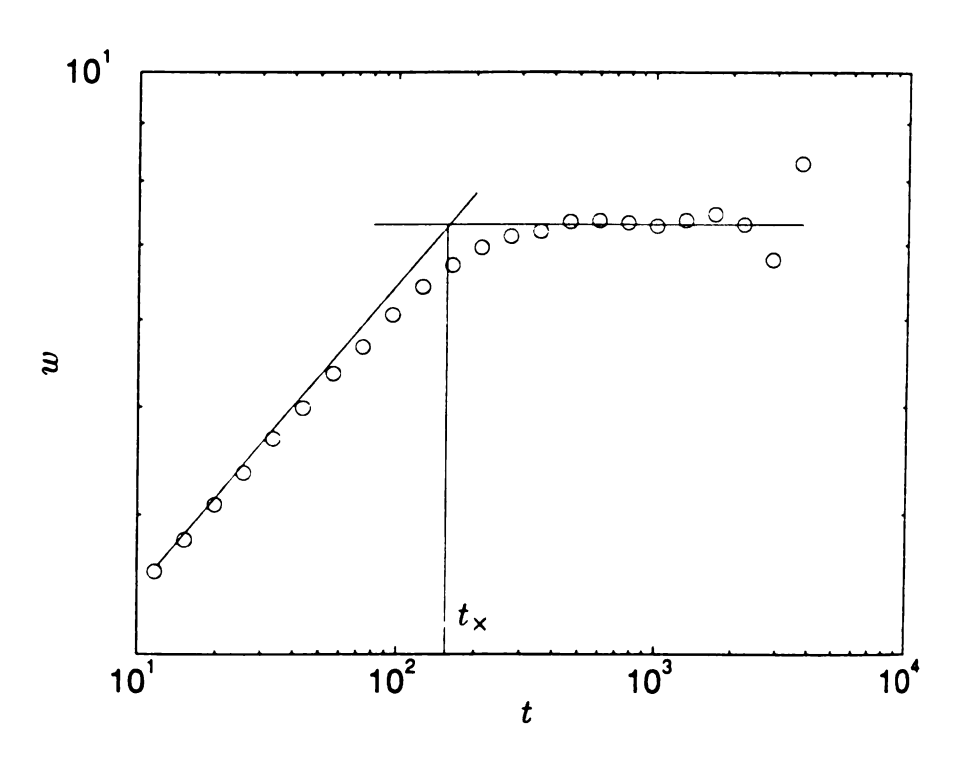


Figure 2.2 Fluctuation width vs. time. There are two characteristic regimes.

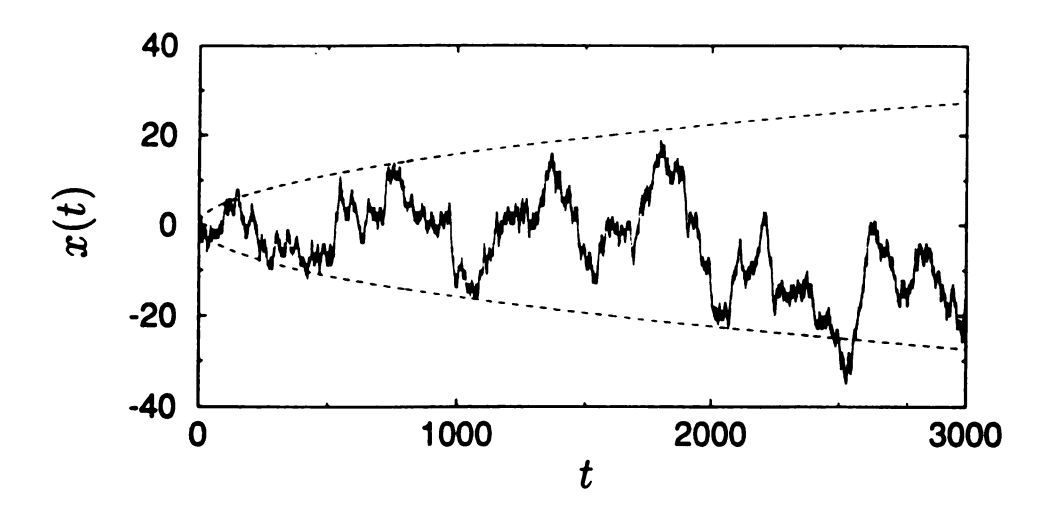


Figure 2.3 A typical trajectory of a random walker. The dashed lines are proportional to $t^{1/2}$ [37]...

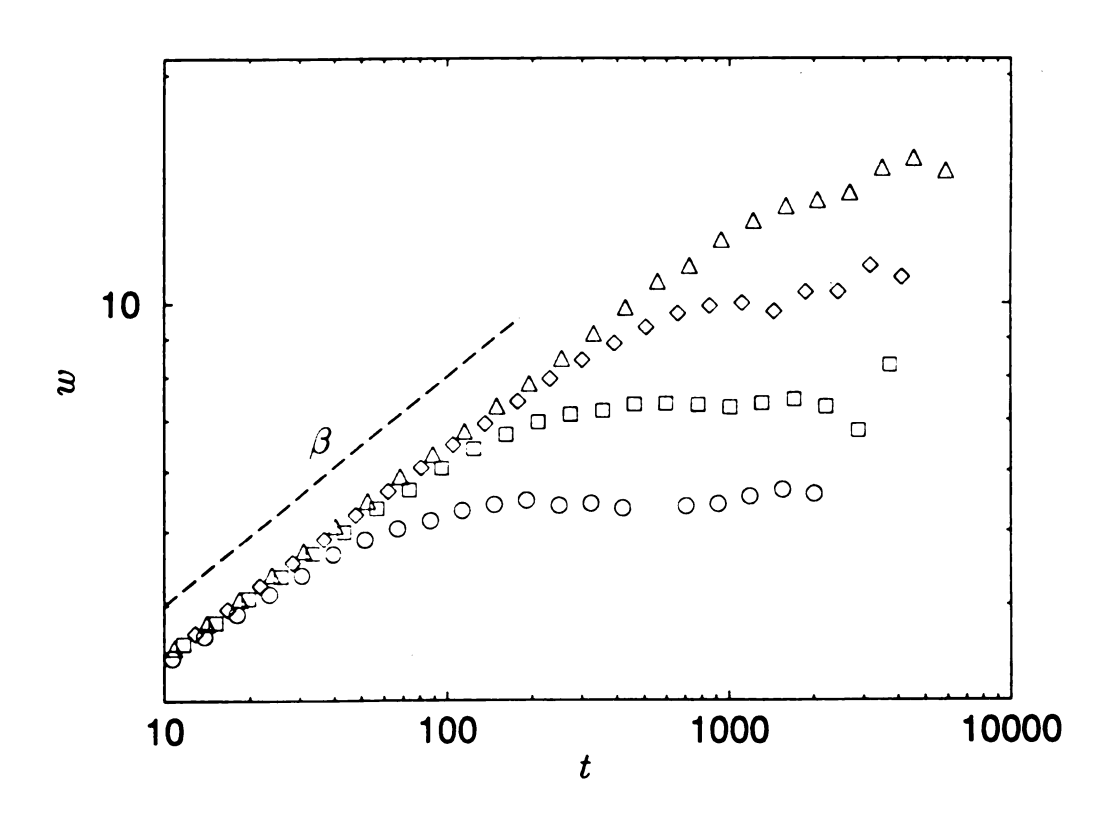


Figure 2.4 Saturation width for different system sizes.

saturation value, w_{sat} . The step fluctuation width saturates when the tendency of the system to keep its free energy smaller (by suppressing the increase of fluctuations) equilibrates with the tendency of the system to increase its entropy. As L increases, the saturation width, w_{sat} increases as well, and the dependence also follows a power law,

$$w_{sal}(L) \sim L^{\alpha} \tag{2.4}$$

The exponent α , called the *roughness exponent*, is a second critical exponent that characterizes the roughness of the saturated step edge fluctuation. As shown in Appendix A, for the free energy expression used in models described in Chapters 3 and 4, $\alpha = 1/2$.

(iii) The crossover time t_{sat} (sometimes called saturation time) at which the step edge crosses over from the behavior of (2.3) to that of (2.4) depends on the system size

$$t_{sat} \sim L^{z} \tag{2.5}$$

where z is called the dynamic exponent. The construction illustrated in Figure 2.2 is a simple way to estimate t_{sat} .

Although the scaling exponents are interesting, perhaps the main reason for studying them is to extract the correct prefactors from the expressions for w(t). These prefactors are related to step-edge kinetic barriers, and the study of w(t) provides an important technique for estimating these critical parameters.

The scaling exponents α , β , and z are not independent, and there exists a simple way to "collapse" the data of Figure 2.4 onto a single curve.

- (A) Plotting $w(t)/w_{sat}(L)$ as a function of time will result in curves that saturate at the same value, independent of the system size L (see Figure 2.5).
- (B) Plotting the width as a function of t/t_{sat} will cause the curves to saturate at the same characteristic time (see Figure 2.5).

These two observations suggest that $w(t)/w_{sat}(L)$ is a function of t/t_{sat} only, i.e

$$\frac{w(t)}{w_{sat}(L)} \sim f\left(\frac{t}{t_{sat}}\right),\tag{2.6}$$

where f(u) is called a scaling function. Replacing w_{sat} and t_{sat} in (2.6) with their scaling forms (2.4) and (2.5) one obtains the Family-Vicsek scaling relation [36]

$$w(L,t) \sim L^{\alpha} f\left(\frac{t}{L^{2}}\right).$$
 (2.7)

The general form of the scaling function f(u) can be read off from Figure 2.5. There are two different scaling regimes depending on its argument $u \equiv t/t_{sat}$.

(a) For small u, the scaling function increases as a power law. Since during the rescaling shown in Figure 2.5 one did not rotate the curves, but only shifted them, it can be seen that in this regime one has

$$f(u) \sim u^{\beta}, \quad u << 1 \tag{2.8}$$

(b) As $t \to \infty$, the width saturates. Saturation is reached for $t >> t_{sat}$, i.e. the argument of the scaling function u >> 1. In this limit we have

$$f(u) = const (2.9)$$

The validity of the scaling relation (2.7) can be tested numerically by replotting the data of Figure 2.4 in a fashion suggested by (2.8) and Figure 2.5.

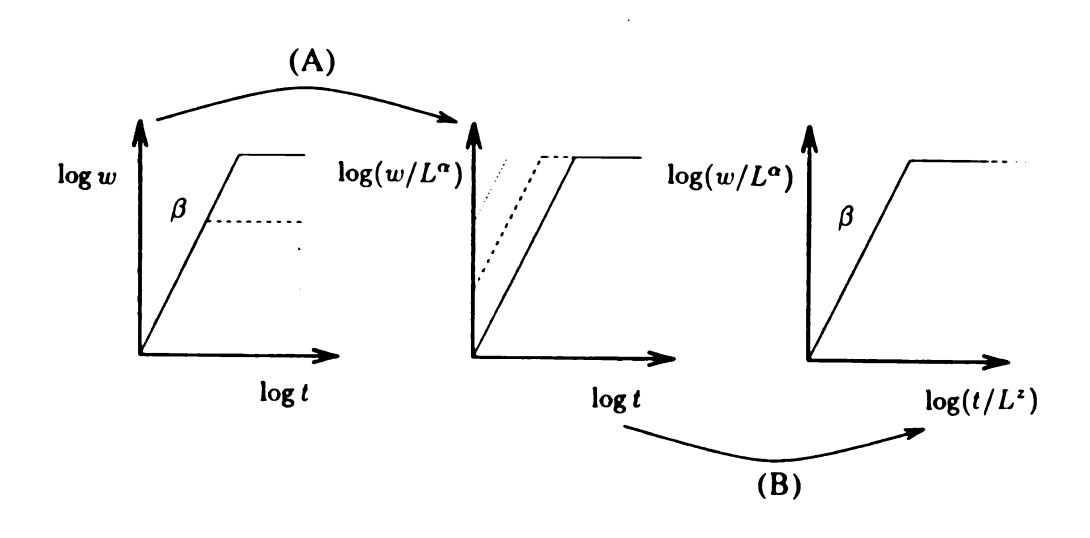


Figure 2.5 Illustration of steps involved in rescaling the time dependent fluctuation width [37].

It can be next shown that the exponents α , β , and z are not independent. In Figure 2.2 if one approaches the crossover point $(t_{sat}, w(t_{sat}))$ from the left one finds, according to (2.3), that $w(t_{sat}) \sim t_{sat}^{\beta}$. However, approaching the same point from the right, one has, from (2.4), $w(t_{sat}) \sim L^{\alpha}$. From these two relations follows $t_{sat}^{\beta} \sim L^{\alpha}$ which, according to (2.5), implies that

$$z = \frac{\alpha}{\beta}. (2.10)$$

Equation (2.10), a scaling law linking the three exponents, is valid for any growth process that obeys the scaling relation (2.7). It will be seen in the following chapter that this relation is also satisfied in the presented formalism.

2.3 Correlation Length

The fact that the saturation time, t_{sat} , and the saturation width, w_{sat} increase with the system size suggests that saturation phenomena constitute a finite size effect [37]. One property of the fluctuation process is that correlations develop along the step edge, which implies that the fluctuations of the different parts of the step are not completely independent. Although the process of attaching and detaching on the step edge is local, the "information" about the height of each of the sites spreads globally. The typical distance over which the heights "know about" each other is the characteristic distance over which they are correlated and is called the *correlation length*, and is denoted by ξ_{\parallel} .

At the beginning of the fluctuation, the sites are uncorrelated. Then ξ_{\parallel} grows with time. For a finite system ξ_{\parallel} cannot grow indefinitely, because it is limited by the size of the system, L. When ξ_{\parallel} reaches the size of the system, the entire step edge becomes correlated, resulting in the saturation of the fluctuation width. Thus at saturation

$$\xi_{\parallel} \sim L$$
 , $t \gg t_{sat}$ (2.11)

According to (2.7), saturation occurs at a time t_{sat} given by (2.5). Replacing L with ξ_{\parallel} , one obtains $\xi_{\parallel} \sim t_{sat}^{1/z}$, which in fact holds for $t < t_{sat}$ as well,

$$\xi_{\parallel} \sim t^{1/z}, \quad t << t_{sat} \tag{2.12}$$

2.4 Analysis of Simulation and Experimental Data

Two main methods to check scaling laws are to analyze the data from computer simulation and experimental measurement. Computer simulation is usually done using the Monte-Carlo method on discrete models. Experimental data are obtained through STM and REM images of the surface. The analysis of data requires special care due to finite size effects, and slow crossover behavior in computer simulations, and unstable condition, and inadequate resolution in experimental measurements. In this section an overview of five methods that are useful in obtaining a thorough analysis of the scaling properties is given [37]. In the ideal case, α and β do not depend on the method one uses. But in practice, α sometimes varies from method to method, and it is useful to use as many methods as possible in order to get a feeling for the range of values of α that are consistent with the data.

Method 1. Assume that the saturation width $w_{sat}(L)$ has been calculated for different system sizes L. Then the roughness exponent α can be estimated using (2.4) by plotting the data on a log-log plot, and measuring the slope of the straight line. To use this method, one must be able to obtain $w_{sat}(L)$ for various system sizes L. In most experimental situations one does not have results for different systems sizes, or in addition there may be strong boundary effects influencing $w_{sat}(L)$. Thus Method 1 is more useful for computer simulations, where one can simulate systems of arbitrary sizes, and can require periodic boundary conditions to reduce the boundary effects. Method 1 cannot always be used, since for sufficiently large systems it is not possible to saturate the step edge fluctuation. According to (2.5), the time necessary for saturation increases with the system size. If the dynamic exponent z is large, this increase can be quite dramatic requiring a prohibitive computation time.

Method 2. In many situations, there is no information on the dynamics of the growth, nor is there the possibility of producing interfaces with different system sizes. Suppose the only data one has are collected at the final stage of an experiment consisting of the value of the height at different points. In this situation, one can study the scaling of the local width $w_l(t)$ defined by

$$w_l^2(t) \equiv \left\langle \left[h_l(x, t) - \left\langle h_l(t) \right\rangle \right]^2 \right\rangle. \tag{2.13}$$

The subscript l means that one selects a portion ("window") of length l on the interface and measures the width and average height $\langle h_l(t) \rangle$ in this window. The brackets $\langle ... \rangle$

denote spatial (over x) and ensemble averages - one chooses many different windows along the surface and averages over the obtained results. For small *l*

$$w_l(t) \sim l^{\alpha}, \quad l \ll \xi_{\parallel}, \tag{2.14}$$

where α is the same roughness exponent defined in (2.4). One can verify that (2.14) reduces to (2.4) in the long time limit, by replacing l with the system size L. Method 2 is also useful for the determination of α in numerical simulations, and is complementary to Method 1.

Method 3. If, in addition to w_{sat} one has the full time evolution of the width, as shown in Figure 2.4, one can use (2.7) to determine both α and z. This can be done by attempting to rescale the data as it is illustrated in Figure 2.5. If the correct exponents for the rescaling is used, it should give good data collapse. Any significant deviation would lead to the breakdown of data collapse.

Method 4. Another quantity that scales in the same way as the step fluctuation width is the correlation function,

$$G(x,t) = \left\langle \left(h(x_1 + x, t_1 + t) - h(x_1, t_1) \right)^2 \right\rangle$$
 (2.15)

The correlation function G(x,t) defined in (2.15) is sensitive to bias in the data, i.e., if the step edge has an overall slope, the scaling is affected. If the step edge is obtained from numerical simulations with periodic boundary conditions, there should be no bias in the data so (2.15) gives the correct scaling. However, step edges obtained from experimental data may have an overall slope. To overcome the effect of the bias, one can use a slightly different height variable from which the overall average slope has been subtracted.

If one is interested only in α , one takes t = 0 (i.e., there is no time delay), and

$$G(x,0) \sim x^{2\alpha}$$
, $x << \xi_{\parallel}$. (2.16)

If one wishes to determine β , one can measure the correlation with a time delay. Provided one studies times shorter than the crossover time t_{sat} where the width saturates, one finds that G(0,t) has the same scaling as $w^2(t)$ (see Appendix B)

$$G(0,t) \sim t^{2\beta}$$
, $t << t_1 \approx t_{sat}$. (2.17)

Method 5. Some experiments measure the power spectrum of the step edge, and not the height h(x, t). Thus one can examine how the dynamic scaling relation (2.7) is modified in Fourier space. Consider the structure factor

$$C_q(t) \equiv \left\langle h_q(t)h_{-q}(t) \right\rangle , \qquad (2.18)$$

where

$$h_q(t) = \sum_{\tau} \left[h(x, t) - \langle h(t) \rangle \right] e^{iq\tau}$$
 (2.19)

The dynamic scaling hypothesis (2.7) can be translated to the structure factor, with result

$$C_a(t) = q^{-1-2a}g(t/q^{-2}).$$
 (2.20)

Here $g(u) \sim u^{(2a+d)}$ for u << 1 and g(u) = const for u >> 1.

Note that $w^2(t) = (1/L)\sum_q C_q(t)$ gives a simple relation between the structure factor and the width of the step edge fluctuation. The calculation of the structure factor provides an alternative way to estimate the scaling exponents. It has the advantage over the real space

methods that only the long wavelength modes contribute to its scaling. The scaling of the real space form (2.7) is determined by all modes, including the short wavelength modes. Thus (2.7) is expected to have stronger finite size effects than (2.20) [37].

2.5 Fluctuation Equation and Symmetry Principles

Symmetry principles can be used to derive the equation that describes the equilibrium step edge [37]. By equilibrium one means that the fluctuation of the step edge is not driven by an external field. Thus an equilibrium step separates two terraces of the surface that are in "equilibrium" in the sense that one terrace is not growing at the expense of the other.

As assumed at the beginning of this chapter, the position of the step edge is characterized by its height h(x,t). Beside that, it should be assumed that h(x,t) is single valued - i.e., there are no "overhangs". The goal is to derive a general fluctuation equation. It is expected that equation has the form

$$\frac{\partial h(x,t)}{\partial t} = F(h,x,t) + \eta(x,t). \tag{2.21}$$

Here F(h,x,t) is the deterministic term, while $\eta(x,t)$ is the noise term. It reflects the random fluctuations in the detachment and attachment process and is an uncorrelated random number that has zero configurational average

$$\langle \eta(x,t) \rangle = 0. \tag{2.22}$$

The second moment of the noise is given by

$$\langle \eta(x,t)\eta(x',t')\rangle \propto \delta(x-x')\delta(t-t')$$
 (2.23)

for nonconservative and

$$\langle \eta(x,t)\eta(x',t')\rangle \propto -\nabla^2 \delta(x-x')\delta(t-t')$$
 (2.24)

for conservative noise. Relations (2.25) and (2.24) imply that noise has no correlations in space and time, since averaging over the product $\langle \eta(x,t)\eta(x',t')\rangle$ produces zero, except for the special case in which t=t' and x=x'. Conditions (2.22) and (2.23) are automatically satisfied if the noise variable η is chosen from a Gaussian distribution. Another type of noise that also satisfies both (2.22) and (2.23) and is often used in numerical simulations is "bounded noise", in which $\eta=+1$ and $\eta=-1$ are chosen with equal probability.

As a first step in obtaining the fluctuation equation, one should consider the basic symmetries of the problem:

- (i) Invariance under translation in time. The equation should not depend on where one defines the origin of time, so the equation must be invariant under the transformation $t \to t + \delta t$. This symmetry rules out an explicit time dependence of F.
- (ii) Translation invariance along the x direction. The equation should not depend on the actual value of x, having the symmetry $x \to x + \delta x$. This excludes explicit x dependence of F.

- (iii) Translation invariance along the h direction. The fluctuation rule should be independent of where one defines h=0, so the fluctuation equation should be invariant under the translation $h \to h + \delta h$. This symmetry rules out the explicit h dependence of F. So that the equation must be constructed from combinations of $\nabla h, \nabla^2 h, ..., \nabla^n h$.
- (iv) Inversion symmetry in x direction. The equation must be invariant under transformation $x \to -x$. This rules out odd order derivatives in the coordinates, excluding vectors such as ∇h , $\nabla(\nabla^2 h)$, etc.
- (v) Inversion symmetry in h direction. The equation must be invariant under transformation $h \to -h$. This rules out even powers of ∇h , terms such as $(\nabla h)^2, (\nabla h)^4$, etc. This symmetry is intimately connected to the equilibrium nature of the step edge, and for nonequilibrium problems this symmetry may be broken.

To find the final form of the fluctuation equation, one considers all terms that can be formed from combinations of powers of $\nabla^n h$. One by one, one can eliminate all those that violate at least one of the symmetries listed above. Thus,

$$\frac{\partial h(x,t)}{\partial t} = \nabla^2 h + \nabla^4 h + ... + \nabla^{2n} h + (\nabla^2 h)(\nabla h)^2 + ... + (\nabla^{2k} h)(\nabla h)^{2j} + \eta(x,t), \quad (2.25)$$

where n, k, j can take any positive integer value. For simplicity of notation, the coefficients in front of the terms are not explicitly indicated.

In the rest of the chapter, the continuum equations for two existing models, step edge diffusion and attachment-detachment, will be derived, analyzed and compared with simulation and experimental results

2.6 Step-Edge Diffusion

In the step edge diffusion model, atoms are only allowed to move along a step edge by reattaching to one of the two closest neighboring sites (see Figure 2.1(a)). That diffusion generates a macroscopic current j(x,t), parallel to the average step edge direction. The local changes in the step height are the result of the nonzero current along the edge. Since the total number of particles remains unchanged during the diffusion process, the current must obey the continuity equation

$$\frac{\partial h(x,t)}{\partial t} = -\nabla j(x,t). \tag{2.26}$$

On the other hand, the step edge current is driven by the differences in the local chemical potential $\mu(x,t)$

$$j(x,t) \propto -\nabla \mu(x,t). \tag{2.27}$$

To determine the local chemical potential, one may use either (a) physical reasoning or (b) symmetry arguments.

(a) Step edge diffusion is an activated process. The motion of an atom does not depend on the local height of the step, but only on the number of bonds that must be broken for diffusion to take place. The number of bonds a particle may form increases with the local curvature of the step edge at that point (see Figure 2.6). If the local radius of

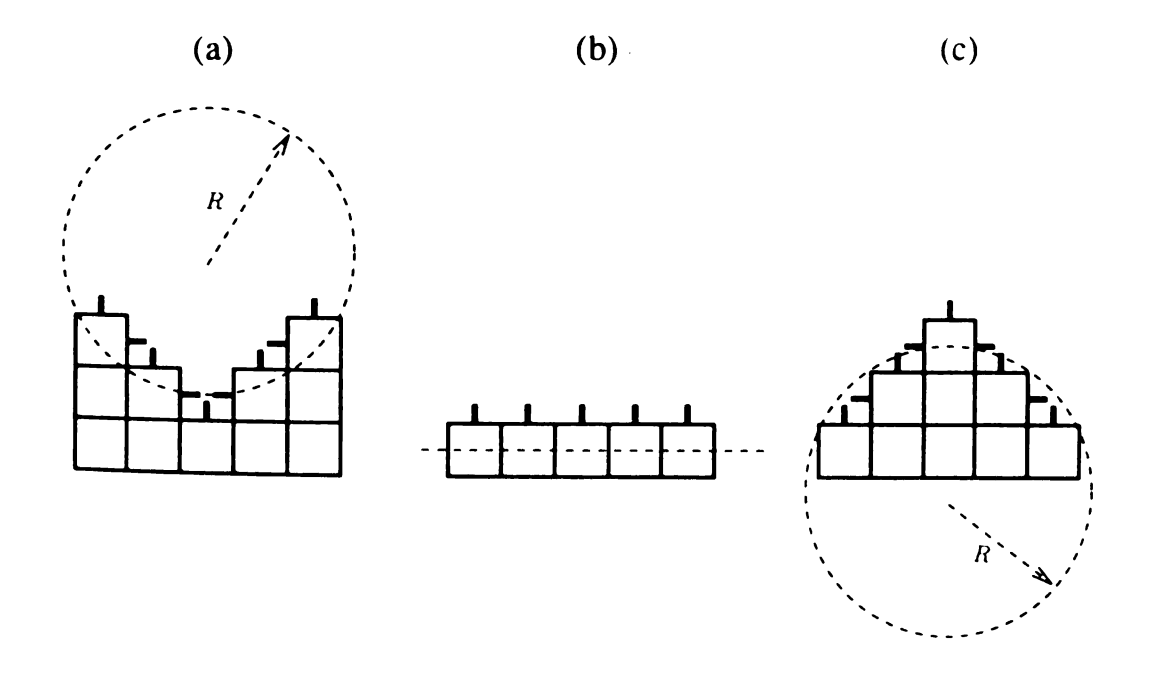


Figure 2.6 Illustration of three possible local geometries [37].

curvature R is positive, the atom has a large number of neighbors, and moving away from the site will be difficult. In contrast, if R is negative, the atom has a few neighbors, and is able to diffuse easily. The simplest assumption is that the chemical potential controlling the diffusion probability is proportional to -1/R, which in turn is proportional to $\nabla^2 h(x,t)$. Hence

$$\mu(x,t) \propto -\nabla^2 h(x,t). \tag{2.28}$$

(b) Symmetry arguments can lead to the same result (2.28) [37]. The diffusion probability of an atom should not depend explicitly on the height h(x,t) of the step edge, since it does not depend on where one defines the origin. Similarly, if the chemical potential were to depend on a power of (∇h) , then the sticking probability would be different if the system of coordinates were tilted. Thus one is left with (2.28) as the lowest order form for the chemical potential.

Combining (2.26)-(2.28), one obtains the equation describing relaxation by step edge diffusion [38]

$$\frac{\partial h}{\partial t} = -K\nabla^4 h + \eta(x, t) \tag{2.29}$$

Noise $\eta(x,t)$ must be added, otherwise equation (2.29) would be *deterministic*. During the detachment process there is an inherent *randomness* in the system. Noise is uncorrelated, but *conserved* (2.24).

By applying a Fourier transform to (2.29) one gets a Langevin equation in the form (B.1) where $\tau_q^{-1} \propto q^4$. Thus, using solution (B.12) derived in Appendix B, it gives the fluctuation width (2.2) as

$$w^2(t) \propto t^{1/4} \tag{2.30}$$

That result has been confirmed with Monte Carlo simulation [8] (see Figure 2.7) and was experimentally observed [11] (see Figure 2.8).

2.7 Attachment-Detachment

In this model, atoms are randomly detaching to the terrace and reattaching from the terrace (see Figure 2.1(b)). Thus, the terrace is a particle reservoir that randomly exchanges atoms with the step edge. The process is governed by the difference between the average chemical potential on the terrace μ_{ter} and the local chemical potential on the surface $\mu(x,t)$

$$\frac{\partial h(x,t)}{\partial t} = -B(\mu(x,t) - \mu_{tcr}) + \eta(x,t) \tag{2.31}$$

where randomness of the process is represented by *nonconservative* noise (2.23). Setting the average chemical potential on the terrace to be $\mu_{ter} = 0$ and using Equation (2.28), one gets

$$\frac{\partial h(x,t)}{\partial t} = v \nabla^2 h(x,t) + \eta(x,t) . \tag{2.32}$$

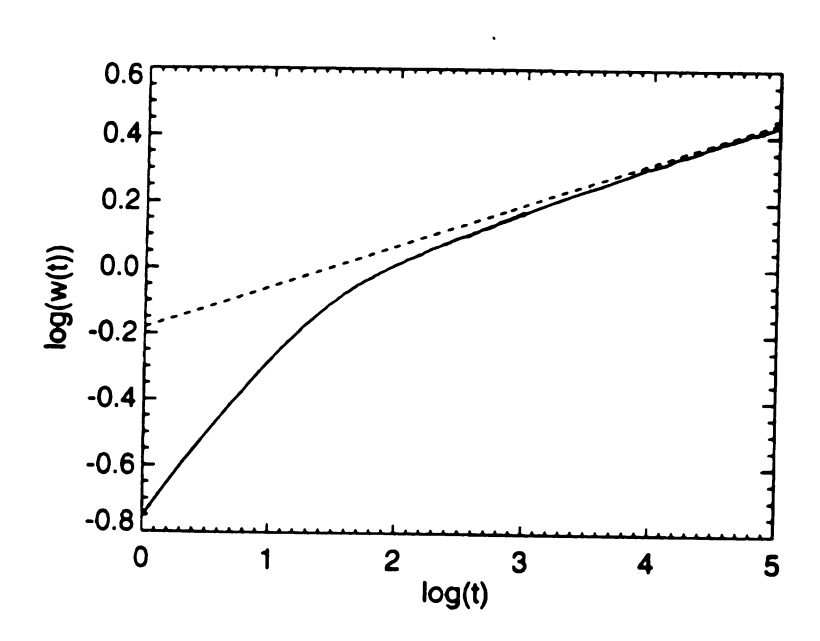


Figure 2.7 Monte Carlo simulation of an isolated step evolving through step-edge diffusion. The dashed line shows the t^{1/8} [8].

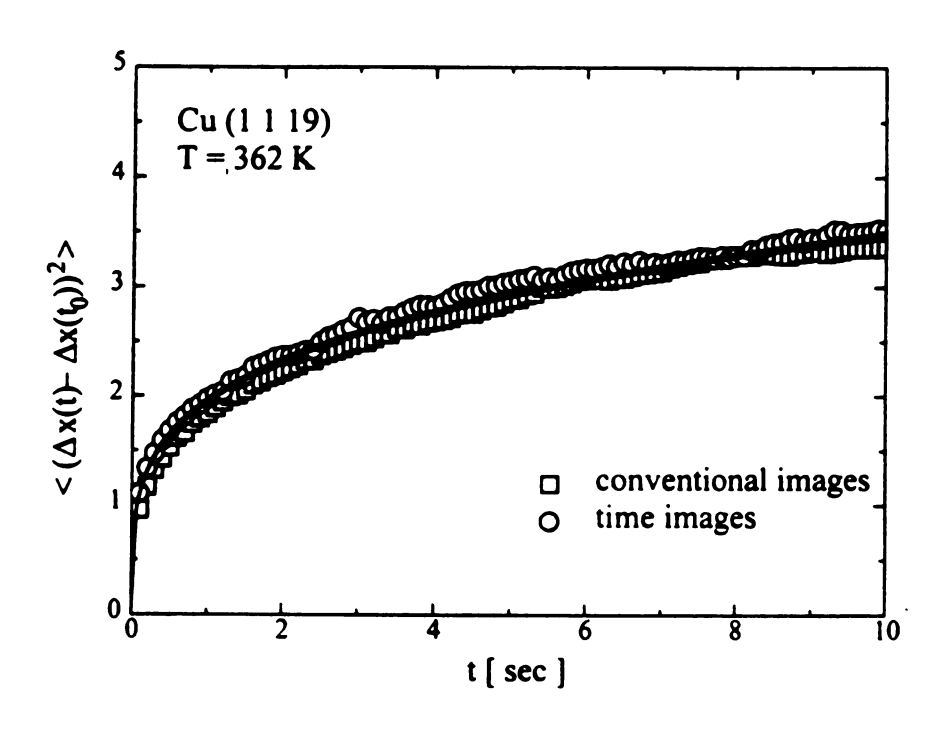


Figure 2.8 Correlation function $G(0,t) \propto w^2(t)$ (see Equation 2.17) averaged over space and time denoted by squares and circles, respectively. The full line represents a fit to a $t^{1/4}$ law [11].

By applying a Fourier transform to (2.32) one also gets a Langevin equation in the form (B.1) where $\tau_q^{-1} \propto q^2$. Thus, using again solution (B.12) derived in Appendix B, it gives the fluctuation width (2.2) as

$$w^2(t) \propto t^{1/2} \tag{2.33}$$

That result has been confirmed with Monte Carlo simulation [8] (see Figure 2.9) and was also experimentally observed [10] (see Figure 2.10).

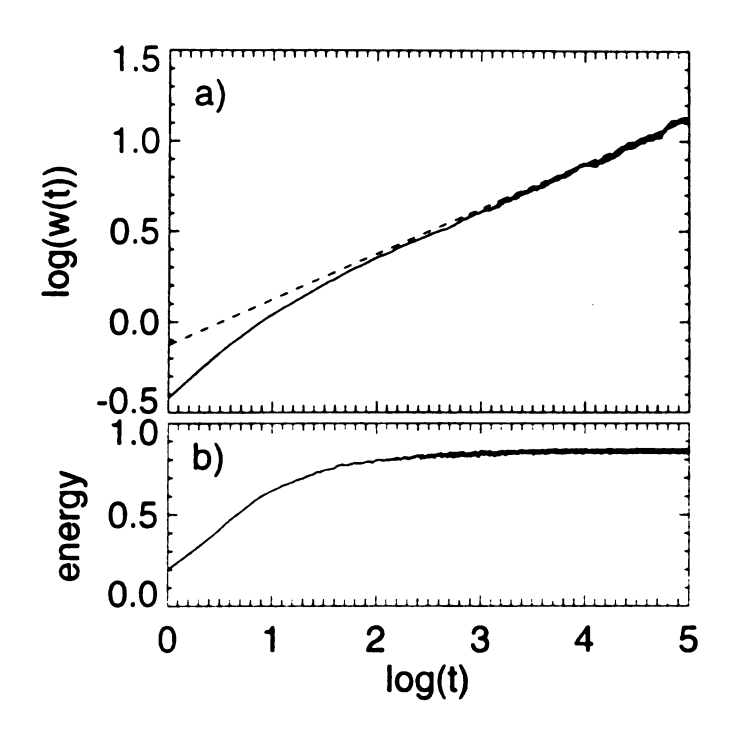


Figure 2.9 Monte Carlo simulation of an isolated step evolving through attachment-detachment . The dashed line shows the $t^{1/4}$ [8].

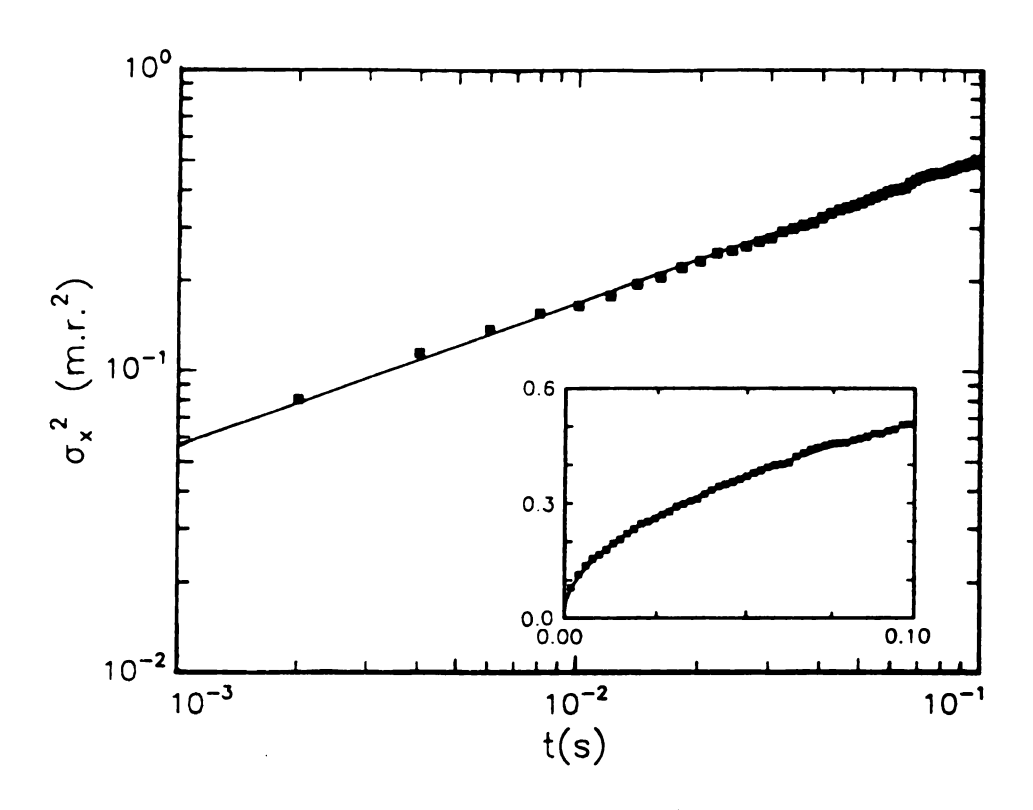


Figure 2.10 Squared fluctuation width for Au(110) at 556K. The full line represents a fit to t^{1/2} [10].

Chapter 3

An Isolated Step

3.1 Description of the Model

Consider a single isolated step at the surface. Its energy is often modeled by,

$$E = J \sum_{i=1}^{L} (h_i - h_{i-1})^{\rho}$$
 (3.1)

where h_i are in discrete units of a_{\perp} , the lattice constant perpendicular to the step edge. p=1 is the solid-on-solid (SOS) model, p=2 is the discrete Gaussian model, while $p=\infty$ is the restricted solid-on-solid model (RSOS).

In analytic work it is more convenient to use a model which takes on continuum values of the variable h_i . Moreover, it can be shown that for an isolated step, the free energy derived from the energy (3.1) is often well approximated (at small slopes) by,

$$F \sim \frac{\widetilde{\Sigma}}{2} \int_{-L/2}^{L/2} (\nabla h)^2 dx \tag{3.2}$$

where the "stiffness" $\widetilde{\Sigma} = \Sigma(0) + \Sigma''(0)$ depends on the value of p in (3.1). The "small-slope approximation" corresponds to w/L << 1. It is assumed that this holds. $\Sigma(\theta)$ is the angle-dependent interface free energy derived from (3.1). h(x) is a continuous height variable. Three cases in which the stiffness can be calculated exactly [39-41] are,

$$\widetilde{\Sigma} = 2k_B T \sinh^2(J/2k_B T) \tag{3.3}$$

for the SOS model,

$$\widetilde{\Sigma} = k_B T \frac{1 + 2e^{-J/k_B T}}{2e^{-J/k_B T}}$$
(3.4)

for the RSOS model

$$\widetilde{\Sigma} = k_B T \sinh(2J/k_B T) \tag{3.5}$$

for the Ising model. J is the kink energy, and in the low temperature and large L limit, Equations (3.3)-(3.5) all reduce to

$$\widetilde{\Sigma} = \frac{k_B T}{2} e^{J/k_B T} \text{ for } k_B T \ll J$$
 (3.6)

From the Hamiltonian (3.2), it is straightforward to find the saturation width, $w_{sat}^2 = \langle h^2(t \to \infty) \rangle - \langle h(t \to \infty) \rangle^2$ (one takes h(x,0)=0 henceforth), of the step edge (see Appendix A),

$$w_{sat} = (\frac{k_B T L}{12\tilde{\Sigma}})^{1/2} = (\frac{L\Omega}{12\tilde{s}})^{1/2}$$
 (3.7)

where $\tilde{s} = \tilde{\Sigma}\Omega/k_BT$ with $\Omega = a \ a_\perp$ as the area of the surface element (a and a_\perp are the lattice spacings perpendicular and parallel to the step edge respectively). As it is seen from expression (3.7), periodic boundaries at the end of the step are assumed.

The chemical potential, $\mu(x,t)$ can be found from Equation (3.2) in the following way. Using the formula for the variation of an integral, (3.2) gives

$$\delta F(h) = -\widetilde{\Sigma} \int_{-L/2}^{+L/2} \nabla^2 h \, \delta h \, dx \, .$$

On the other hand, variation of the energy can be expressed through the local chemical potential [22] as

$$\delta F(h) = \frac{1}{\Omega} \int_{-L/2}^{+L/2} \mu \, \delta h \, dx \, .$$

Finally, equating those equations gives the expression for the chemical potential as

$$\mu(x,t) = -\Omega \widetilde{\Sigma} \nabla^2 h(x,t) . \tag{3.8}$$

Note that this agrees with assumptions (2.28). Within non-equilibrium thermodynamics, the driving force for relaxation is provided by deviations in the local chemical potential from its equilibrium value. The rate at which such deviations relax is determined by the dominant *kinetics* in the physical system of interest. In addition, the thermal noise in the system randomly generates fluctuations. One thus describes the dynamics of a step edge by the equation,

$$\frac{\partial h(x,t)}{\partial t} = \frac{\Gamma_h}{k_B T} J(x,t) + \eta(x,t). \tag{3.9}$$

where:

$$J(x,t) = \int_0^{L-2} P_i(l) \{ \mu(x+l,t) - 2\mu(x,t) + \mu(x-l,t) \} dl$$
 (3.10)

L is the length of the step along the x-direction and Γ_h is the rate

$$\Gamma_{k} = a_{\perp} / \tau_{k}, \tag{3.11}$$

where τ_h is the time between detachment events from a site on the step edge. $\eta(x,t)$ is the noise term, which must reproduce the equilibrium fluctuations of the step at long times (see Appendix B). Equation (3.9) states that the relaxation rate of a chemical potential difference between two step positions (separated by distance l) is a product of the chemical potential difference between those sites and the flux of atoms which is exchanged between the two positions. Thus, $P_i(l)$ is the probability that an atom will be

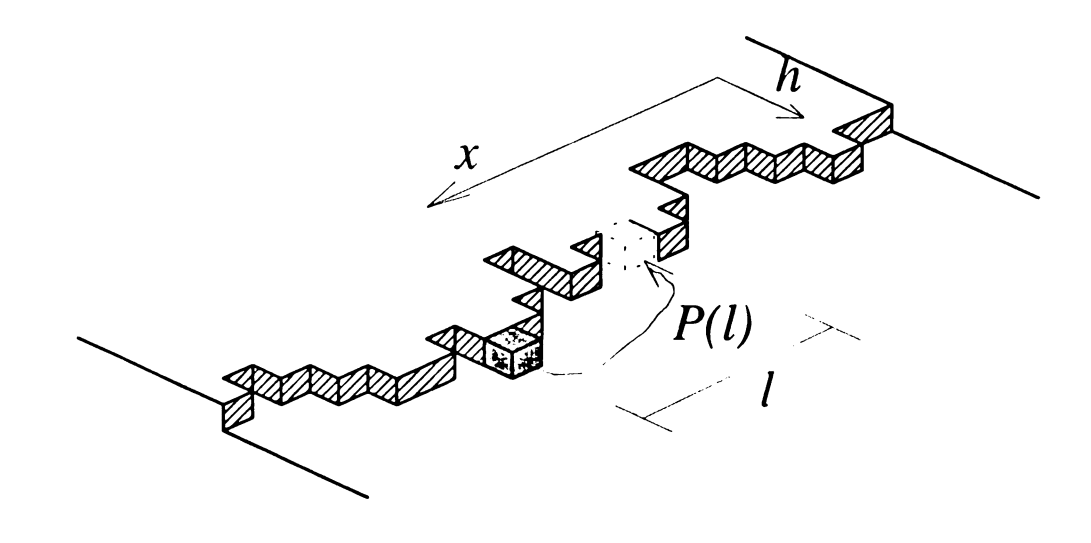


Figure 3.1 Terrace diffusion with diffusion kernel $P_i(l)$.

exchanged between sites separated by distance *l* along the isolated step edge (see Figure 3.1). It is normalized

$$2\int_{0}^{L/2} P_{i}(l) dl = 1$$

A Fourier transform of (3.9) and (3.10) using normalization yields Langevin equation,

$$\frac{\partial h_q(t)}{\partial t} = -\frac{h_q(t)}{\tau_q} + \eta_q(t) \tag{3.11}$$

where

$$\tau_q^{-1} = \frac{\widetilde{s} \, q^2 a_\perp}{\tau_h} \left\{ 1 - 2 \int_0^{L/2} P_i(l) \cos q l \, dl \right\}$$
 (3.12)

and (periodic boundaries),

$$h(x,t) = \sum_{q} h_{q}(t)e^{iqx}$$
, with $q = \pm 2\pi n/L$, $n = 1,..., L/a_{\parallel}$.

Note that if the noise is removed from the right hand side of Equation (3.11), one has

$$h_q(t) = h_q(0) e^{-t/\tau_q}$$
 with no noise (3.13)

A general expression for τ_q^{-1} was found by Bales and Zangwill [14] (corrected by Pimpinelli et al. [13]). Their expressions will be derived from a different physical perspective later in this chapter.

In the presence of Gaussian white noise

$$\langle \eta_{q_1}(t_1)\eta_{q_2}^{\bullet}(t_2)\rangle = f(q_1,q_2)\delta_{q_1,q_2}\delta(t_1-t_2),$$

the solution to the linear Langevin Equation (3.11) is (see Appendix B)

$$<\left|h_{q}(t)\right|^{2}>=\frac{\Omega}{L\widetilde{s}q^{2}}(1-e^{-2t/\tau_{q}}).$$
 (3.15)

An inverse transform of $\left|h_q(t)\right|^2$ then gives,

$$w^{2}(t) = \langle h^{2}(x,t) \rangle - \langle h(x,t) \rangle^{2} = \langle h^{2}(x,t) \rangle = \sum_{q} \frac{\Omega}{L\widetilde{s}q^{2}} (1 - e^{-t/\tau_{q}})$$
 (3.16)

since $\langle h(x,t) \rangle = 0$ (center of the mass of the step does not move from its initial position at x = 0) Besides, $w^2(t) = G(2t)$, where (see Appendix B)

$$G(t) = \frac{1}{2} \left\langle \left(h(x, t_1 + t) - h(x, t_1) \right)^2 \right\rangle, \quad t << t_1 \approx t_{sat}$$
 (3.17)

and t_{sat} is the saturation time. w(t) is a fluctuation width, while G(t) is a time dependent equilibrium correlation function. Within the linear Langevin Equation (3.11) they are essentially equivalent. At long times, the exponential part in Equation (3.16) is dominated by the n = 1 term in the sum. One thus defines the saturation time t_{sat} , by the time it takes for the (n = 1) exponential term to decay to e^{-1} so that,

$$t_{sat} = \tau_{q=2\pi/L}. \tag{3.18}$$

This gives a simple and accurate estimate of the saturation time. Thus the "natural" scaled variables are $G(t)/w_{sat}^2$ and t/t_{sat} .

In several cases, one finds that

$$\tau_q^{-1} \sim Aq^{\gamma}, \tag{3.19}$$

in which case, the continuum limit of Equation (3.16) yields (see (B.12))

$$w^{2}(t) = G(2t) \sim \frac{\Omega}{\pi \, \tilde{s}} \Gamma(1 - \frac{1}{\gamma})(2At)^{\frac{1}{\gamma}},$$
 (3.20)

where Γ is the Gamma integral as defined for example in [34]. Thus, scaling assumed in (2.3) holds if (3.19) holds.

3.2 Step-Edge Diffusion

The diffusion is restricted to nearest neighbors along the step edge (see Section 2.6 and Figure 2.1(a)) by defining,

$$P_{i}(l) = \frac{1}{2} \left\{ \delta(l - a_{\parallel}) + \delta(l + a_{\parallel}) \right\}$$
 (3.21)

The characteristic time τ_h is now the time between atomic hopping events between nearest neighbors. Let us assume simple activated behavior $\tau_h^{-1} = v \exp(-E_{SE}/k_BT) \{ \exp(-E_I/k_BT) + \exp(-E_r/k_BT) \}$, where v is a characteristic phonon frequency, E_{SE} is a step-edge diffusion activation energy, while E_I and E_r are the energy barriers that an atom, once activated, has to overcome to move to the left or to the right site respectively. In the simplest simetric case $E_I = E_r = 0$, thus $\tau_h^{-1} = 2\tau_{SE}^{-1}$ where $\tau_{SE}^{-1} = v \exp(-E_{SE}/k_BT)$. Using Equation (3.12) then yields

$$\tau_q^{-1} = \frac{2\tilde{s} a_{\perp}}{\tau_{sc}} q^2 \{1 - \cos q a_{\parallel}\}. \tag{3.22}$$

An expansion of τ_q^{-1} at small q yields the behavior (3.19), with $A = \tilde{s} a_{\parallel}^2 / \tau_{SE}$, $\gamma = 4$ for $|q| < 1/a_{\parallel}$. The region $|q| > 1/a_{\parallel}$ is very small and has negligible influence to the correlation function. Thus, in the intermediate time regime one finds (using Equation (3.20)),

$$w^{2}(t) = G(2t) = \frac{1}{\pi} \Gamma(\frac{3}{4}) \left(\frac{\Omega^{5} a_{\parallel}}{\widetilde{s}^{3}}\right)^{\frac{1}{4}} \left(\frac{2t}{\tau_{SF}}\right)^{\frac{1}{4}}.$$
 (3.23)

This agrees with Equation (2.30) and case F of [13]. It is the essentially the same as the result previously obtained in [8].

A behavior similar to Equation (3.23) occurs for any short range diffusion kernel. For example, taking

$$P_i(l) = \frac{1}{2\xi_{\parallel}} e^{-\frac{l}{\xi_{\parallel}}}, \text{ with } a_{\parallel} << \xi_{\parallel} << L$$
 (3.24)

yields

$$w^{2}(t) = G(2t) = const \left(\frac{\xi^{2}t}{\widetilde{s}^{3}\tau_{SE}}\right)^{1/4}.$$
 (3.25)

A little later in this chapter, it will be shown that if $P_i(l) = B/l^{\alpha}$, with $\alpha \ge 3$, then a similar behavior pertains.

3.3 Attachment-Detachment Model

The attachment-detachment (see Section 2.7) assumes that a step is randomly exchanging atoms with the terrace (see Figure 2.1(b)). It can be described by using the probability function Equation (3.24) but now assuming that the correlation length, $\xi_{\parallel} >> L$. Physically this means that infinite range conserved-order-parameter dynamics is the same as non-conserved order parameter dynamics. To simplify the calculation, one can use the normalized uniform probability $P_i(l)$ as,

$$P_i(l) = const = \frac{1}{L} \tag{3.26}$$

The characteristic time τ_h is the time between atomic detachment events from a step edge onto the terrace. In the simplest case one would expect activated behavior $\tau_q^{-1} = \tau_{AD}^{-1} = v \exp(-E_{AD}/k_BT)$, where v is a characteristic phonon frequency and E_{AD} is an attachment-detachment activation energy. However, this simplified theory remains valid even if many different processes (and barriers) play a role, provided they can be treated as independent. Equation (3.12) then yields,

$$\tau_q^{-1} = \frac{\widetilde{s}a_\perp}{\tau_{AD}} q^2, \tag{3.29}$$

for all values of q. Thus, the q dependence (3.19) holds with $A = \tilde{s} a_{\perp} / \tau_{EC}$ and $\gamma = 2$. Using (3.20), one has

$$w^{2}(t) = G(2t) = \Omega(\frac{a_{\perp}}{\pi \widetilde{s}})^{1/2} (\frac{2t}{\tau_{AD}})^{1/2}.$$
 (3.28)

This agrees with Equation (2.33) and case A of [13]. It is essentially the same result as the one obtained by prior workers in [8] and [42].

3.4 Terrace Diffusion

Over broad temperature regimes, terrace diffusion is the dominant kinetic mechanism. In this model, an atom detaches onto the terrace below the step edge with probability p_L , and onto the terrace above the step edge with probability p_U . It then diffuses on the terrace until it reattaches to the same or one of the adjacent step edges. Let us define α_L to be the sticking coefficient of an atom which approaches a step edge from the lower

terrace and α_U to be the sticking coefficient on approach to the step edge from the upper terrace. One assumes simple behavior where E_{TD} is the terrace diffusion activation energy, and E_L and E_U are the energy barriers that an atom, once activated, has to overcome to move to the lower or to the upper terrace respectively (see Figure 3.2). E_L and E_U are also energy barriers that an atom has to overcome to stick to the step edge on its approach from the lower and upper terrace respectively. E_U is known as the "Schwoebel barrier" [45] and one expects in general $E_U >> E_L$. This is understood by noting that the atom that sticks to a step on its approach from the upper terrace has to go through the position where it has fewer neighbors. This is unfavorable energetically. One then finds that probabilities of detaching

$$p_{L} = \frac{e^{-E_{L}/k_{B}T}}{e^{-E_{L}/k_{B}T} + e^{-E_{U}/k_{B}T}}, \quad p_{U} = \frac{e^{-E_{U}/k_{B}T}}{e^{-E_{L}/k_{B}T} + e^{-E_{U}/k_{B}T}}$$
(3.29)

and sticking coefficients (see Appendix C)

$$\alpha_{L} = \frac{e^{-E_{L}/k_{B}T}}{(1 - e^{-E_{L}/k_{B}T})a_{\perp}}, \quad \alpha_{U} = \frac{e^{-E_{U}/k_{B}T}}{(1 - e^{-E_{U}/k_{B}T})a_{\perp}}.$$
 (3.30)

are related to the step edge barriers. Sticking coefficients can have any value in the range $[0.\infty)$ where 0 corresponds to no sticking and ∞ to perfect sticking.

In terms of the energies defined in Figure 3.2, the characteristic time τ_h is,

$$\tau_h^{-1} = \tau_{TD}^{-1} \left\{ e^{-E_L/k_B T} + e^{-E_U/k_B T} \right\},\tag{3.31}$$

where $\tau_{TD}^{-1} = v \exp(-E_{TD}/k_B T)$ and v is a characteristic phonon frequency. Therefore, for the terrace diffusion case, the fundamental activation energies are E_{TD} , E_L and E_U , as

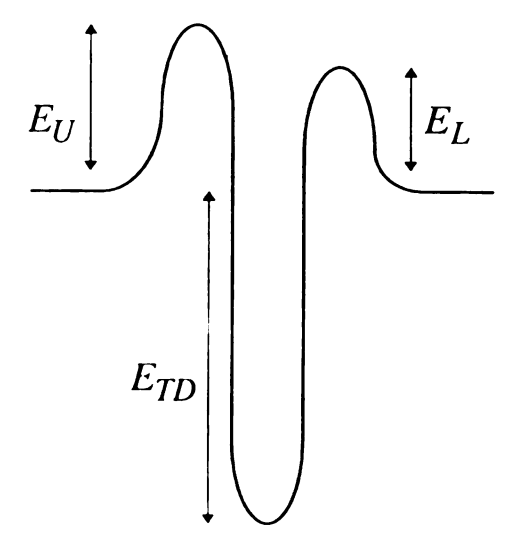


Figure 3.2 Key energy barriers at a step edge.

defined in Figure 3.2, while the "natural" parameters appearing in the dynamics are τ_{TD} , α_{U} and α_{L} .

 $P_i(l)$ for terrace diffusion is

$$P_{i}(l) = p_{U}P'(\alpha_{U}, \alpha_{L}, l) + p_{L}P'(\alpha_{L}, \alpha_{U}, l)$$
(3.32)

where P'=P with $d\to\infty$ given by Equation (C.14) derived in Appendix C (see also Equation (C.17)), from which one finds,

$$P_{i}(l) = p_{U} \frac{\alpha_{U}}{\pi} \int_{0}^{\infty} \frac{\cos kl \, e^{-ka_{\perp}} dk}{k + \alpha_{U}} + p_{L} \frac{\alpha_{L}}{\pi} \int_{0}^{\infty} \frac{\cos kl \, e^{-ka_{\perp}} dk}{k + \alpha_{L}}$$
(3.33)

On Figure 3.3, $P' = \frac{\alpha}{\pi} \int_0^\infty \frac{\cos kl \, e^{-ka_-} \, dk}{k + \alpha}$ vs. l is plotted for four different values of the sticking coefficient α . Note that for the large values of α (perfect sticking) $P' \propto 1/l^2$ for all l, while for the small values of α (weak sticking) $P' \propto -\ln(l)$ for small l and $P' \propto 1/l^2$ for large l.

Using expression (3.33) in (3.12) leads to,

$$\tau_q^{-1} = \frac{\widetilde{s} q^2 a_\perp}{\tau_h} \left(1 - \alpha_U p_U \frac{e^{-iq a_\perp}}{\alpha_U + q} - \alpha_L p_L \frac{e^{-iq a_\perp}}{\alpha_L + q} \right)$$
(3.34)

Using this inverse time and doing numerical summations over q, G(t), defined by Equation (B.10), is plotted on Figure 3.4 for $\alpha_L = \alpha_U = 10^{-2} / a_\perp$ (weak sticking), $\alpha_L = 10^3 / a_\perp$, $\alpha_U = 10^{-2} / a_\perp$ (Schwoebel barrier), and $\alpha_L = \alpha_U = 10^3 / a_\perp$ (perfect sticking). As will be shown below, $G(t) \propto t^{1/3}$ for perfect sticking, Schwoebel barrier and

Single Step: probability

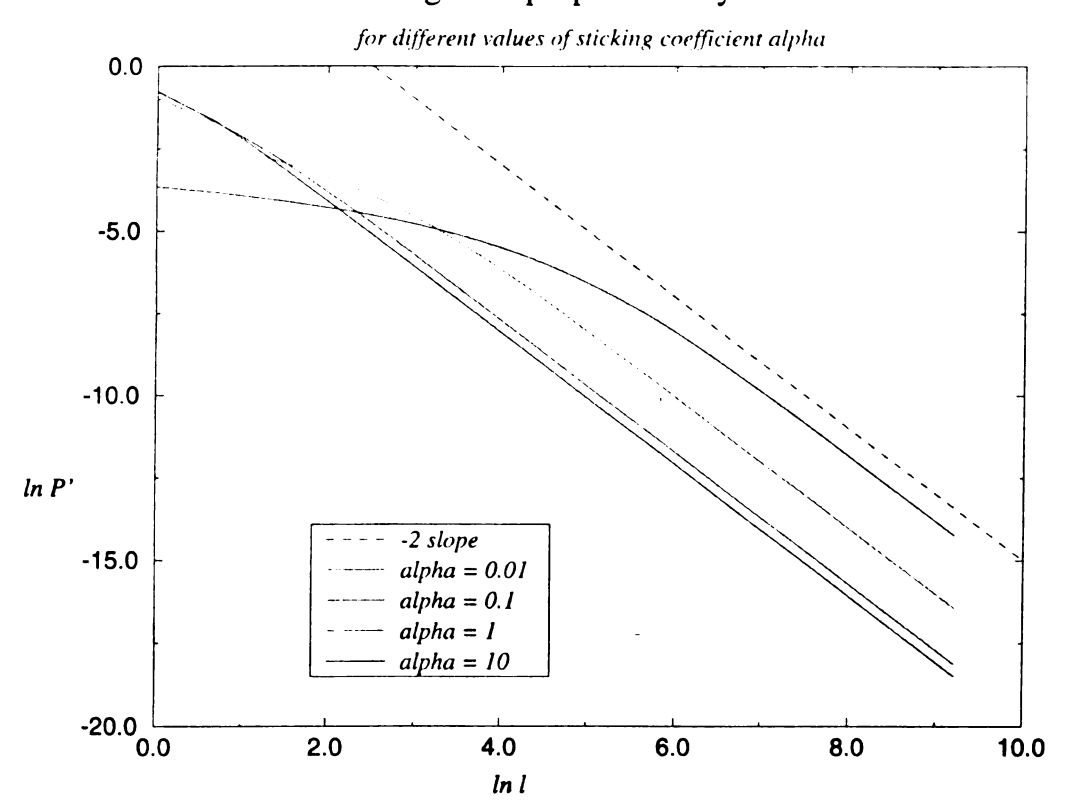


Figure 3.3 Diffusion kernel (C.17) is plotted vs. l for four different values of sticking coefficient (from the top): $\alpha_L = \alpha_U = 0.01/a_\perp$, $\alpha_L = \alpha_U = 0.1/a_\perp$, $\alpha_L = \alpha_U = 1/a_\perp$, and $\alpha_L = \alpha_U = 10/a_\perp$. Note that for large values of α (perfect sticking) $P' \propto 1/l^2$ for all l, while for small values of α (weak sticking) $P' \propto -\ln(l)$ for small l and $P' \propto 1/l^2$ for large l.

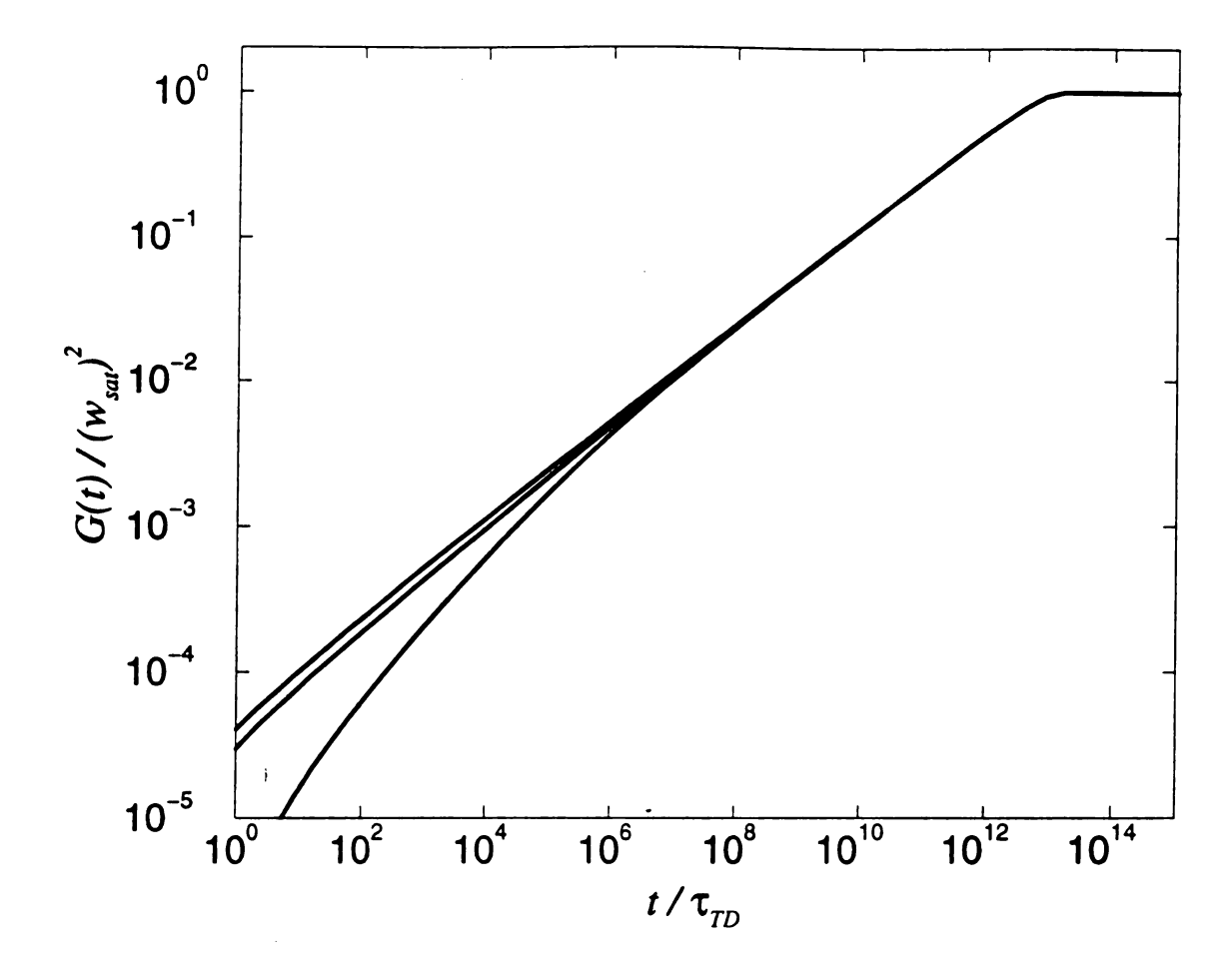


Figure 3.4 The correlation function G(t) for (from the top): $\alpha_L = \alpha_U = 10^3 / a_{\perp}$; $\alpha_L = 10^3 / a_{\perp}$; $\alpha_L = \alpha_U = 10^{-2} / a_{\perp}$. In all cases $L = 10^5 a_{\parallel}$, $k_B T / \tilde{\Sigma} = 1$. It is plotted using inverse times (3.34) and doing numerical summations over q, defined by Equation (B.10), As shown in Equations (3.39)-(3.41), $G(t) \propto t^{1/3}$ for perfect sticking, Schwoebel barrier, and weak sticking case at large times, while $G(t) \propto t^{1/2}$ for weak sticking case at small times.

weak sticking case (the last one at large times only), while $G(t) \propto t^{1/2}$ for weak sticking case at small times.

For $|q| < 1/a_{\perp}$, (3.34) reduces to,

$$\tau_q^{-1} = \frac{\widetilde{s} a_\perp^2}{\tau_{TD}} |q|^3 \left(\frac{\alpha_U}{\alpha_U + |q|} + \frac{\alpha_L}{\alpha_L + |q|}\right). \tag{3.35}$$

From Equation (3.35) it is seen that there are three possible regimes:

(i) when $\alpha_{U,L} << |q|$ then

$$\tau_q^{-1} = \widetilde{s} a_\perp^2 (\alpha_U + \alpha_L) q^2 / \tau_{TD} \tag{3.36}$$

 $(q^2$ dependence for small sticking coefficients has been also suggested in [16]);

(ii) when $\alpha_U \ll |q| \ll \alpha_L$ (assuming $\alpha_{t'} \ll \alpha_L$) then

$$\tau_q^{-1} = \tilde{s} a_{\perp}^2 |q|^3 / \tau_{TD};$$
 (3.37)

(iii) and when $\alpha_{U,L} >> |q|$ then

$$\tau_q^{-1} = 2\tilde{s} a_\perp^2 |q|^3 / \tau_{TD} \tag{3.38}$$

(last expression has been derived using different formalism in [16]).

Thus, extreme values of sticking coefficients leads to three different time dependences of the width and correlation function. In the case of small sticking coefficients, an atom has to bounce off the step edge many times before it sticks. Thus, terrace diffusion with weak sticking has the same effect as attachment-detachment process (see Equation 3.28). After substituting (3.36) to (3.20) one has

$$w^{2}(t) = G(2t) = \Omega a_{\perp} \left(\frac{\alpha_{U} + \alpha_{L}}{\pi \widetilde{s}}\right)^{1/2} \left(\frac{2t}{t_{TD}}\right)^{1/2}, \text{ for } \alpha_{U,L} \ll 1.$$
 (3.39)

In the large Schwoebel barrier case, one of the terraces (the upper one for the case $\alpha_U \ll \alpha_L$) is not contributing since approach to the step edge from that terrace has such a small sticking coefficient. After substituting (3.37) to (3.20) one has,

$$w^{2}(t) = G(2t) = \frac{\Omega\Gamma(2/3)}{\pi} \left(\frac{a_{\perp}^{2}}{\widetilde{s}^{2}}\right)^{1/3} \left(\frac{2t}{\tau_{TD}}\right)^{1/3}, \text{ for } \alpha_{U} << 1 << \alpha_{L}$$
 (3.40)

However, for very small values of q (3.36) and (3.37) do not hold. Instead, (3.38) then holds for all values of sticking coefficients. Thus at large enough times, weak sticking and Schwoebel barrier case have the same correlation function as perfect sticking case for all times (after substituting (3.38) to (3.20)),

$$w^{2}(t) = G(2t) = \frac{\Omega\Gamma(2/3)}{\pi} \left(\frac{2a_{\perp}^{2}}{\tilde{s}^{2}}\right)^{1/3} \left(\frac{2t}{\tau_{TD}}\right)^{1/3}. \quad \text{for } \alpha_{U,L} >> 1$$
 (3.41)

That is visible on Figure 3.4, where correlation function of weak sticking (bottom line) and Schwoebel barrier (middle line) at certain time cross to (3.41) from (3.39) and (3.38) respectively.

In experiment, the step-edge, terrace diffusion and attachment-detachment mechanisms all occur, albeit with different activation energies. It is straightforward to combine the diffusion kernels (3.21), (3.26) and (3.33), with arbitrary weights and hence find,

$$\tau_{q}^{-1} = \widetilde{s} a_{\perp} q^{2} \left(a \frac{a_{\parallel}^{2}}{\tau_{SE}} q^{2} + b \frac{1}{\tau_{AD}} + c \frac{a_{\perp}}{\tau_{TD}} q \left(\frac{\alpha_{U}}{\alpha_{U} + |q|} + \frac{\alpha_{L}}{\alpha_{L} + |q|} \right) \right)$$
(3.42)

with a+b+c=1 to preserve the normalization of the kernel $P_i(l)$. The weights a,b,c are expected to have an activated form, dependent on the various step-edge and kink energies, so the crossover between the various mechanisms as a function of temperature is quite sharp. At present atomistic simulations are not sufficiently precise to predict in detail the relative importance of the various terms in Equation (3.42).

3.5 Anomalous Diffusion

It is interesting to note that there are cases in which the step dynamics is non-universal.

One can illustrate this point through use of the probability distribution

$$P_i(l) = \frac{B}{l^{\alpha}} \text{ for } l \ge a_{\parallel}$$
 (3.43)

where $\alpha=0$ recovers the attachment-detachment limit, $\alpha=2$ corresponds to terrace diffusion with perfect sticking, while $\alpha>3$ (see below) corresponds to "short-range" hopping and recovers the step-edge diffusion behavior. $B^{-1}=2((L/2)^{1-\alpha}-a_{\parallel}^{1-\alpha})/(1-\alpha)$ normalizes the probability on the interval (a_{\parallel},∞) . By evaluating the integral Equation (3.12), one finds that:

$$\tau_q^{-1} \approx \frac{\widetilde{s} a_\perp}{\tau_L} q^2 (1 + O((\frac{2q a_\perp^2}{L})^{2-2\alpha}) \quad \text{for } 0 \le \alpha < 1.0;$$
(3.44)

$$\tau_{q}^{-1} \approx \frac{\widetilde{s} a_{\perp}}{\tau_{h}} q^{2} \left(\frac{1 - \alpha}{2} \Gamma(1 - \alpha) \cos \frac{(1 - \alpha)\pi}{2} (q a_{\parallel})^{\alpha - 1} + \frac{1 - \alpha}{4(3 - \alpha)} (q a_{\parallel})^{2} \right) \text{ for } 1 < \alpha < 3 \quad (3.45)$$

(Note that for integer α , τ_q^{-1} is finite despite the divergence in $\Gamma(1-\alpha)$);

$$\tau_q^{-1} \approx \frac{\widetilde{s} a_{\perp}}{\tau_h} q^2 \left(\frac{\alpha - 1}{4(\alpha - 1)} (q a_{\parallel})^2 - \frac{\alpha - 1}{48(\alpha - 5)} (q a_{\parallel})^4 \right) \quad \text{for } \alpha > 3$$
 (3.46)

Using Equation (3.20), one then finds

$$w^{2}(t) = G(2t) \sim t^{1/2}$$
 for $0 < \alpha < 1$, (3.47)

$$w^{2}(t) = G(2t) \sim t^{\frac{1}{\alpha+1}}$$
 for $1 \le \alpha \le 3$, (3.48)

and

$$w^{2}(t) = G(2t) \sim t^{1/4} \quad \text{for} \quad \alpha \ge 3.$$
 (3.49)

Equations (3.47-3.49) show a continuous variation in the dynamical exponent for $1 \le \alpha \le 3$, while the attachment-detachment universality class holds for $0 < \alpha < 1$ and the step-edge universality class holds for $\alpha \ge 3$. Figure 3.5 shows fluctuation exponent β (see (2.3)) vs. α . The points on the graph are obtained using diffusion kernel (3.43) in (3.12) to numerically find q dependence and than using (3.20) to get exponent β . As it can be seen, there is a continuous variation for $0 \le \alpha \le 3$. Thus, (3.47-3.49) holds as an approximate dependence around $\alpha = 1$. This is due to complex forms of (3.44-3.46).

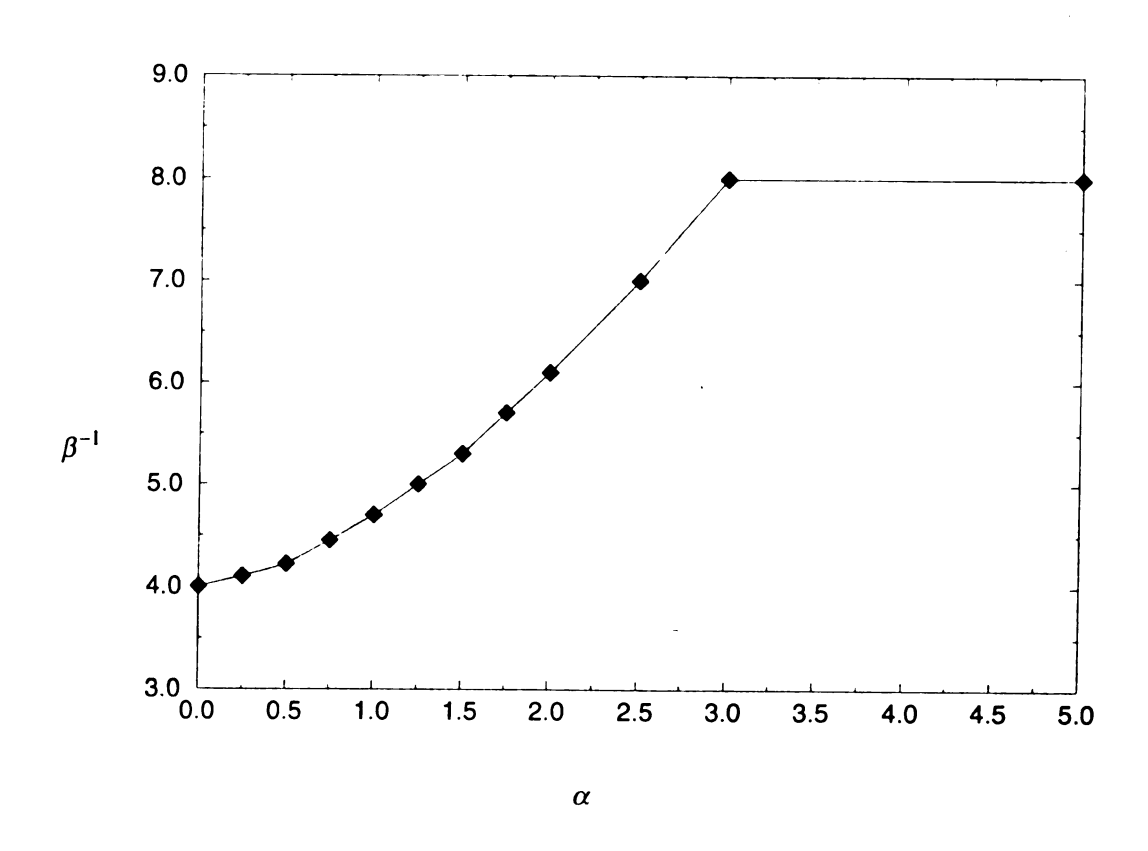


Figure 3.5 The fluctuation exponent β (see (2.3)) is plotted vs. α from (3.43). The points on the graph are obtained using diffusion kernel (3.43) in (3.12) to numerically find q dependence and than using (3.20) to get exponent β .

Chapter 4

Array of Steps

4.1 Introduction

In this chapter, the step train (array) is treated (see Figure 4.1). The model introduced in Chapter 3 is extended to include the exchange of atoms between neighboring steps. The pair correlation function between two steps $C_k(x,t)$ is introduced [48]. It is an averaged product of two step positions separated by distance x parallel to the step edge and located k steps away. The relaxation time τ_{pq} for steps which are modulated along the steps (with wave number q), and perpendicular to the steps (with wave number p) is calculated. By summing over all modes, one derives $C_k(x,t)$. It is shown that the pair correlation function between two different steps, $C_{k\neq 0}(x,t)$, can often differentiate between terrace diffusion and attachment-detachment or step-edge diffusion. $C_{k\neq 0}(x,t)$ is identically zero for the cases of attachment-detachment and step-edge diffusion. In contrast, $C_{k\neq 0}(x,t)$ is finite and quite large in the case of terrace diffusion. This means that measurement of a finite value for $C_{k\neq 0}(x,t)$ implies that terrace diffusion is important. Since G(t) quantifies the cumulative effect of all mass transport mechanisms, by combining the results of G(t)and $C_{k\neq 0}(x,t)$ it is then possible to determine the relative importance of terrace diffusion to the other types of mass transport in surface dynamics. In addition, G(t) used in Chapter 3 is generalized by introducing G(x,t) as the averaged square fluctuation of the difference between two step positions separated by distance x parallel to the step edge and located at the same step. It enables one to derive initial time-independent fluctuation for nonzero x. The currently used correlation function is included as $G(t) \equiv G(0,t)$.

The next section contains the real-space formulation of step dynamics, extended from the one in Chapter 3. The key equations are Equation (4.17) for the relaxation time τ_{pq} , and Equation (4.24) for the correlation function $C_k(x,t)$. Section 4.3 contains an analysis of $C_k(x,t)$ and G(x,t) in a variety of time regimes. This section can be skipped by those uninterested in the detailed analysis. Section 4.4 treats the terrace diffusion case. Since there is no correlated mass exchange between steps in attachment-detachment and stepedge diffusion case, in these cases the step train model essentially gives the same results as for an isolated step model. For that reason, those two models are not treated in Section 4.4. Analytic results for G(x,t) and $C_k(0,t)$ for all three solvable limiting cases are summarized in Tables 4.1 and 4.2 respectively. Examples illustrating some of the more interesting crossovers between these limiting cases are illustrated in Figures 4.3 and 4.4.

4.2. The Model

Consider a train of N steps, all with length L (see Figure 4.1). Steps are numbered with k=1,2,...,N and periodic boundary conditions both along the step train, and along each step are assumed. (this simplifies the analysis and is typical of steps away from the edges of a finite step train). Let $h_k(x,t)$ describe the random motion of the k^{th} step in the train about its center of mass, which is assumed to be fixed - there are no "direct" interaction terms to produce center of mass dynamics. The average distance between centers of mass

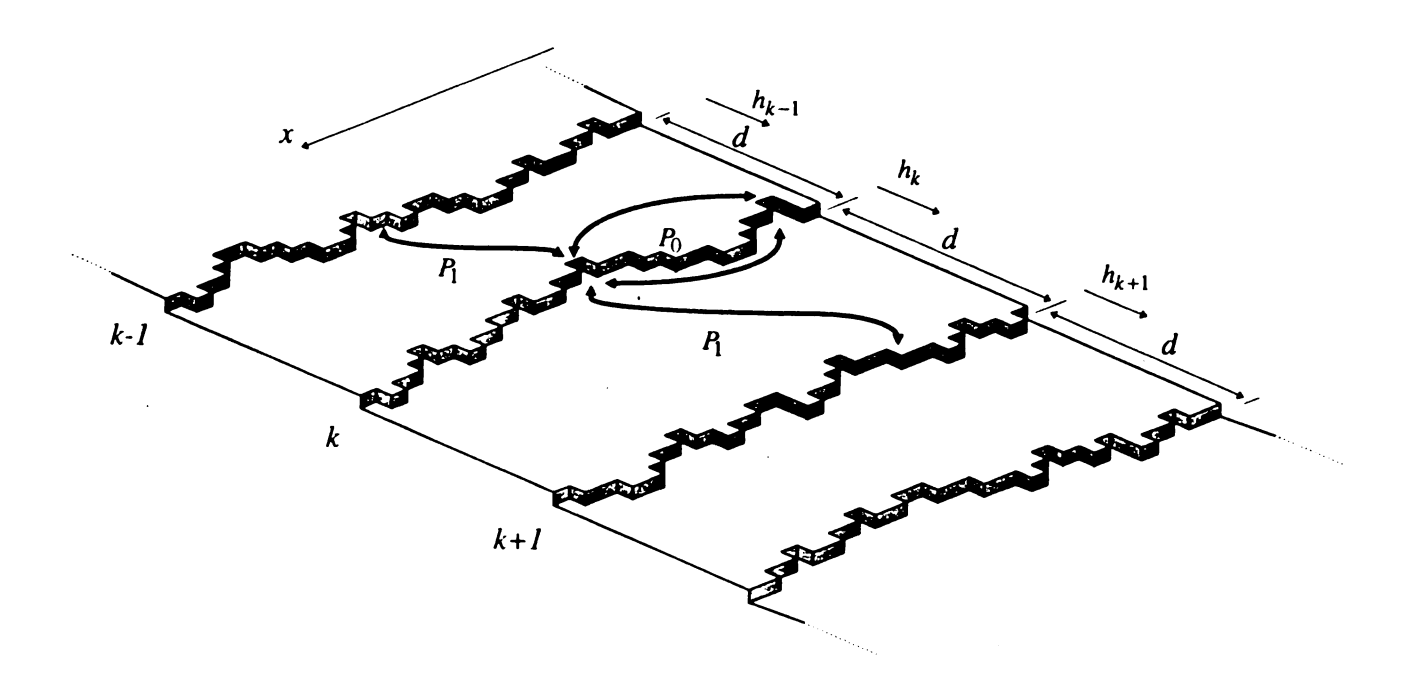


Figure 4.1 Diffusion kernels on the vicinal surface.

of adjacent steps is the same everywhere on the surface and equals d. The existence of direct interaction would cause the centers of mass of the steps to move. That would lead to the change in surface morphology. That is analyzed in Chapter 5.

Let us define the equilibrium ($t \ll t_1 \rightarrow \infty$) correlation functions

$$G(x,t) = \frac{1}{2} < [h_{k_1}(x_1 + x, t_1 + t) - h_{k_1}(x_1, t_1)]^2 >$$
(4.1)

and

$$C_k(x,t) = \langle h_{k_1+k}(x_1 + x, t_1 + t) h_{k_1}(x_1, t_1) \rangle. \tag{4.2}$$

While G(x,t) measures the fluctuation width, the pair correlation function $C_k(x,t)$ quantifies the correlation between the fluctuation of two points. Because of the periodic boundaries, G(x,t) and $C_k(x,t)$ do not depend on x_1 and k_1 . By squaring the bracket in Equation (4.1) and taking an average of each term individually, one finds that these two functions are related as

$$G(x,t) = C_0(0,0) - C_k(x,t)$$
(4.3)

where $C_0(0,0)$ is actually the squared equilibrium width of the step fluctuation.

The local chemical potential, $\mu_k(x,t)$, one associates with k^{th} step is,

$$\mu_{k}(x,t) = -\Omega \widetilde{\Sigma} \nabla^{2} h_{k}(x,t). \tag{4.4}$$

It is derived using (see derivation of Equation (3.8))

$$F_k \approx \frac{\widetilde{\Sigma}}{2} \int_{-L/2}^{L/2} (\nabla h_k)^2 dx \tag{4.5}$$

as the energy cost of Gaussian fluctuations of the step edge about its mean position. As introduced before, $\Omega = a_{\perp} a_{\parallel}$ is the area of a surface element, with a_{\perp} and a_{\parallel} being the

lattice spacings perpendicular and parallel to the step edge respectively. Time dependent fluctuations of the steps is described using a coupled set of Langevin equations.

$$\frac{\partial h_k(x,t)}{\partial t} = \frac{\Gamma_h}{k_B T} \left\{ \frac{1}{2} J_{k-1,k}(x,t) + J_{k,k}(x,t) + \frac{1}{2} J_{k+1,k}(x,t) \right\} + \eta_k(x,t) . \tag{4.6}$$

 $J_{k,k}$ describes the healing of the step fluctuation due to mass transport along a step, while $J_{k-1,k}$ and $J_{k+1,k}$ describe the healing of such fluctuations due to mass transport between step k and steps k-1 and k+1 respectively. The healing of fluctuations is driven by differences in the step chemical potential, and the rate of that healing is controlled by the rate at which mass may be transferred in order to heal unfavorable chemical potential differences. The rate

$$\Gamma_h = \frac{a_\perp}{\tau_h} \tag{4.7}$$

where τ_h is the time between detachment events, depends on the energy barriers which exist at the step edges. This will be discussed further in the context of specific types of mass transport.

Considering first healing due to mass transport along a step edge, the integral $J_{k,k}$ is given by

$$J_{k,k}(x,t) = \int_0^{L/2} P_0(l) \{ \mu_k(x+l,t) - 2\mu_k(x,t) + \mu_k(x-l,t) \} dl$$
 (4.8)

where the chemical potential difference between sites separated by distance l is contained in the curly brackets, and the "mobility" is described by $P_0(l)$. This mobility is the probability that an atom is exchanged between two sites separated by distance l along x-axis and located on the same step edge. The form of $P_0(l)$ depends on the mass transport mechanism as it is elucidate later in this section. As in Chapter 3, one can do the

analysis to a large degree without knowing the explicit form for this quantity. The integral describing the way in which fluctuations heal due to mass transport between steps is very similar to Equation (4.8)

$$J_{k\pm l,k}(x,t) = \int_0^{L/2} P_1(l) \{ \mu_{k\pm l}(x+l,t) - 2\mu_k(x,t) + \mu_{k\pm l}(x-l,t) \} dl$$
 (4.9)

 $P_1(l)$ is the probability that an atom is exchanged between two sites separated by distance l along x-axis but located on the adjacent step edges. The probability functions are even and normalized,

$$2\int_0^{L/2} (P_0(l) + P_1(l)) = 1$$
 (4.10)

Step perturbations or fluctuations are randomly generated by the noise term $\eta_k(x,t)$ and then healed by the processes described in the integrals $J_{k,k}$ and $J_{k\pm 1,k}$. The noise must be constructed so that the time independent equilibrium properties of the steps are reproduced. Since it is assumed that there are no interactions between steps, the equilibrium correlations of the step train are simply those of non-interacting steps.

A Fourier transform

$$h_k(x,t) = \sum_q h_{kq}(t)e^{iqx}$$
 (4.11)

and similarly for $\eta_k(x,t)$ with $q=2\pi n/L$, $n=\pm 1,\pm 2,...\pm L/a_{\parallel}$ in Equation (4.6) yields the N-dimensional set of linear first-order differential equations,

$$\frac{\partial \vec{h}_q(t)}{\partial t} = -\widetilde{M}(q)\vec{h}_q(t) + \vec{\eta}_q(t) \tag{4.12}$$

with \widetilde{M} given by,

$$\widetilde{M}(q) = \begin{pmatrix} g_0(q) & -\frac{1}{2}g_1(q) & 0 & \cdots & -\frac{1}{2}g_1(q) \\ -\frac{1}{2}g_1(q) & g_0(q) & -\frac{1}{2}g_1(q) & \cdots & 0 \\ \vdots & \ddots & \ddots & \vdots \\ 0 & \cdots & -\frac{1}{2}g_1(q) & g_0(q) & -\frac{1}{2}g_1(q) \\ -\frac{1}{2}g_1(q) & \cdots & 0 & -\frac{1}{2}g_1(q) & g_0(q) \end{pmatrix}$$
(4.13)

where

$$g_{0}(q) = \frac{\widetilde{s} q^{2} a_{\perp}}{\tau_{h}} \{1 - 2 \int_{0}^{L/2} P_{0}(l) \cos q l \, dl \}$$

$$g_{1}(q) = \frac{2\widetilde{s} q^{2} a_{\perp}}{\tau_{h}} \int_{0}^{L/2} P_{1}(l) \cos q l \, dl$$
(4.14)

with the reduced stiffness $\tilde{s} = \tilde{\Sigma}\Omega/k_BT$ having units of length.

In order to decouple the system of equations (4.12), one needs to diagonalize the matrix \widetilde{M} . Since this matrix is circulant, it is also diagonalized by a Fourier transform [46]

$$\vec{v}_q(t) = \widetilde{U}^+ \vec{h}_q(t) \text{ with } U_{km} = \frac{1}{\sqrt{N}} e^{i(k-1)p}$$
 (4.15)

where $p = 2\pi m/N$, m = 0.1, 2, ..., N-1. When this is completed one arrives at a set of decoupled linear Langevin equations,

$$\frac{\partial v_{pq}(t)}{\partial t} = -\frac{v_{pq}(t)}{\tau_{pq}} + \eta_{pq}(t) \tag{4.16}$$

where each mode (p,q) has a relaxation time τ_{pq} given by,

$$\tau_{pq}^{-1} = g_0(q) - g_1(q)\cos p \tag{4.17}$$

and is associated with the noise $\eta_{pq}(t)$. The statistics of the noise is unaltered and therefore one can keep the same symbol $\vec{\eta}$. In the absence of noise, equation (4.16)

describes the relaxation of a periodic mode (e.g. sinusoidal with wavenumber q along the steps and p perpendicular to the steps) with relaxation time τ_{pq} . This mode relaxes as,

$$v_{pq}(t) = v_{pq}(0)e^{-t/\tau_{pq}},$$
 (4.18)

where $v_{pq}(0)$ is the initial (small) amplitude of the mode.

In the presence of Gaussian white noise

$$<\eta_{p_1q_1}(t_1)\eta_{p_2q_2}^{\bullet}(t_2)>=f(p_1,p_2,q_1,q_2)\delta_{p_1,p_2}\delta_{q_1,q_2}\delta(t_1-t_2)$$
 (4.19)

the correlation function becomes (see Equation (B.18))

$$C_k(x,t) = \frac{\Omega}{NL\widetilde{s}} \sum_{q} \frac{\cos qx \, e^{-R \cdot (q)t}}{q^2} \sum_{p} \cos pk \, e^{g_1(q)t\cos p} \tag{4.20}$$

where $p = 2\pi n / N$, m = 0,1,2,...,N-1, and $q = 2\pi n / L$, $n = \pm 1,\pm 2,...,\pm L / a_{\parallel}$.

The next Section 4.3 presents an analysis of Equation (4.20) in a variety of solvable limits. This section is used in Section 4.4 which discusses physical cases, but may be skipped by those uninterested in the detailed analysis.

4.3 Analysis of Various Time Regimes

Taking the continuum limit of the p sum gives (p376-9.6.19 of [34]),

$$C_{k}(x,t) = \frac{2\Omega}{L\tilde{s}} \sum_{q>0} \frac{\cos qx \, e^{-g_{0}(q)t}}{q^{2}} I_{k}(g_{1}(q)t), \qquad (4.21)$$

where $I_k(z)$ is the modified Bessel function of order k and argument z. To make the analysis in this section simpler, summation over positive q only will be considered.

At t = 0, Equation (4.21) reduces (because $I_{k\neq 0}(0) = 0$ and $I_0(0) = 1$, p375-9.6.7 of [34]) to (p39-1.443(3) of [47])

$$C_0(x,t) = \frac{L\Omega}{2\tilde{s}} \left(\frac{1}{6} - \frac{x}{L} + \left(\frac{x}{L} \right)^2 \right), \tag{4.22}$$

which is the equilibrium correlation function along a step, while the equilibrium correlations between steps are zero ($C_{k\neq 0}(x,0)=0$). At x=0, Equation (4.22) reduces to the squared equilibrium width $\frac{L\Omega}{12\tilde{s}}$ of the step edge. The equilibrium correlations between steps $C_{k\neq 0}(x,0)$ are zero due to the fact that there are no direct energy terms between steps in this model. Nevertheless, as demonstrated below, there are strong time dependent correlations $C_{k\neq 0}(x,t>0)$ between steps when there is correlated mass transport across the terraces (e.g. terrace diffusion). These correlations are absent in the case of attachment-detachment and step-edge diffusion. The analysis of the correlations between different steps thus provides a method to distinguish between attachment-detachment and terrace diffusion, which have very similar trends in the correlation function on the same step.

Due to the difference between the equilibrium behavior of the correlation functions between the same and different steps, these two cases differently will be treated differently. For correlations between different steps $C_{k\neq 0}(x,t)$ is used. It increases from zero at short time. For the step self-correlation, G(x,t) is used. It also increases from zero at the short time, rather then $C_0(x,t)$ that starts at its equilibrium value. This way is

more convenient for analyzing log-log plots to test the power law behaviors so typical of step dynamics.

To proceed to an analytic analysis of the time dependence of $C_{k\neq 0}(x,t)$ and G(x,t), one needs more detailed expressions for $g_0(q)$ and $g_1(q)$. It will shown later in this section that the important asymptotic behaviors of these functions can be expressed in relatively simple forms. There are two cases, one for terrace diffusion (case A) and the other applies to attachment-detachment, step edge diffusion or terrace diffusion with an infinite Schwoebel barrier (case B).

CASE A (terrace diffusion)

$$g_0(q) \approx A_1 |q|^{r_1} + B|q|^{\beta}, \ g_1(q) \approx A_1 |q|^{r_1} \text{ for } |q| < q_0$$

$$g_0(q) \approx A_2 |q|^{r_2}, \ g_1(q) = 0 \text{ for } |q| > q_0.$$
(4.23)

For $|q| < q_0$, $B|q|^{\beta} << A_1|q|^{\gamma_1}$ is always satisfied and term $B|q|^{\beta}$ will be neglected in the following calculation except in expression $g_0(q) - g_1(q)$.

CASE B (attachment-detachment, step-edge diffusion, terrace diffusion with an infinite Schwoebel barrier)

$$g_0(q) \approx A_1 |q|^{r_1}, \ g_1(q) = 0 \text{ for } |q| < q_0$$

 $g_0(q) \approx A_2 |q|^{r_2}, \ g_1(q) = 0 \text{ for } |q| > q_0.$ (4.24)

The details of the system of interest (terrace width, energies, diffusion constants, etc.) are primarily contained in the prefactors $A_{1,2}$, the crossover wavenumber q_0 and lower limit

of $q = 2\pi/L$. The exponents $\gamma_{1,2}$ take on quite universal values depending of the mass transport mechanism. Nevertheless, a complete asymptotic analysis will now be done without knowing these details, and then those results will be used in the next section. In the next section these asymptotic results will also be compared with direct numerical evaluations of Equation (4.20) for physically interesting cases.

There are three important asymptotic time regimes in the step dynamics:

- (i) Early times $t \rightarrow 0$
- (ii) Intermediate times $0 << t << t_{sat}$
- (iii) Very long times $t \gg t_{sat}$

Here, the saturation time,

$$t_{sat} = (L/2\pi)^{\gamma_1}/A_1 \tag{4.25}$$

is the decay time of slowest mode in the system. The asymptotic forms for $C_{k\neq 0}(x,t)$ and G(x,t) in these three regimes will be presented, though frequently (ii) is the most experimentally accessible one.

Correlations between different steps - $C_{k\neq 0}(x,t)$ (only case A)

Starting from zero at t=0, the correlation between steps $C_{k\neq 0}(x,t)$ grows due to correlated mass transport between steps. Neither step-edge diffusion, attachment-detachment nor terrace diffusion with an infinite Schwoebel barrier (case B) produce this correlation, so $C_{k\neq 0}(x,t)=0$ in these cases. Considering case A (4.23), the sum (4.21)

ceases to contribute for $q>q_0$, due to the fact that the Bessel function $I_{k\neq 0}(0)=0$. One then has (combining (4.21) and (4.23))

$$C_{k\neq 0}(x,t) = \frac{2\Omega}{L\widetilde{s}} \sum_{q < q_0} \frac{\cos qx \, e^{-A_1 q^{\gamma_1} t}}{q^2} I_k(A_1 q^{\gamma_1} t). \tag{4.26}$$

(i) Short times $t \rightarrow 0$

At short times, one expands Bessel function for small argument (p375-9.6.7 of [34]),

$$I_k(z) = (\frac{z}{2})^k \frac{1}{k!}, \ z \to 0$$
 (4.27)

and sets the exponential to one, which yields,

$$C_{k \neq 0}(x, t) = \frac{2\Omega}{L\widetilde{s}} \sum_{q \leq q_0} \frac{\cos qx}{q^2} \frac{(A_1 q^{\gamma_1} t)^k}{2^k k!}.$$
 (4.28)

This is valid provided $t \ll 1/(A_1 q_0^{\gamma_1})$. Turning the sum into an integral and evaluating shows that at small x, one has,

$$C_{k\neq 0}(x,t) = \frac{\Omega}{\widetilde{s}\,\pi} \frac{q_0^{k\gamma_1-1}}{k!(k\gamma_1-1)} (\frac{A_1 t}{2})^k \,, \quad q_0 x \to 0 \,. \tag{4.29}$$

(ii) Intermediate times $0 << t << t_{sat}$

In this regime, the sum (4.21) is dominated by small q, so one can take the upper limit to ∞ . However all values of q contribute, so one can take the continuum limit, and rewriting in terms of more convenient variables one then finds,

$$C_{k\neq 0}(x,t) = \frac{\Omega}{\pi \widehat{s}} \frac{(A_1 t)^{1/\gamma_1}}{\gamma_1} \int_0^\infty \frac{e^{-y} \cos(x(\frac{y}{A_1 t})^{1/\gamma_1}) I_k(y)}{y^{1+1/\gamma_1}} dy.$$
 (4.30)

For small x, the cosine tends to unity, and the integral may be written in terms of Gamma functions (p486-11.4.13 of [34]),

$$C_{k\neq 0}(x,t) = \frac{\Omega}{\widetilde{s} \, \pi^{3/2}} \frac{2^{1/\gamma_1} \Gamma(k-\frac{1}{\gamma_1}) \Gamma(\frac{1}{2}+\frac{1}{\gamma_1})}{\gamma_1 \Gamma(k+\frac{1}{\gamma_1}+1)} (A_1 t)^{1/\gamma_1}, \ x \to 0.$$
 (4.31)

(iii) Long time limit $t >> t_{sat}$

One may then use the large argument expansion for the Bessel function (p377-9.7.1 of [34])

$$I_k(z) \approx \frac{e^z}{(2\pi z)^{1/2}}$$
 (4.32)

Now, small correction $B|q|^{\beta}$ is the only term that survives in (4.21). The first term in the sum is dominant, thus for small x

$$C_k(x,t) \approx \frac{2\Omega}{L\widetilde{s}} \left(\frac{L}{2\pi}\right)^{2+\gamma_1/2} \frac{e^{-B(\frac{2\pi}{L})^{\beta_t}}}{(2\pi A_t t)^{1/2}}, \quad \frac{x}{L} \to 0$$
 (4.33)

A surprising feature of this expression is that it is independent of k indicating that asymptotically all of the steps are correlated in the same way. Besides, it is also valid for k = 0, i.e. both correlations on the same and different steps behave in the same manner.

Correlations on the same step - G(x,t) (Both cases A and B)

One considers (combining (4.3) and (4.21)),

$$G(x,t) = \frac{2\Omega}{L\widetilde{s}} \sum_{q} \frac{1 - \cos qx \, e^{-g_0(q)t} I_0(g_1(q)t)}{q^2}. \tag{4.34}$$

First, this equation for small x (when cosine tends to unity) is analyzed for three time regimes.

(i) Short times $t \rightarrow 0$

At short times, using $I_0(0) = 1$, $g_0(q) = A_1 q^{\gamma_1}$ for $q < q_0$, $g_0(q) = A_2 q^{\gamma_2}$ for $q > q_0$, and expanding the exponential in (4.34) to the second order, one finds

$$G(x \to 0, t) = \frac{\Omega}{\pi \tilde{s}} \left(\frac{A_1 q_0^{\gamma_1 - 1}}{\gamma_1 - 1} + A_2 \frac{(2\pi / a_{\parallel})^{\gamma_2 - 1} - q_0^{\gamma_2 - 1}}{\gamma_2 - 1} \right) t \tag{4.35}$$

for both the case A and the case B.

(ii) Intermediate times $0 \ll t \ll t_{sat}$

This regime actually breaks up into two regimes. The first $0 << t << t_x$ is dominated by the modes in the regime $q >> q_0$, while the second $t_x << t << \tau_s$ is dominated by modes in the regime $q << q_0$. These regimes are quite distinct due to the fact that τ_{pq} only appears in the exponential. It is then quite a good approximation to treat the first early time regime using $A_1q^{r_1}$. One can do an analysis similar to that leading to Equation (4.30) to find,

$$G(x \to 0, t) = \frac{\Omega}{\widetilde{s} \pi} \Gamma(1 - \frac{1}{\gamma_2}) (A_2 t)^{\frac{1}{\gamma_2}}, \quad t << t_{\tau}$$
 (4.36)

for both cases A and B, and

$$G(x \to 0, t) = C \frac{\Omega}{\widetilde{s} \pi} \Gamma(1 - \frac{1}{\gamma_1}) (A_1 t)^{\frac{1}{\gamma_1}}, \quad t >> t_x,$$
 (4.37)

where $C = (2^{1/\gamma_1} \dot{\gamma}_1 \Gamma(1/2 + 1/\gamma_1)) / (\sqrt{\pi} \Gamma(1/\gamma_1))$ (integration by parts using p486-11.4.13 of [34]) for the case A, and C=1 (p333-3.434(1) of [47]) for the case B. The crossover

time t_x is found by equating (4.36) to (4.37), and solving for the time. In the physical cases, there may be several different crossovers in this intermediate time regime, but the same general principles can be applied. Naturally this complexity makes experimental data difficult to analyze in general.

(iii) Long times $t > t_{sat}$

 $C_0(x \to 0, t)$ for long times is first found. In case A, it is given by Equation (4.33). In case B, the argument of the Bessel function in (4.21) is zero. One then has $I_0(0) = 1$ and since first term in the sum is dominant,

$$C_0(x \to 0, t) \approx \frac{2\Omega}{L\tilde{s}} (\frac{L}{2\pi})^2 e^{-t/t_{\text{tar}}},$$
 (4.38)

whose time scale is set by the slowest mode in the system, t_{sat} . Then, using Equation (4.3),

$$G(x \to 0, t) \approx \frac{L\Omega}{12\tilde{s}} - C_0(x \to 0, t). \tag{4.39}$$

For larger x, one finds combining (4.3) and (4.22)

$$G(x \neq 0, t) = \frac{\Omega x}{2\widetilde{s}} (1 - \frac{x}{L})$$
 (4.40)

for short times. On the other hand, one finds $G(x \neq 0, t) = G(0, t)$ for longer times. Therefore, $G(x \neq 0, t)$ is initially constant in time until the correlation length along the step increases approximately to value x. If Aq^{r} is the dominant regime, one finds that Equation (4.40) is valid for $t << x^{r}/A$. This time depends on the kind of dynamics through γ and A and defines the propagation speed of the nonlinear fluctuation. As

expected, initial fluctuation (4.40) depends on x and \tilde{s} , but not on the kind of dynamics i.e. γ and A.

4.4. Terrace Diffusion

Assumptions of the terrace diffusion model are explained in Section 3.4. Since atoms diffuse on the terrace, $P_0(l)$ and $P_1(l)$ are the probabilities for random walk on the surface between two fluctuating semi-sticking walls. The calculation of these probabilities for straight step edges is done in Appendix C,

$$P_{0}(l) = p_{U}P(\alpha_{U}, \alpha_{L}, d, d - a_{\perp}, l) + p_{L}P(\alpha_{L}, \alpha_{U}, d, d - a_{\perp}, l)$$
(4.41)

and

$$P_{1}(l) = p_{U}P(\alpha_{L}, \alpha_{U}, d, a_{\perp}, l) + p_{L}P(\alpha_{U}, \alpha_{L}, d, a_{\perp}, l)$$

$$(4.42)$$

where

$$P(\alpha_1, \alpha_2, d, b, l) = \frac{1}{2\pi} \int_{-\infty}^{\infty} dk \frac{\alpha_1(k \cosh kb + \alpha_2 \sinh kb)}{(k^2 + \alpha_U \alpha_L) \sinh kd + k(\alpha_U + \alpha_L) \cosh kd} \cos kl . \tag{4.43}$$

These results for two straight edges can be used as the diffusion kernels mediating the dynamics of the fluctuations provided the fluctuations are relatively weak (the small slope limit). The integrals (4.14) may be evaluated to find

$$g_0(q) = \frac{\widetilde{s}a_{\perp}}{\tau_h} q^2 \{1 - p_U g(\alpha_U, \alpha_L, d, d - a_{\perp}, q) - p_L g(\alpha_L, \alpha_U, d, d - a_{\perp}, q)\}$$
(4.44)

$$g_{1}(q) = \frac{\widetilde{s} a_{\perp}}{\tau_{h}} q^{2} \{ p_{L} g(\alpha_{U}, \alpha_{L}, d, a_{\perp}, q) + p_{U} g(\alpha_{L}, \alpha_{U}, d, a_{\perp}, q) \}$$
(4.45)

where

$$g(\alpha_1, \alpha_2, d, b, q) = \frac{\alpha_1(q \cosh qb + \alpha_2 \sinh qb)}{(q^2 + \alpha_{l'}\alpha_{l}) \sinh qd + q(\alpha_{l'} + \alpha_{l}) \cosh qd}.$$
 (4.46)

Here, the characteristic time is related to step edge energies by

$$\tau_h^{-1} = \tau_{TD}^{-1} \left\{ e^{-E_L/k_B T} + e^{-E_C/k_B T} \right\},\tag{4.47}$$

where $\tau_{TD}^{-1} = v \exp(-E_{TD}/k_BT)$ and v is a characteristic phonon frequency. On Figure 4.2, the spectrum of inverse relaxation times is plotted using Equations (4.44) and (4.45) different cases: $\alpha_L = \alpha_U = 10^3 / a_1$ (perfect sticking), (4.17)four in $\alpha_L = \alpha_U = 10^{-2} / a_\perp$ (weak sticking), $\alpha_L = 10^3 / a_\perp$, $\alpha_U = 10^{-3} / a_\perp$ (finite Schwoebel barrier $E_L \ll E_U$), and $\alpha_L = 10^3 / a_\perp$, $\alpha_U = 0$ (infinite Schwoebel barrier $E_U \to \infty$). Note on the Figure 4.2 that, except in the infinite Schwoebel barrier case when there in no atom exchange between the steps, the spectrum of relaxation times is spreaded for small values of q. This means that there is a mutual step-step correlation of the large wave length fluctuations. On the other hand, the spectrum shrinks to one value for larger values of q, since there is much less mutual step-step correlation of small wave length fluctuations. As it will be derived later, for large q, $\tau_{pq}^{-1} \propto q^3$ for perfect sticking, finite and infinite Schwoebel barrier case , while $au_{pq}^{-1} \propto q^2$ for weak sticking case. For small q, spectrum au_{pq}^{-1} spreads between q^2 and q^4 for finite Schwoebel barrier, perfect and weak sticking case, while $\tau_{pq}^{-1} \propto q^4$ for infinite Schoebel barrier case. Using this spectrum from Figure 4.2 and doing numerical summations over q and p, G(x,t) and $C_k(0,t)$, defined by Equations (4.3) and (4.20), are plotted on Figures 4.3 and 4.4. G(x,t) are plotted for all four different cases of sticking coefficient, defined above for Figure 4.2. Each case has different scaling and is shown for a couple of values of x (for $x \neq 0$ time independent regime (4.40) holds). $C_{t}(0,t)$ is plotted just for perfect sticking case for a couple of nonzero values of k. The other cases of non-zero sticking coefficients are not plotted

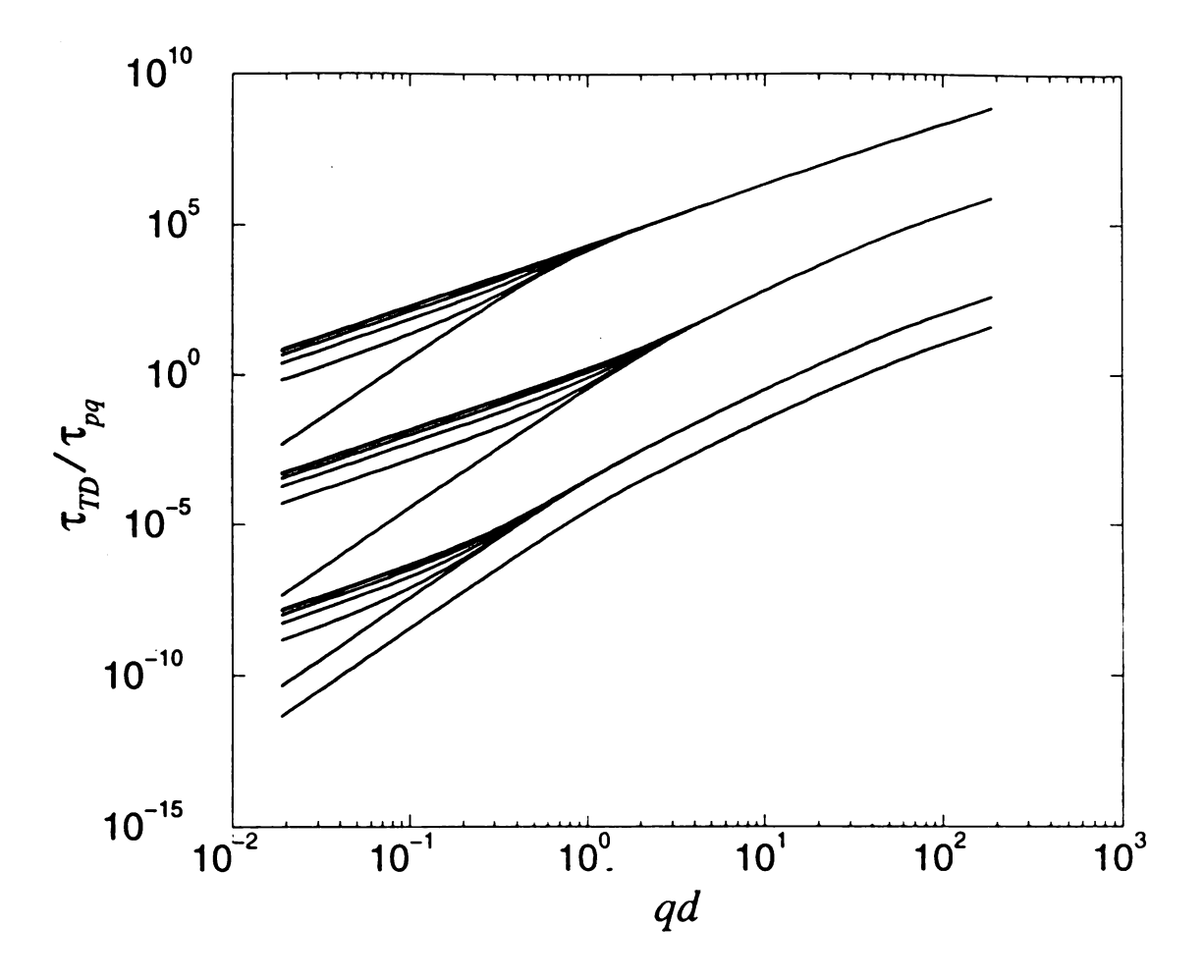


Figure 4.2 Four spectrums of inverse relaxation times in the terrace diffusion case for the surface with N=10 steps (there are only up to 6 visible lines in each spectrum since four pairs overlap); $d=30a_{\perp}$, $L=10^4 a_{\parallel}$. Different ratios $\tilde{s}a_{\perp}/a_{\parallel}^2$ for each spectrum are used to avoid overlapping. They are plotted for the following sticking coefficients (from the top): $\alpha_L = \alpha_U = 10^{-2}/a_{\perp}$, $\tilde{s}a_{\perp}/a_{\parallel}^2 = 10^9$, $\alpha_L = \alpha_U = 10^3/a_{\perp}$, $\tilde{s}a_{\perp}/a_{\parallel}^2 = 10^4$, $\alpha_L^l = 10^3/a_{\perp}$, $\alpha_U^l = 10^{-3}/a_{\perp}$,

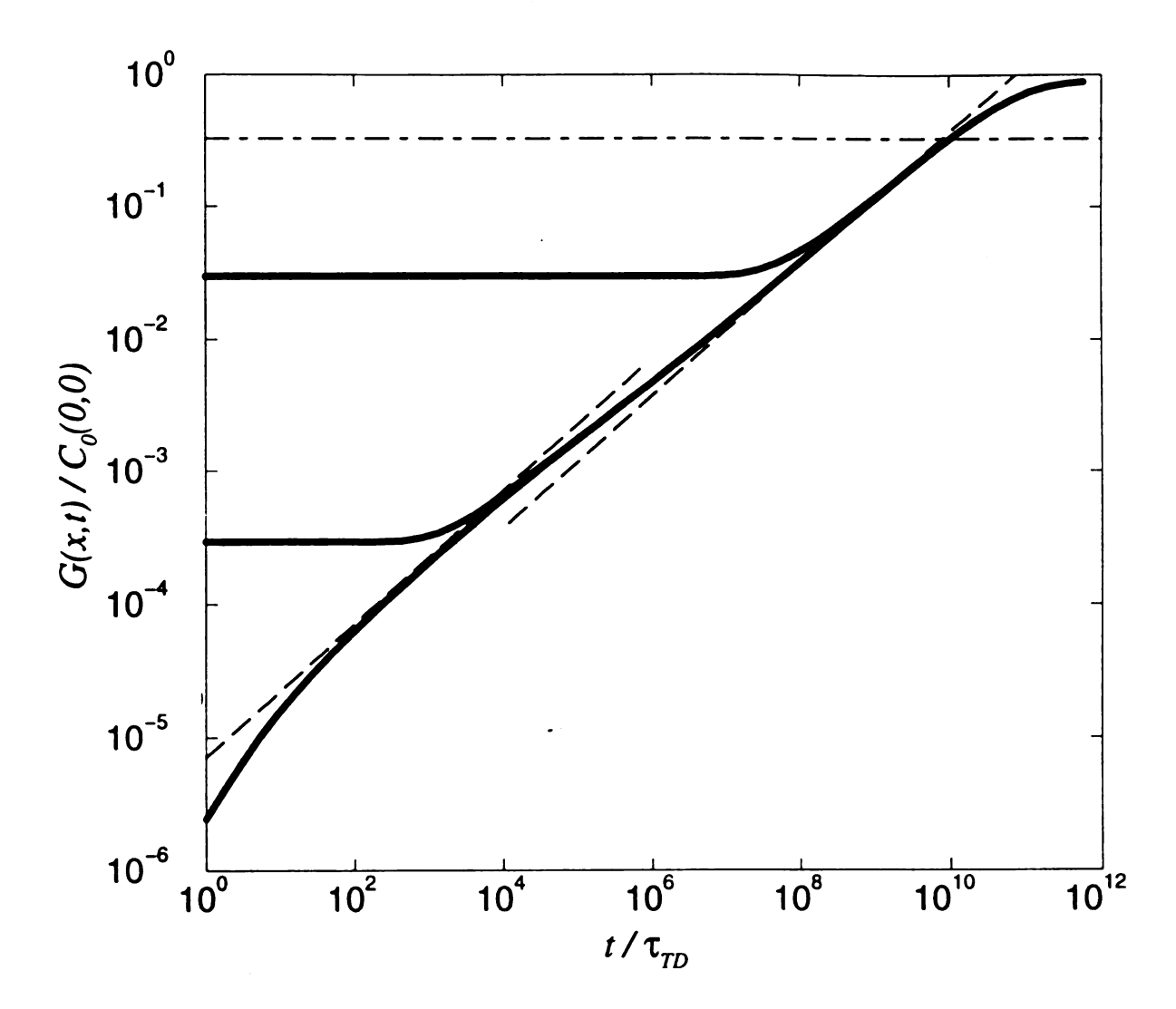


Figure 4.3(a) The autocorrelation function in the terrace diffusion limit. N=10, $L=10^5 a_{\parallel}$, $d=100 a_{\perp}$ and $k_B T/\widetilde{\Sigma}=1$. Solid lines are Equation (4.3) plotted doing numerical summation (4.20) using (4.44)-(4.47), dashed lines are equations listed in Table 4.1 and horizontal dashed-dotted line is d^2 , all divided by $C_0(0,0)$, for the sticking coefficients $\alpha_L=\alpha_U=10^{-2}/a_{\perp}$ (case T3), x=0, x=5, x=500 from the bottom.

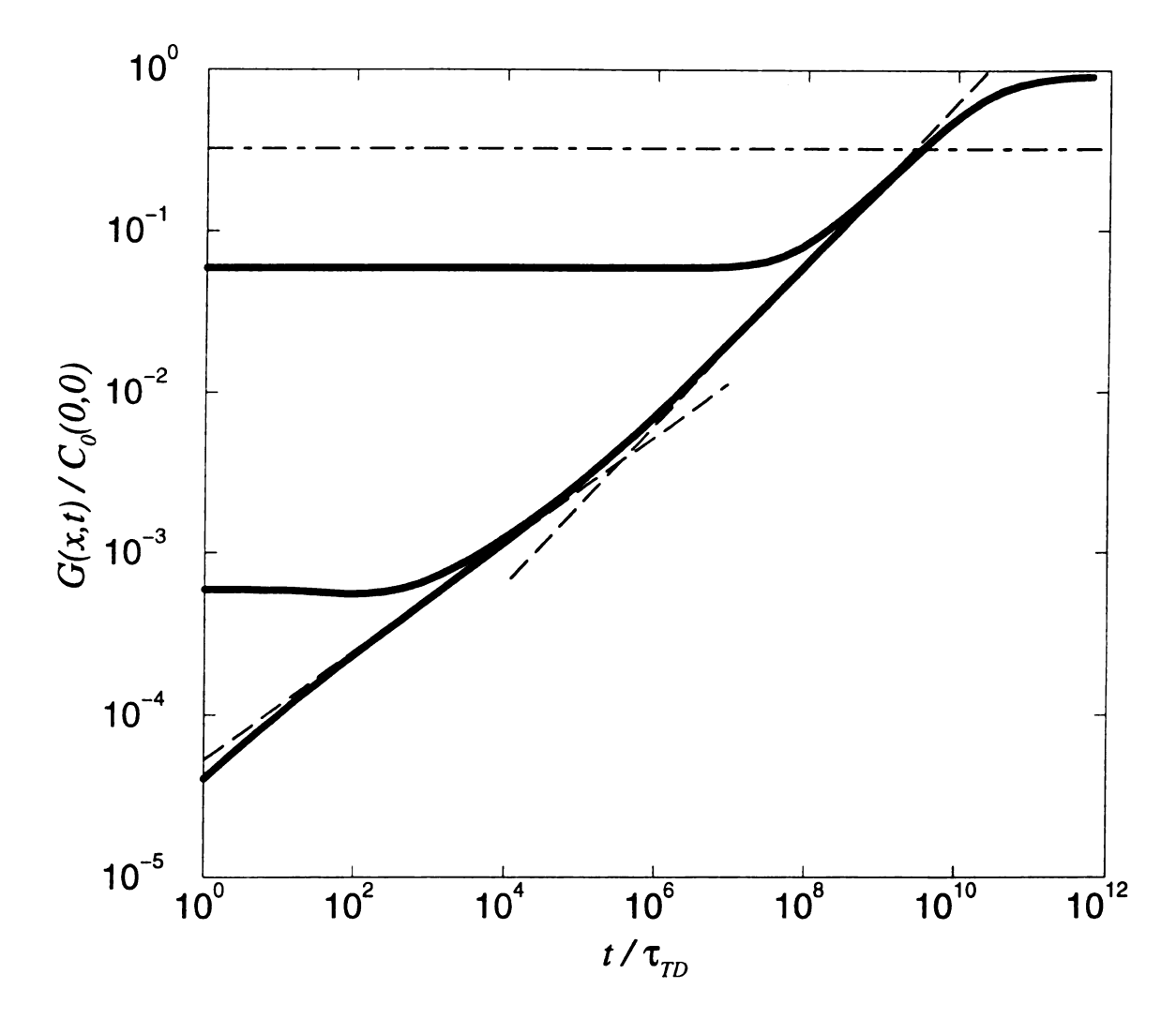


Figure 4.3(b) The autocorrelation function in the terrace diffusion limit. N=10, $L=10^5 a_{\parallel}$, $d=100 a_{\perp}$ and $k_B T/\widetilde{\Sigma}=1$. Solid lines are Equation (4.3) plotted doing numerical summation (4.20) using (4.44)-(4.47), dashed lines are equations listed in Table 4.1 and horizontal dashed-dotted line is d^2 , all divided by $C_0(0,0)$, for the sticking coefficients $\alpha_L=\alpha_U=10^3/a_{\perp}$ (case T3), x=0, x=10, x=1000 from the bottom.

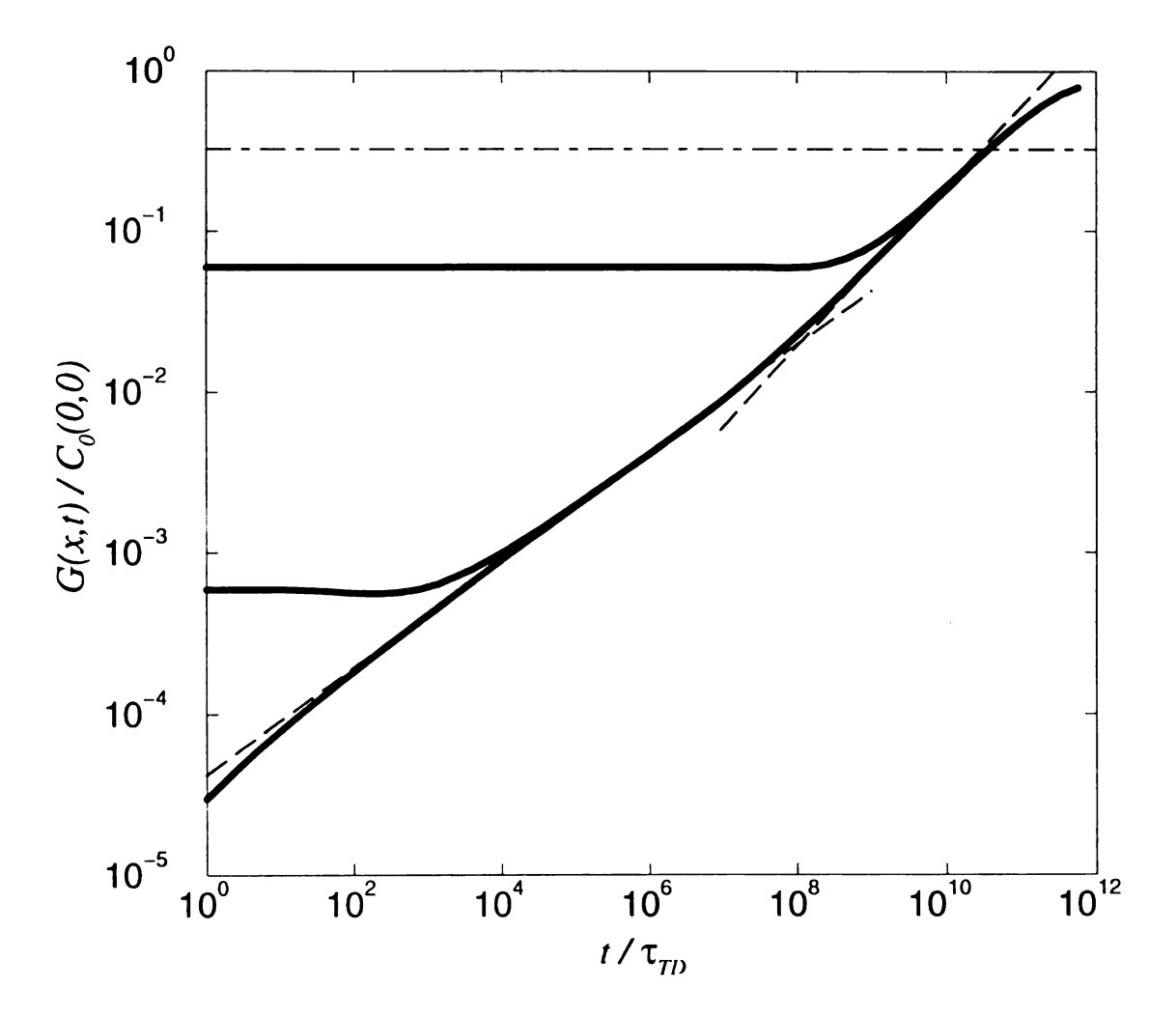


Figure 4.3(c) The autocorrelation function in the terrace diffusion limit. N=10, $L=10^5 a_{\parallel}$, $d=100a_{\perp}$ and $k_BT/\widetilde{\Sigma}=1$. Solid lines are Equation (4.3) plotted doing numerical summation (4.20) using (4.44)-(4.47), dashed lines are equations listed in Table 4.1 and horizontal dashed-dotted line is d^2 , all divided by $C_0(0,0)$, for the sticking coefficients $\alpha_L=10^3/a_{\perp}$, $\alpha_{t'}=10^{-3}/a_{\perp}$ (case T3), x=0, x=10, x=1000 from the bottom.

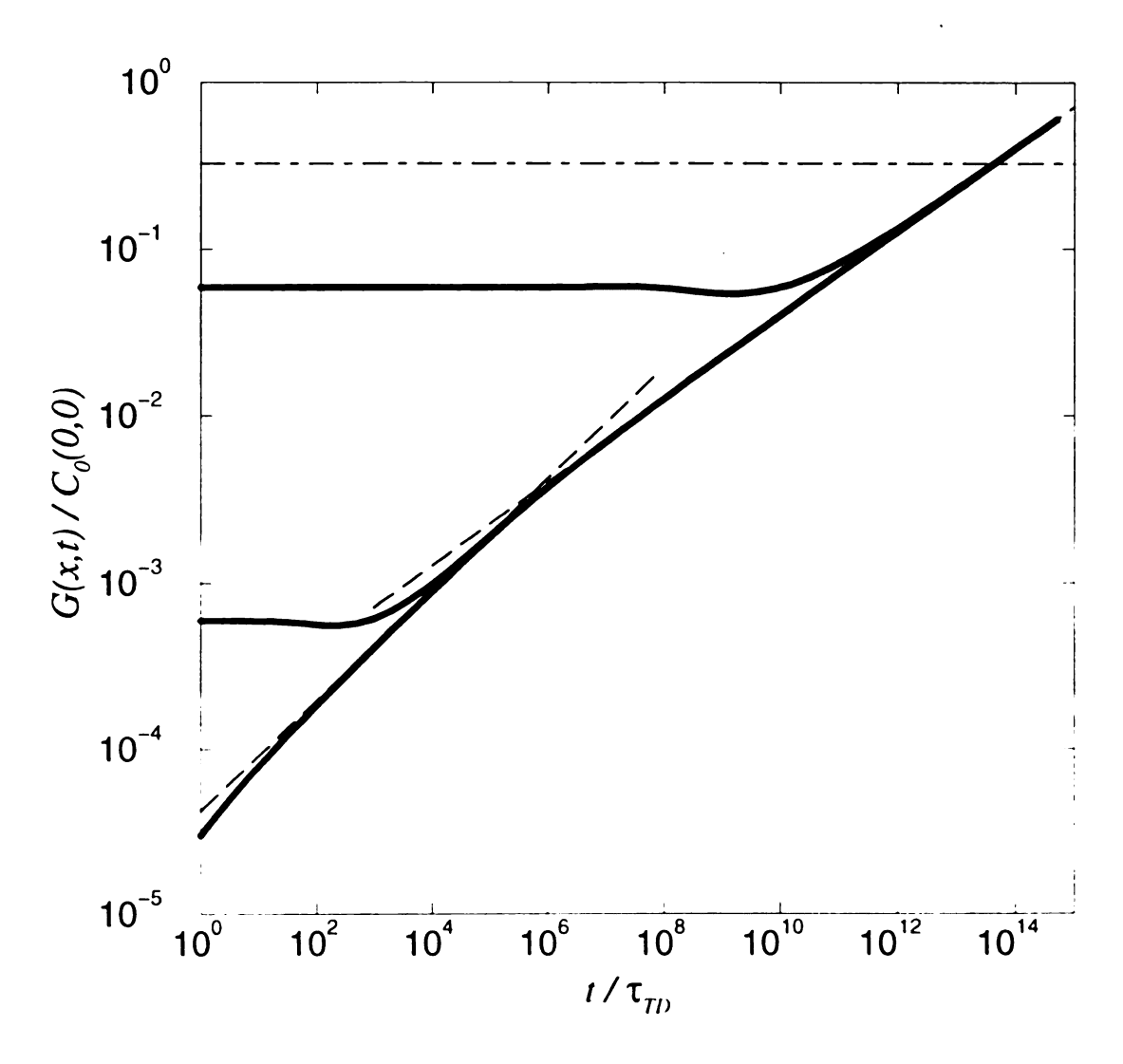


Figure 4.3(d) The autocorrelation function in the terrace diffusion limit. N = 10, $L = 10^5 a_{\parallel}$, $d = 100 a_{\perp}$ and $k_B T \cdot \tilde{\Sigma} = 1$. Solid lines are Equation (4.3) plotted doing numerical summation (4.20) using (4.44)-(4.47), dashed lines are equations listed in Table 4.1 and horizontal dashed-dotted line is d^2 , all divided by $C_0(0,0)$, for the sticking coefficients $\alpha_L = 10^3 / a_{\perp}$, $\alpha_U = 0$ (case T2), x = 0, x = 10, x = 1000 from the bottom.

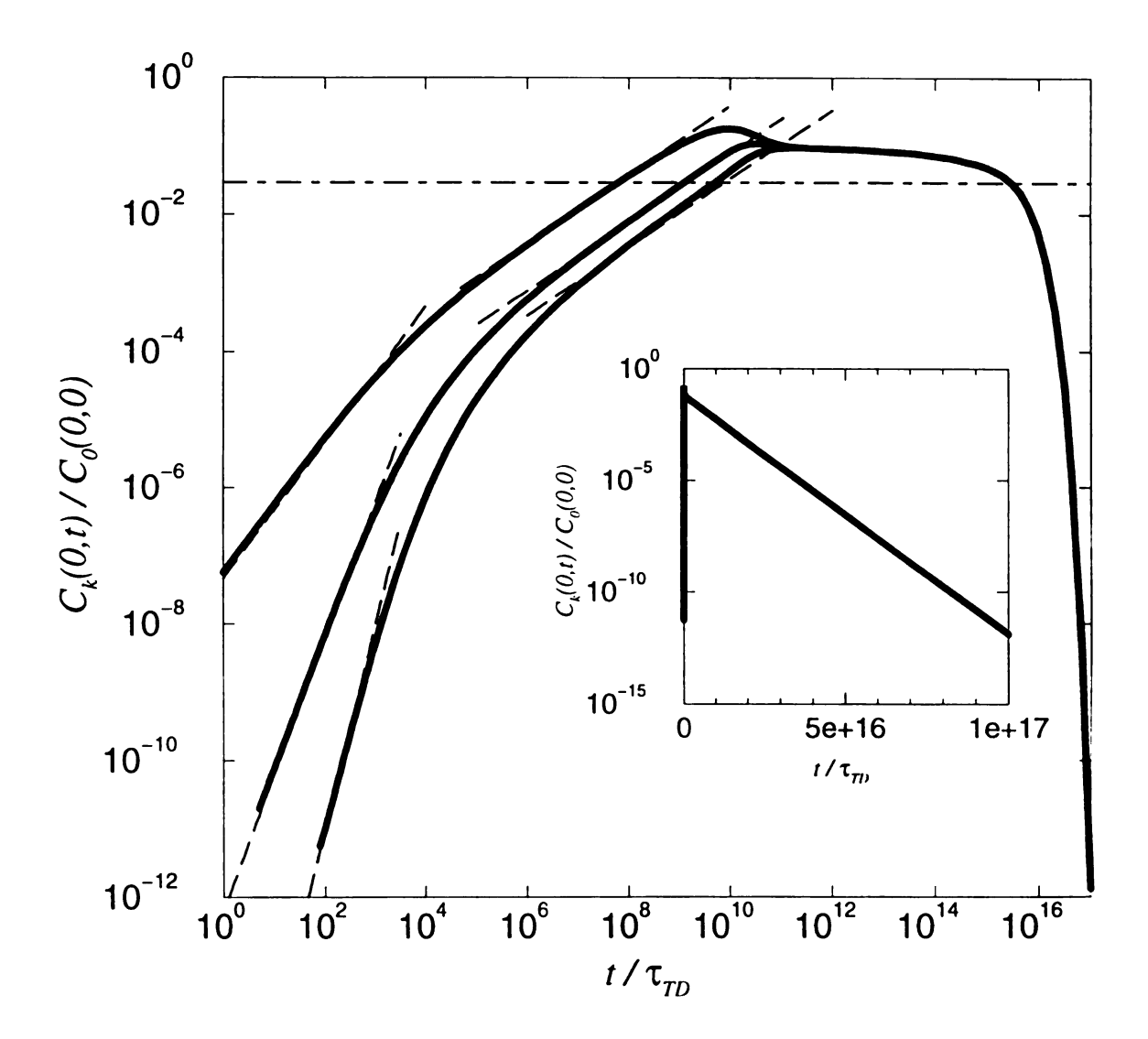


Figure 4.4 The step-step correlation function in the terrace diffusion T3 limit. N=10, $L=10^5 a$, $d=30a_{\perp}$, $k_BT/\widetilde{\Sigma}=1$ and $\alpha_L=\alpha_U=10^3/a_{\perp}$. Solid lines are plotted doing numerical summation (4.20) using (4.44)-(4.47), dashed lines are equations listed in Table 4.2 and horizontal dashed-dotted line is d^2 , all divided by $C_0(0,0)$, for k=1,2,3 (from the top). Inner graph is linear-log plot that shows exponential time dependence at large times.

since they show the same scaling. These numerical results are then compared to approximate analytical forms plotted as dashed lines on Figures 4.3 and 4.4. Those analytical forms, listed in Tables 4.1 and 4.2, are obtained substituting expressions for relaxation times derived below, to Equations (4.36), (4.37), (4.29) and (4.31). d^2 as an horizontal dashed-dotted line is also plotted to show when step fluctuation width exceeds the distance between the steps. Since this model does not include the direct step-step interaction, it fails above the d^2 line.

In the limit $q \ll 1/a_1$ expressions (4.44)-(4.46) reduce to,

$$g_0(q) = \frac{\widetilde{s} a_\perp^2}{\tau_{TD}} |q|^3 \frac{2\alpha_U \alpha_L \cosh qd + (\alpha_U + \alpha_L)q \sinh qd}{(q^2 + \alpha_U \alpha_L) \sinh qd + q(\alpha_U + \alpha_L) \cosh qd}$$
(4.48)

and

$$g_1(q) = \frac{\widetilde{s} a_{\perp}^2}{\tau_{TD}} |q|^3 \frac{2\alpha_U \alpha_L}{(q^2 + \alpha_U \alpha_L) \sinh qd + q(\alpha_U + \alpha_L) \cosh qd}. \tag{4.49}$$

These expressions then lead to the relaxation time of a mode of (p,q) according to $\tau_{pq}^{-1} = g_0(q) - g_1(q)\cos p$. Approximate expressions for this relaxation time have been found in [13] in a variety of limiting cases, though they implicitly assume "in phase motion". Khare and Einstein [17] consider only in phase and out of phase motion $(A_q \pm 2B_q = g_0(q) \pm g_1(q))$, while Ihle et al. [43] consider the full spectrum (all values of p). In Appendix D, an brief overview of those two models [17,43] is given. The following is the discussion of limiting cases in which the time dependent correlations may be explicitly evaluated.

T1 - Terrace diffusion $l(d \rightarrow \infty)$

The large d limit eliminates the flux from neighboring steps, so the steps act independently. This is essentially the isolated step case discussed in Chapter 3. In this limit, Equations (4.48) and (4.49) reduce to,

$$g_0(q) = \frac{\tilde{s}|q|^3 a_\perp^2}{\tau_{TD}} \left(\frac{\alpha_U}{\alpha_U + |q|} + \frac{\alpha_L}{\alpha_L + |q|} \right), \ g_1(q) = 0$$
 (4.50)

Since $g_1(q) = 0$, $\tau_{pq}^{-1} = g_0(q)$ and $C_{k\neq 0}(x,t) = 0$ (case B). From Equation (4.50) it is seen that even isolated steps have some of three possible regimes: when $|q| >> \alpha_{U,L}$ then $g_0(q) = \tilde{s} a_\perp^2 (\alpha_U + \alpha_L) q^2 / \tau_{TD}$; when $\alpha_U \ll |q| \ll \alpha_L$ (assuming $\alpha_U \ll \alpha_L$) then $g_{0}(q) = \widetilde{s} a_{\perp}^{2} |q|^{3} / \tau_{TD}$; and when $|q| << \alpha_{U,L}$ then $g_{0}(q) = 2\widetilde{s} a_{\perp}^{2} |q|^{3} / \tau_{TD}$. This leads to three different time regimes in the correlation function G(0,t) as summarized in Table 4.1. After the non-interacting diffuser regime $t \to 0$, there is an early time $0 << t << t_1^{T_1}$ (large q), in which short range processes must overcome the sticking coefficients to proceed. For this reason $\alpha_U + \alpha_L$ appears as a prefactor. This regime is not well defined if $\alpha_{UL} \to \infty$. In the regime $t_1^{T_1} << t << t_2^{T_1}$, one of the terraces (the upper one for the case $\alpha_{l'} \ll \alpha_L$) is not contributing since approach to the step edge from that terrace has such a small sticking coefficient. This regime is only well defined if the two sticking coefficients are very different (e.g. the large Schwoebel barrier case, when $\alpha_{\scriptscriptstyle U} << \alpha_{\scriptscriptstyle L}$). In the regime $t_2^{T_1} \ll t \ll t_{sat}^{T_1}$, both of the terraces are contributing equally and small sticking coefficients do not play a role. It is rather interesting that in this limit only τ_{TD} appears in the time dependent correlation function. This regime is not well defined if α_{U} or $\alpha_{L} \approx 0$. Finally at long enough time the relaxation is controlled by the slowest mode in the system.

Note that these forms apply, at sufficiently short times, even for quite closely spaced steps in a step train, as discussed below.

T2 - Terrace diffusion 2 (d finite, $\alpha_U = 0$ or $\alpha_U = 0$).

Setting $\alpha_U = 0$ or $\alpha_U = 0$ implies that no mass is transported from one step to either of its neighbors ("large barrier limit", e.g. the large Schwoebel barrier corresponds to $\alpha_U = 0$). At short time (large q dominant), the isolated terrace behavior occurs, especially for well separated steps. For small q, Equations (4.48) and (4.49) reduce to,

$$g_0(q) = \frac{\tilde{s} da_\perp^2}{\tau_{TD}} q^4, \ g_1(q) = 0$$
 (4.51)

thus, $C_{k\neq 0}(x,t)=0$ (case B). The q^4 dependence leads to the long times behavior like that of step-edge diffusion, as seen by comparing the correlation functions for this case with that of step edge diffusion (see Table 4.1). The results in Table 4.1 are found using Equations (4.37), (4.39) and (4.51).

T3 - Terrace diffusion 3 (d finite, $\alpha_{U,L} \neq 0$).

In this case the T1 (isolated step) processes occur at short times (large q dominant). For analysis of the long times behavior (small q dominant), it is useful to define the length

$$d_0 = \frac{\alpha_U + \alpha_L}{\alpha_U \alpha_I}. \tag{4.52}$$

If d_0 is finite ($d \to \infty$ leads to T2 limit), mass transport between steps is dominant. The approximate forms of Equations (4.48) and (4.49) for this case are,

$$g_0(q) = \frac{\tilde{s} a_\perp^2}{\tau_{TD}} \left(\frac{2}{d + d_0} q^2 + dq^4 \right), \quad g_1(q) = \frac{2\tilde{s} a_\perp^2}{\tau_{TD} (d + d_0)} q^2. \tag{4.53}$$

Due to the mass transport occurring between steps $g_1(q) \neq 0$, and this is the mathematical origin of a finite value of $C_{k\neq 0}(x,t)$. Results for this limit are summarized in Tables 4.1 and 4.2, where $q_0 \approx 2/d$ is used. (see Figure 4.2). This case is probably very important in many experiments and leads to a correlation between step fluctuations on neighboring steps which becomes the "signature" of the T3 process. The autocorrelation function G(0,t) (Table 4.1) can have a wide variety of different behaviors. But the pair correlation function only measures the T3 process, as it depends on having a finite $g_1(q)$ corresponding to correlated mass transfer between steps. This makes the pair correlation function a useful diagnostic of the dominant surface transport modes.

Table 4.1 – Limiting behaviors for G(0,t)

Mass transport mechanism	Time regime	G(0,t)
Attachment-detachment (AD)	$t \to 0$	~1
	$0 << t << t_{sat}^{AD}$	$\Omega(\frac{a_{\perp}}{\pi\widetilde{s}})^{1/2}(\frac{t}{ au_{AD}})^{1/2}$
	$t \gg t_{sat}^{AD}$	$\frac{L\Omega}{12\widetilde{s}}(1-\frac{6}{\pi^2}e^{-t/t_{sat}^{AD}})$
Step-edge diffusion (SE)	$t \to 0$	~1
	$0 << t << t_{sat}^{SE}$	$\frac{\Gamma(\frac{3}{4})}{\pi} (\frac{\Omega^5 a_{\parallel}}{\widetilde{s}^3})^{1/4} (\frac{t}{\tau_{SE}})^{1/4}$
	$t >> t_{sat}^{SE}$	$\frac{L\Omega}{12\widetilde{s}}\left(1-\frac{6}{\pi^2}e^{-t/l_{\text{init}}^{SE}}\right)$
Terrace diffusion 1 (T1)	$t \to 0$	~1
$d \to \infty$ (isolated step)	$0 << t << t_1^{T_1}$	$\Omega a_{\perp} \left(\frac{\alpha_{U} + \alpha_{L}}{\pi \widetilde{s}}\right)^{1/2} \left(\frac{t}{\tau_{TD}}\right)^{1/2}$
	$t_1^{T1} << t << t_2^{T1}$	$\frac{\Omega\Gamma(\frac{2}{3})}{\pi}(\frac{a_{\perp}^{2}}{\widetilde{s}^{2}})^{1/3}(\frac{t}{\tau_{TD}})^{1/3}$
	$t_2^{T1} << t << t_{sat}^{T1}$	$\frac{\Omega\Gamma(\frac{2}{3})}{\pi} (\frac{2a_{\perp}^{2}}{\widetilde{s}^{2}})^{1/3} (\frac{t}{\tau_{TD}})^{1/3}$
	$t \gg t_{sat}^{T1}$	$\frac{L}{12\widetilde{s}}(1-\frac{6}{\pi^2}e^{-t/t_{cat}^{T_1}})$
Terrace diffusion 2 (T2)	$t \ll t_1^{T_2}$	as for isolated step (T1)
d finite, $\alpha_U = 0$ or $\alpha_L = 0$ (e.g. Schwoebel barrier = ∞)	$t_1^{T2} << t << t_{sat}^{T2}$	$\frac{\Omega\Gamma(\frac{3}{4})}{\pi} (\frac{da_{\perp}^{2}}{\widetilde{s}^{3}})^{1/4} (\frac{t}{\tau_{TD}})^{1/4}$
	$t \gg t_{sat}^{T2}$	$\frac{L}{12\widetilde{s}}\left(1-\frac{6}{\pi^2}e^{-t/t_{uat}^{T^2}}\right)$
Terrace diffusion 3 (T3)	$t \ll t_1^{T_3}$	as for isolated step (T1)
d finite, $\alpha_{U,L} \neq 0$	$t_1^{T3} << t << t_{sat}^{T3}$	$4\Omega a_{\perp} \left(\frac{1}{\pi^{3} \tilde{s} (d+d_{0})}\right)^{1/2} \left(\frac{t}{\tau_{TD}}\right)^{1/2}$
	$t \gg t_{sat}^{T3}$	$\frac{L\Omega}{12\tilde{s}} (1 - \frac{3L}{2\pi^3} (\frac{d + d_0}{\pi a_\perp^2 \tilde{s}})^{1/2} (\frac{t}{\tau_{TD}})^{-1/2} \times$
		$e^{-(\frac{2\pi}{L})^4 \tilde{s} a_1^2 d \frac{t}{t_{7D}}}$

Table 4.2 – Limiting behaviors for $C_{k\neq 0}(0,t)$

Mass transport mechanism	Time regime	$C_{k\neq 0}(t)$
Terrace diffusion 3 (T3) d finite, $\alpha_{U,L} \neq 0$	$t \rightarrow 0$	$\frac{\Omega d}{2\pi \widetilde{s} k! (2k-1)} \left(\frac{4\widetilde{s} a_{\perp}^2}{(d+d_0)d^2}\right)^k \left(\frac{t}{\tau_{TD}}\right)^k$
	$0 << t << t_{sat}^{T3}$	$\frac{4\Omega}{4k^2-1}(\frac{a_{\perp}^2}{(d+d_0)\pi^3\widetilde{s}})^{1/2}(\frac{t}{\tau_{TD}})^{1/2}$
	$t \gg t_{sat}^{T3}$	$\frac{\Omega L^{2}}{8\tilde{s}\pi^{3}} \left(\frac{d+d_{0}}{\pi a_{\perp}^{2}\tilde{s}}\right)^{1/2} \left(\frac{t}{\tau_{TD}}\right)^{-1/2} e^{-\left(\frac{2\pi}{L}\right)^{4} \tilde{s} a_{\perp}^{2} d \frac{t}{\tau_{TD}}}$

Table 4.3 – Equations for limiting timescales

Characteristic time

Physical origin

Attachment-detachment (AD)

$$\tau_{AD} = \frac{e^{E_{AD}/k_BT}}{V}$$

Time related to the binding energy (E_{AD}) at the step edge

$$t_{sat}^{AD} = \frac{\tau_{AD}}{\widetilde{s}a_{\perp}} (\frac{L}{2\pi})^2$$

Saturation time

Step-edge diffusion (SE)

$$\tau_{SE} = \frac{e^{E_{SE}/k_BT}}{v}$$

Time related to the binding energy $(E_{\it SE})$ at the step edge

 $t_{sat}^{SE} = \frac{\tau_{SE}}{\widetilde{s}a_{\perp}a_{\perp}^{2}} \left(\frac{L}{2\pi}\right)^{4}$

Saturation time

Terrace diffusion

$$\tau_{TD} = \frac{e^{E_{TD}/k_BT}}{v}$$

Time related to the binding energy (E_{TD}) at the step edge

$$t_{sat}^{T1} = \frac{\tau_{TD}}{2\widetilde{s}a_{\perp}} \left(\frac{L}{2\pi}\right)^3$$

Saturation time: terrace diffusion T1 (isolated step limit)

$$t_{sai}^{T2} = \frac{\tau_{TD}}{d\widetilde{s} a_{\perp}} (\frac{L}{2\pi})^4$$

Saturation time: terrace diffusion T2 (large barrier limit)

$$t_{sat}^{T3} = \frac{\tau_{TD}(d+d_0)}{2\widetilde{s}a_\perp} \left(\frac{L}{2\pi}\right)^2$$

Saturation time: terrace diffusion T3 (step to step limit)

 $t_1^{T1}, t_2^{T1} \\ t_1^{T2} \\ t_1^{T3}$

Crossover times for isolated step limit (T1)

Crossover time for large barrier limit (T2)

Crossover time for step to step limit (T3)

Chapter 5

Surface Evolution Due to Step Interactions

5.1 Introduction

The model that describes the dynamics of a step train with direct step-step interaction is introduced in this chapter [49]. The steps exchange atoms through terrace diffusion. The direct interaction term is included in the expression for the free energy (Equation 4.5). There are many possible origins of step-step interactions: the fact that steps cannot cross (delta function repulsion, which leads to the so called "entropic" repulsion), strain terms (either due to dipole terms or applied stress terms) and electronic structure effects (which sometime are oscillatory). Due to direct interactions, the centers of mass of steps are not fixed. The evolution of large scale surface morphology is mediated by this step motion. Here, repulsive step-step interaction is assumed. At long times the morphology of the surface approaches a steady state profile shape, which spreads with a characteristic exponent.

5.2 Chemical Potential of Interacting Steps

Let us assume that the free energy F of N steps (see Figure 5.1) is given by,

$$F(t) \approx \sum_{k=1}^{N} \int_{-L/2}^{L/2} \left\{ \frac{\tilde{\Sigma}}{2} (\nabla H_k(x,t))^2 + g(H_{k+1}(x,t) - H_k(x,t)) \right\} dx$$
 (5.1)

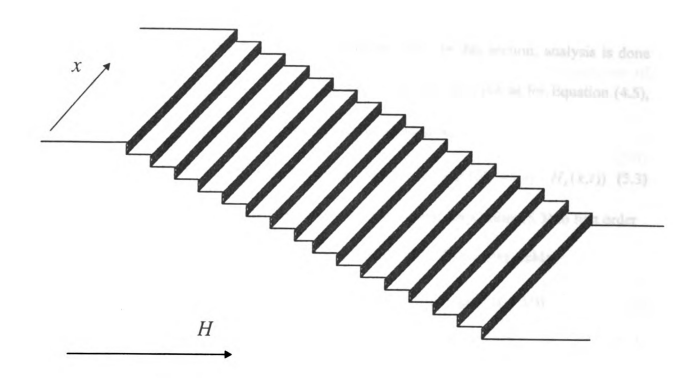


Figure 5.1 Geometry of the step train.

where the "stiffness" $\widetilde{\Sigma} = \Sigma(0) + \Sigma''(0)$ depends on $\Sigma(\theta)$, the angle-dependent interface free energy (see Equations (3.1)-(3.6)). $H_k(x,t)$ is the position of site at x on the k^{th} step at the time t. It is the sum of its center of mass motion $\overline{H}_k(t)$ and its fluctuation $h_k(x,t)$,

$$H_k(x,t) = \overline{H}_k(t) + h_k(x,t). \tag{5.2}$$

the term g(y) describes the interaction between steps. In this section, analysis is done without specifying form of g(y). Using the similar manipulation as for Equation (4.5), the chemical potential of the k^{th} step $\mu_k(x,t)$ is found to be,

$$\mu_{k}(x,t) = -\Omega \widetilde{\Sigma} \nabla^{2} H_{k}(x,t) + \Omega g'(H_{k}(x,t) - H_{k-1}(x,t)) - \Omega g'(H_{k+1}(x,t) - H_{k}(x,t))$$
 (5.3)

where primes denote derivatives with respect to argument. Expanding (5.3) to first order in the fluctuations δd_k and using Equation (5.2) (with $\nabla^2 \overline{H}_k(t) = 0$) yields,

$$\mu_{k}(x,t) \approx -\Omega \widetilde{\Sigma} \nabla^{2} h_{k}(x,t) + \Omega g'(d_{k-1}(t)) + \Omega \delta d_{k-1}(x,t) g''(d_{k-1}(t)) -$$

$$-\Omega g'(d_{k}(t)) - \Omega \delta d_{k}(x,t) g''(d_{k}(t))$$

$$(5.4)$$

where $\delta d_k(x,t) = h_{k+1}(x,t) - h_k(x,t)$ describes fluctuations of the terrace spacing.

$$d_{k}(t) = \overline{H}_{k}(t) - \overline{H}_{k-1}(t) \tag{5.5}$$

is the average distance between two adjacent steps (i.e. the average terrace width). Comparing (5.4) with Equation.(4.5) for non-interacting steps, one sees that, in the first order approximation, the direct interaction g adds four additional terms. While the third and fifth term in (5.4) are corrections to the chemical potential of step fluctuations due to interaction g, the second and fourth terms lead to center-of-mass motion of the steps. Equation (5.4) can be rewritten in the following simpler form,

$$\mu_{k}(x,t) \approx \mu_{k}^{0}(x,t) + \delta \mu_{k}^{0}(x,t) + \mu_{k}^{C}(t)$$
 (5.6)

where substitutions

$$\mu_k^0(x,t) = -\Omega \widetilde{\Sigma} \nabla^2 h_k(x,t)$$

$$\delta \mu_k^0(x,t) = \Omega \delta d_{k-1}(x,t) g''(d_{k-1}(t)) - \Omega \delta d_k(x,t) g''(d_k(t))$$

$$\mu_k^C(t) = \Omega g'(d_{k-1}(t)) - \Omega g'(d_k(t))$$
(5.7)

are introduced.

As explained in Chapter 4, one can describe step dynamics with a coupled set of Langevin equations,

$$\frac{\partial H_k(x,t)}{\partial t} = \frac{\Gamma_h}{k_B T} \left\{ \frac{1}{2} J_{k-1,k}(x,t) + J_{k,k}(x,t) + \frac{1}{2} J_{k+1,k}(x,t) \right\} + \eta_k(x,t)$$
 (5.8)

where

$$J_{k,k}(x,t) = \int_0^{L/2} P_0(l,d(t)) \{ \mu_k(x+l,t) - 2\mu_k(x,t) + \mu_k(x-l,t) \} dl$$

$$J_{k\pm 1,k}(x,t) = \int_0^{L/2} P_1(l,d(t)) \{ \mu_{k\pm 1}(x+l,t) - 2\mu_k(x,t) + \mu_{k\pm 1}(x-l,t) \} dl.$$
 (5.9)

After substituting (5.2) and (5.6) in (5.8) and averaging it, one obtains an equation that describes the center-of-mass motion as

$$\frac{d\overline{H}_{k}(t)}{dt} = -\frac{\Gamma_{h}\Omega}{k_{B}T} \left\{ m_{k}(t) \left(g'(d_{k+1}(t)) - 2g'(d_{k}(t)) + g'(d_{k-1}(t)) \right) - m_{k-1}(t) \left(g'(d_{k}(t)) - 2g'(d_{k-1}(t)) + g'(d_{k-2}(t)) \right) \right\}$$
(5.10)

where (see Equation (4.40) for P_1)

$$m_k(t) = \int_0^{L/2} P_1(l, d(t)) dl = \frac{2a_\perp^2}{\tau_{TD} \Gamma_h} \frac{1}{d_k(t) + d_0}$$
 (5.11)

and $d_0 = (\alpha_U + \alpha_L)/\alpha_U \alpha_L$. Subtracting equation (5.10) from (5.8) gives the coupled system of equations for step fluctuations. Similarly to Equation (4.13) in Chapter 4, the

Fourier transform can be applied on that system. Then, it is possible to numerically decouple the system and find the correlation function.

In the following section, short range entropic (contact) repulsion for g is assumed. In that case, $\delta\mu_k^0 \ll \mu_k^0$ and results for step fluctuation derived in Chapter 4 hold as a good approximation. For that reason, the rest of the chapter will deal only with the analysis of the center-of mass equation (5.10).

5.3 Continuum Limit, The Entropic Repulsion

In the continuum k limit, Equation (5.10) becomes

$$\frac{\partial \overline{H}_{k}(t)}{\partial t} = -\frac{2a_{\perp}^{2}\Omega}{k_{B}T\tau_{TD}}\frac{\partial}{\partial k}\left(\frac{1}{d_{k}(t) + d_{0}}\frac{\partial^{2}g'(d_{k}(t))}{\partial k^{2}}\right). \tag{5.12}$$

By writing the similar equation for $\overline{H}_{k+1}(t)$ and subtracting (5.12) from it, one has

$$\frac{\partial d_k(t)}{\partial t} = -\frac{2a_\perp^2 \Omega}{k_B T \tau_{TD}} \frac{\partial^2}{\partial k^2} \left(\frac{1}{d_k(t) + d_0} \frac{\partial^2 g'(d_k(t))}{\partial k^2} \right)$$
 (5.13)

which is the general equation for the profile evolution.

The entropic repulsion between adjacent steps is given by,

$$g_{ER}(y) = C \frac{e^{-y/2w_{sat}}}{y^2} \approx \frac{C}{y^2}$$
 (5.14)

The exponential ensures that the repulsion "cuts-off" when two steps are separated by more than twice their saturation width w_{sat} . In the following it is assumed that $w_{sat} \to \infty$, so the last expression in Equation (5.14) will be used. By substituting (5.14) to (5.13),

and introducing the slope $u_k(t) \equiv a/d_k(t)$, where a is the height of the step edge (difference in height between two adjacent terraces), one gets

$$\frac{\partial u_k(t)}{\partial t} = -\frac{4C\Omega a_\perp^2}{a^4 k_B T \tau_{TD} d_0} u_k^2(t) \frac{\partial^2}{\partial k^2} \left(\frac{u_k(t)}{u_k(t) + a/d_0} \frac{\partial^2 u_k^3(t)}{\partial k^2} \right). \tag{5.15}$$

Equation (5.15) was obtained by Ozdemir and Zangwill [29] using a different approach. It is easy to show by separation of variables that Equation (5.15) has shape preserving solution in time in two limiting cases:

(i) perfect sticking ($d_0 \rightarrow 0$)

$$\frac{\partial u_k(t)}{\partial t} = -\frac{4C\Omega a_\perp^2}{a^5 k_B T \tau_{TD}} u_k^2(t) \frac{\partial^2}{\partial k^2} \left(u_k(t) \frac{\partial^2 u_k^3(t)}{\partial k^2} \right)$$
 (5.16)

with solution

$$u_k(t) = t^{-1/5} A_k (5.17)$$

where A_k satisfies

$$1 = \frac{20C\Omega a_{\perp}^2}{a^5 k_B T \tau_{TD}} A_k \frac{d^2}{dk^2} \left(A_k \frac{d^2 A_k^3}{dk^2} \right).$$
 (5.18)

(ii) weak sticking ($d_0 \rightarrow \infty$)

$$\frac{\partial u_k(t)}{\partial t} = -\frac{4C\Omega a_\perp^2}{a^4 k_B T \tau_{TD} d_0} u_k^2(t) \frac{\partial^4 u_k^3(t)}{\partial k^4}$$
 (5.19)

with solution

$$u_k(t) = t^{-1/4} B_k ag{5.20}$$

where B_k satisfies

$$1 = \frac{16C\Omega a_{\perp}^{2}}{a^{4}k_{o}T\tau_{\tau o}d_{o}}B_{k}\frac{d^{4}B_{k}^{3}}{dk^{4}}.$$
 (5.21)

On Figure 5.2, slope evolution obtained doing numerical integration of Equation (5.15) for (i) $\alpha_L = \alpha_U = 10^3/a_1$ and (ii) $\alpha_L = \alpha_U = 10^{-3}/a_1$ for uniform initial profile is plotted. It shows interesting oscillatory shape in the transition period until it assumes the steady profile. It is interesting to note that the slope in the center of the train actually increases for small times. This means that steps in the center are bunching at small times despite the repulsive potential between them. The slope in the center of the train vs. time is plotted on Figure 5.3. It shows that the slope in the center in initially unchanged, then rises and finally decreases with the power law. The Figure 5.4 compares the steady form of u_k for large time for weak and prefect sticking. On Figure 5.5, the evolution of the profile for perfect sticking is shown.

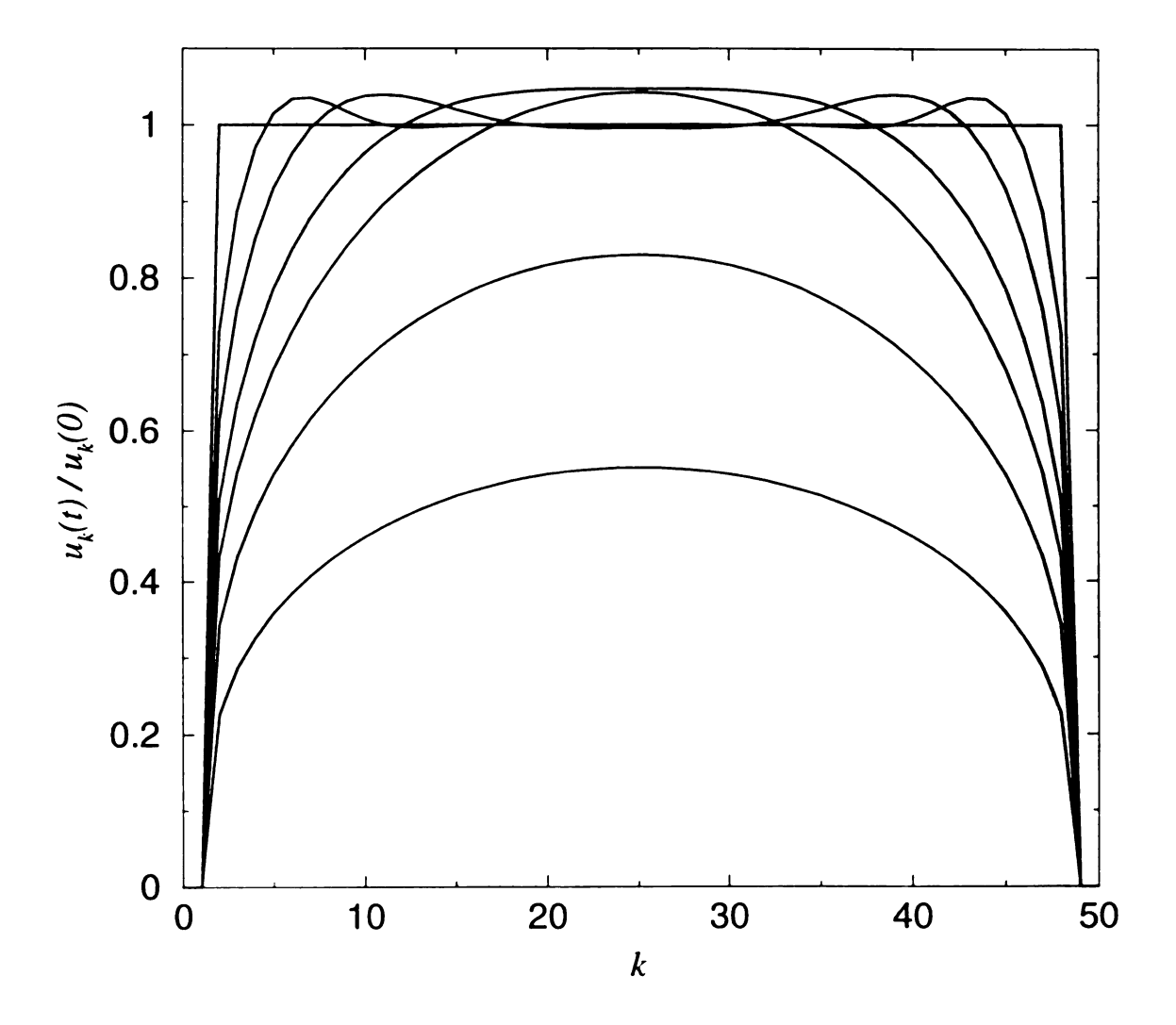


Figure 5.2(a) Slope evolution at times $t/\tau_{TD}=0.10^2.10^3.10^4.10^5.10^6.10^7$ obtained doing numerical integration of Equation (5.15) for $\alpha_L=\alpha_U=10^3/a_\perp$ and $4C\Omega a_\perp^2/a^5k_BT=1$ for uniform initial profile $u_k(0)=const$. Number of steps in the train is N=50.

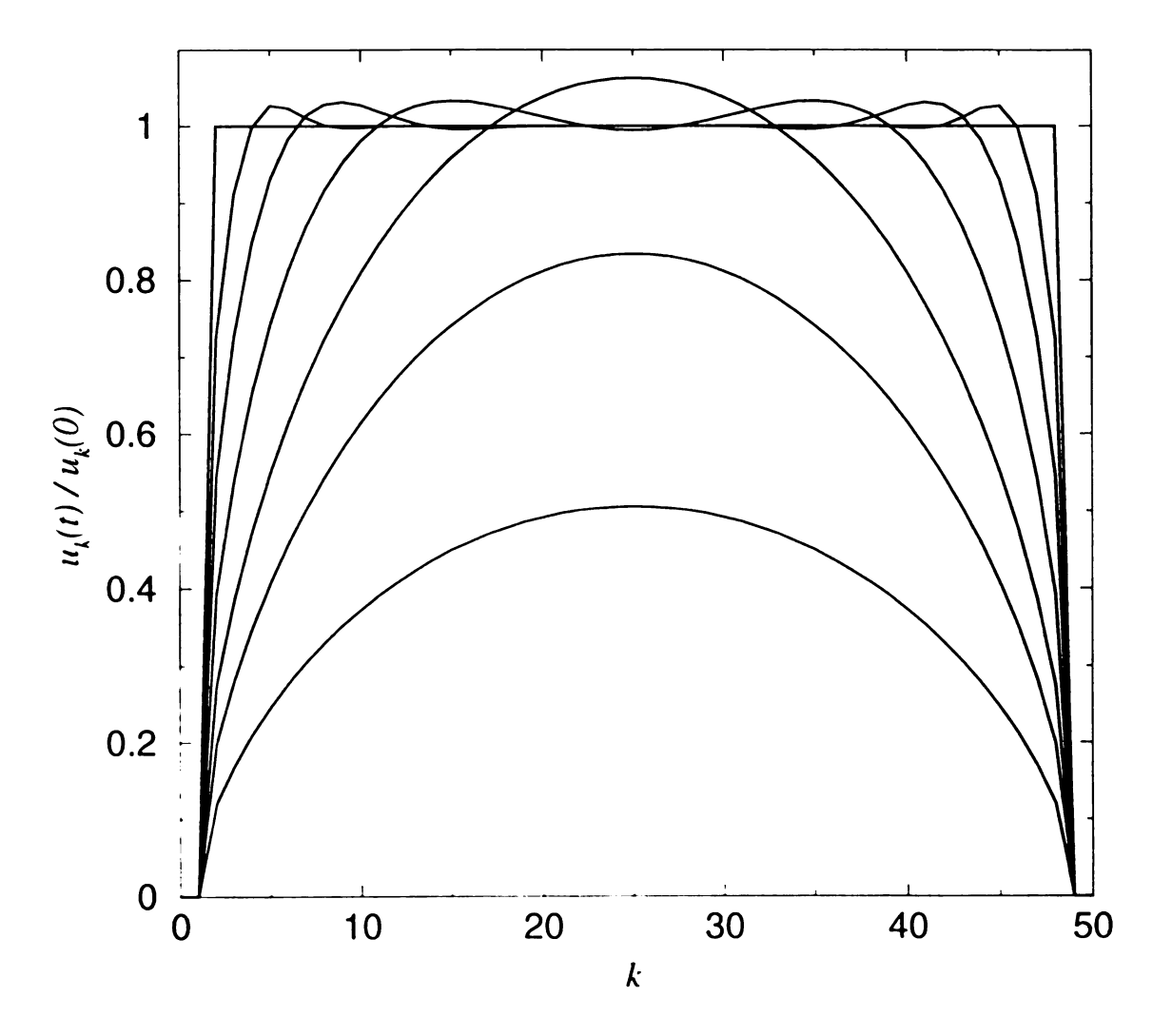


Figure 5.2(b) Slope evolution at times $t/\tau_{TD}=0.10^2.10^3.10^4.10^5.10^6.10^7$ obtained doing numerical integration of Equation (5.15) for $\alpha_L=\alpha_U=10^{-3}/a_\perp$ and $4C\Omega a_\perp^2/a^4k_BTd_0=1$ for uniform initial profile $u_k(0)=const$. Number of steps in the train is N=50.

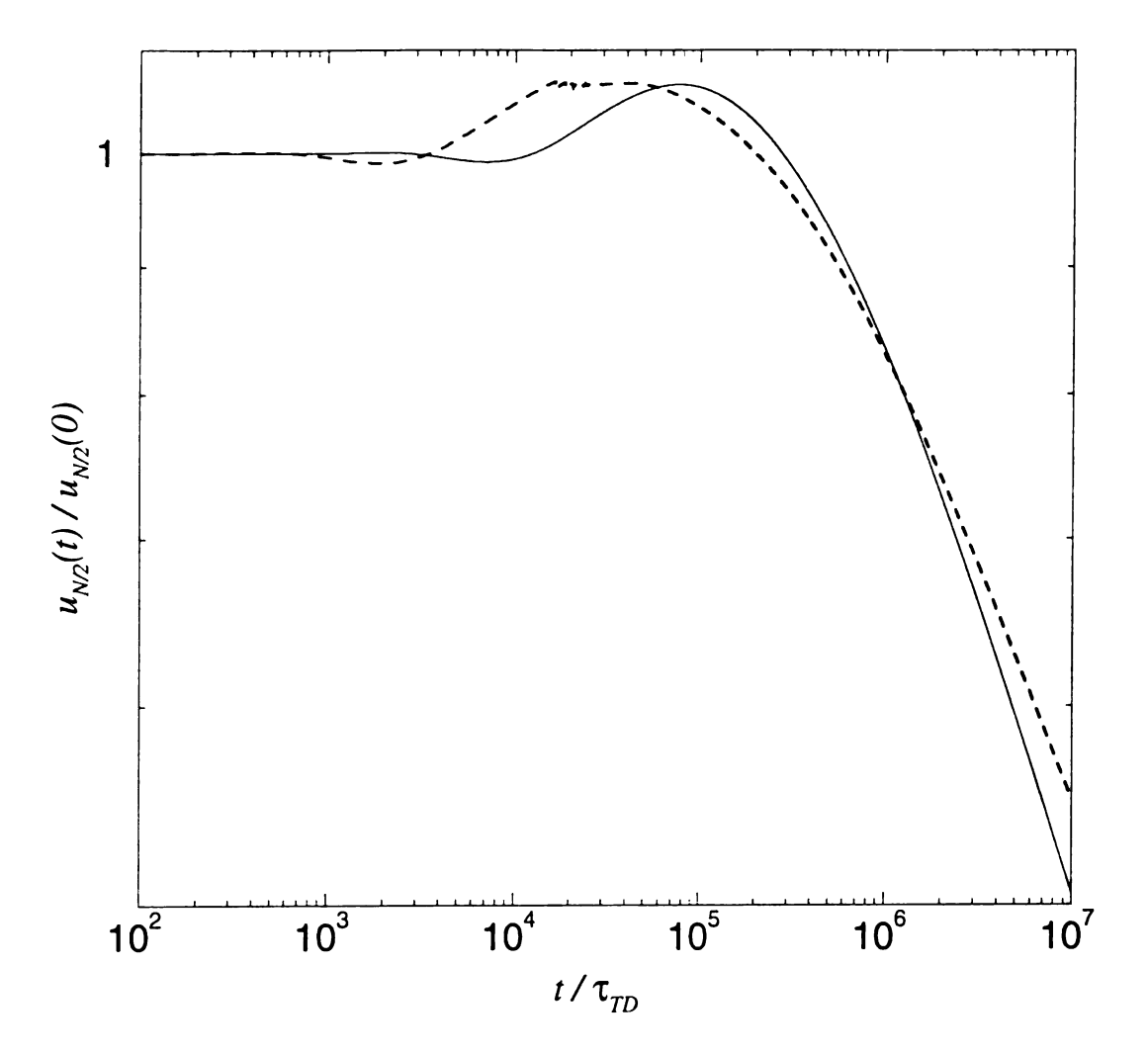


Figure 5.3 The slope in the center of the train vs. time for $\alpha_L = \alpha_U = 10^3/a_{\perp}$, $4C\Omega a_{\perp}^2/a^5k_BT=1$ (dashed line), and $\alpha_L = \alpha_U = 10^{-3}/a_{\perp}$, $4C\Omega a_{\perp}^2/a^4k_BTd_0 = 0.1$ (solid line) for uniform initial profile $u_k(0) = const$. Number of steps in the train is N=50. For large times u_k approaches $\sim t^{-1/5}$ for perfect sticking and $\sim t^{-1/4}$ for weak sticking.

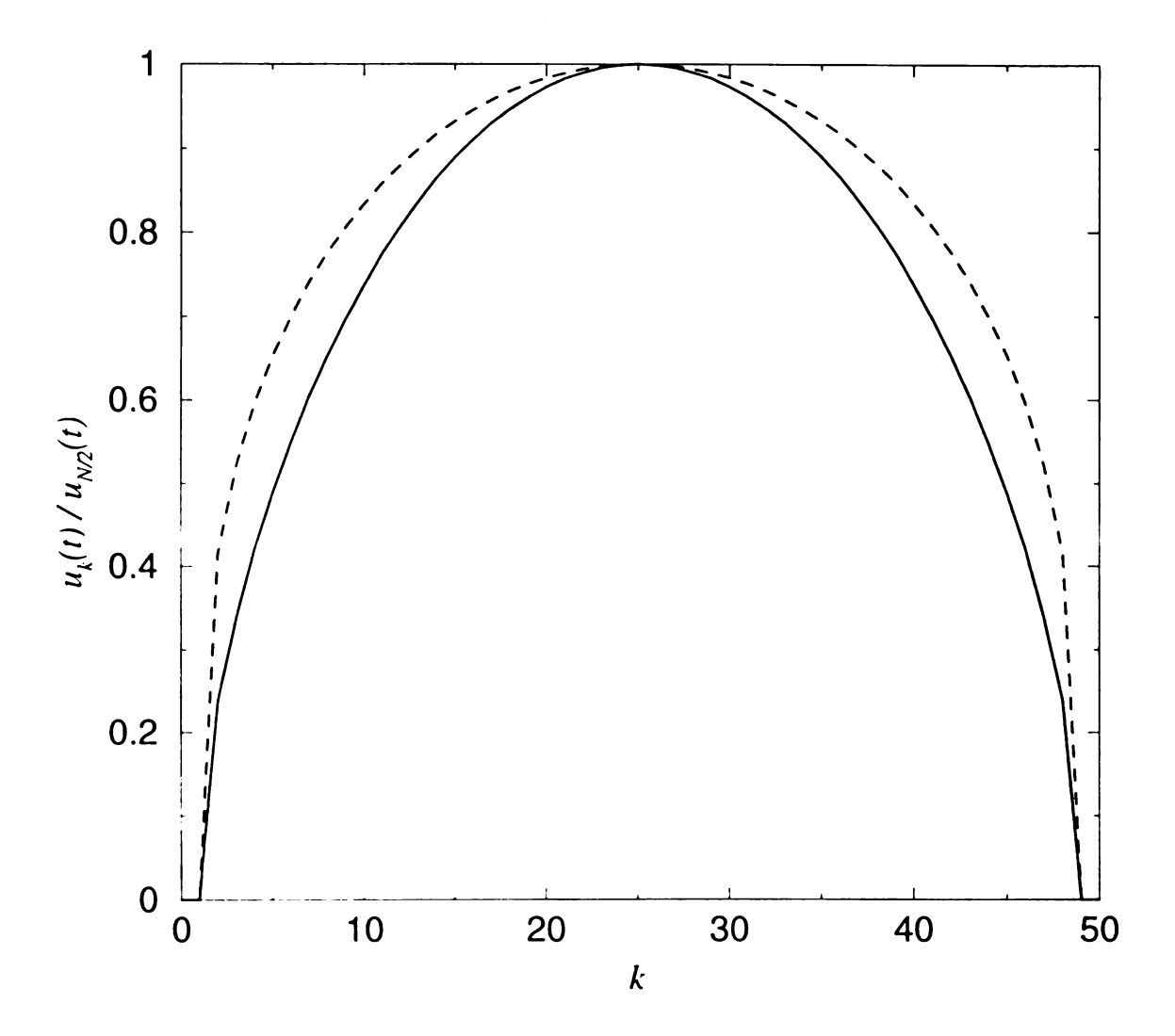


Figure 5.4 Comparison of steady shapes of u_k for $\alpha_L = \alpha_U = 10^3/a_{\perp}$, $4C\Omega a_{\perp}^2/a^5k_BT = 1$ (dashed line), and $\alpha_L = \alpha_U = 10^{-3}/a_{\perp}$, $4C\Omega a_{\perp}^2/a^4k_BTd_0 = 0.1$ (solid line) at time $t/\tau_{TD} = 10^7$. Number of steps in the train is N = 50.

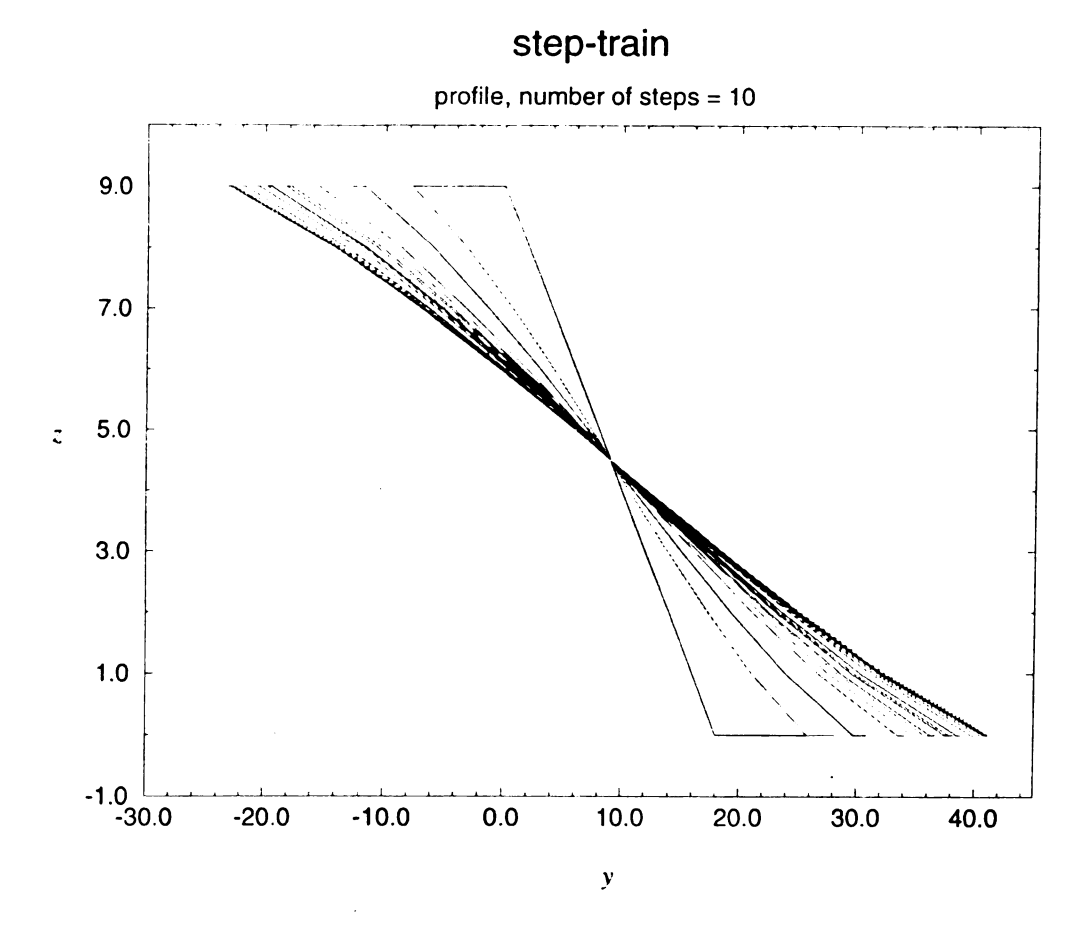


Figure 5.5 Evolution of the profile for $\alpha_L = \alpha_U = 10^3 / a_{\perp}$, $4C\Omega a_{\perp}^2 / a^5 k_B T = 1$ of N = 10 steps in the train.

Chapter 6

Monte-Carlo Simulations and Numerical Analysis

6.1 Introduction

In this chapter, some results of the Monte-Carlo simulation and numerical analysis are summarized. The purpose of performing the simulation is to check whether the continuum equation is properly formed based on initial assumptions. On the other hand, the numerical analysis is the nice way to check whether the analytical analysis of the continuum equation is correctly done.

6.2 Monte-Carlo Simulations

The most common type of Monte-Carlo simulation of surface evolution is the SOS model. As stated at the beginning of Chapter 2, it assumes the step energy in the form (3.1) with p = 1. The way the simulation is performed is to first randomly choose the possible change of the step shape according to model (as it is discussed below). Then the random number $p \in [0,1]$ with uniform distribution is generated. If the following relation between Bolzmann factor and p is satisfied,

$$e^{-(E_i - E_i)/k_B T} \ge p \,, \tag{6.1}$$

the change is done (where E_i and E_f are the initial and final step energy, according to (3.1), before and after the change respectively). Otherwise, the step shape stays unchanged. Then the other possible change of the step shape is chosen and so on. Due to the stochastic fluctuation, the results have to be averaged over many possible configurations to smooth the obtained curves.

In attachment-detachment case, one randomly (with uniform distribution) picks one site on one of the steps at the surface. Then with uniform probability it is randomly chosen to either detach or attach an atom to that particular step site. Finally, after generating random number p, the change is done if (6.1) is satisfied. In the step-edge diffusion model, after randomly picking the site on one of the steps, one chooses with uniform probability to either move the atom from that site to the left or to the right along the step-edge. Again, whether or not to do that particular change is determined according to (6.1).

In terrace diffusion case, after randomly picking the site on the step edge, one chooses upper or lower terrace according to probabilities p_U and p_L (see (3.29)). Then the second site on the same step or on the step across the chosen terrace is picked according to diffusion kernels p_1 and p_2 (see (C.14)). It is uniformly chosen in which direction to move the atom from one site to the other. Then according to (6.1) the change is made or not.

On the Figure 6.1, a snap-shot of the step shape in the equilibrium is shown. It is obtained by doing SOS Monte-Carlo of terrace diffusion with perfect sticking. Figure 6.2 is the

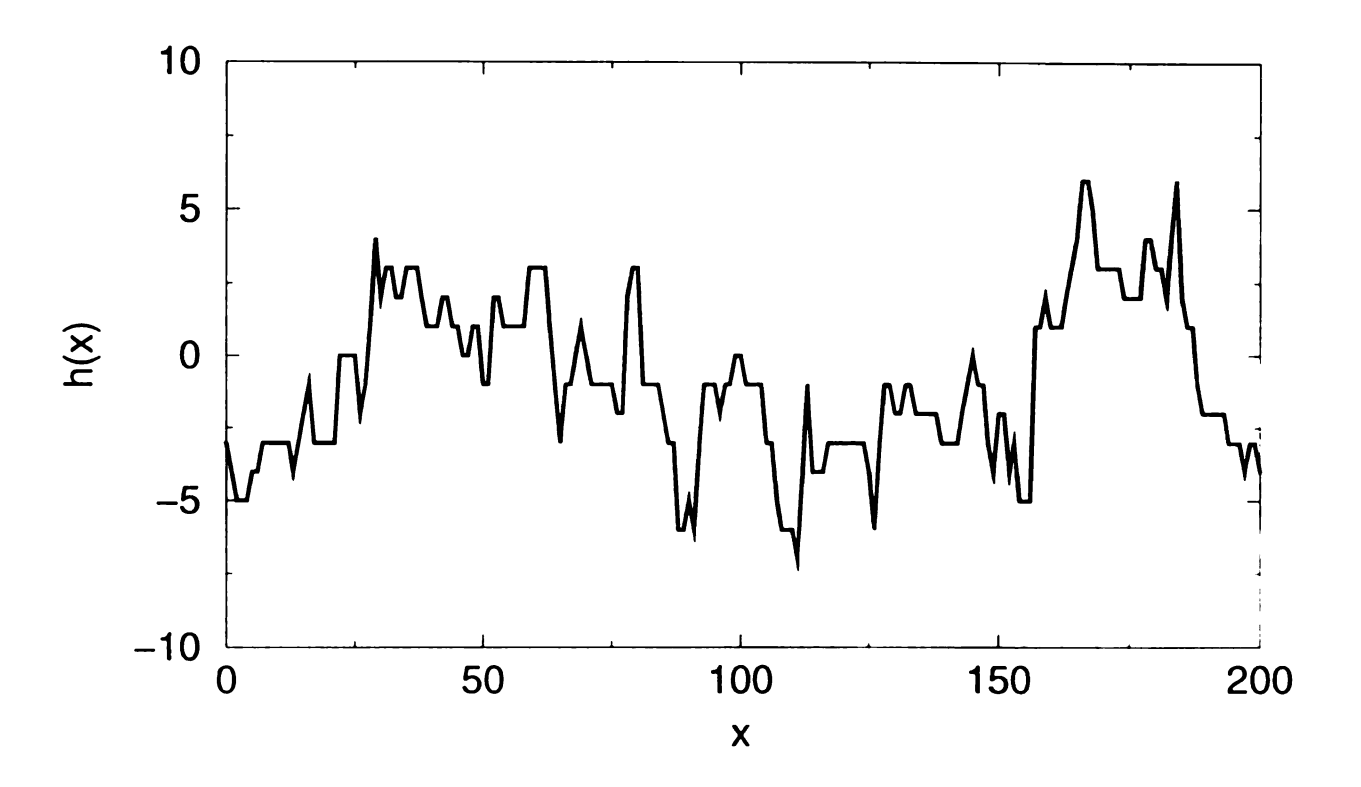


Figure 6.1 A snap-shot of the step shape in the equilibrium. It is obtained by doing SOS Monte-Carlo of terrace diffusion with perfect sticking.

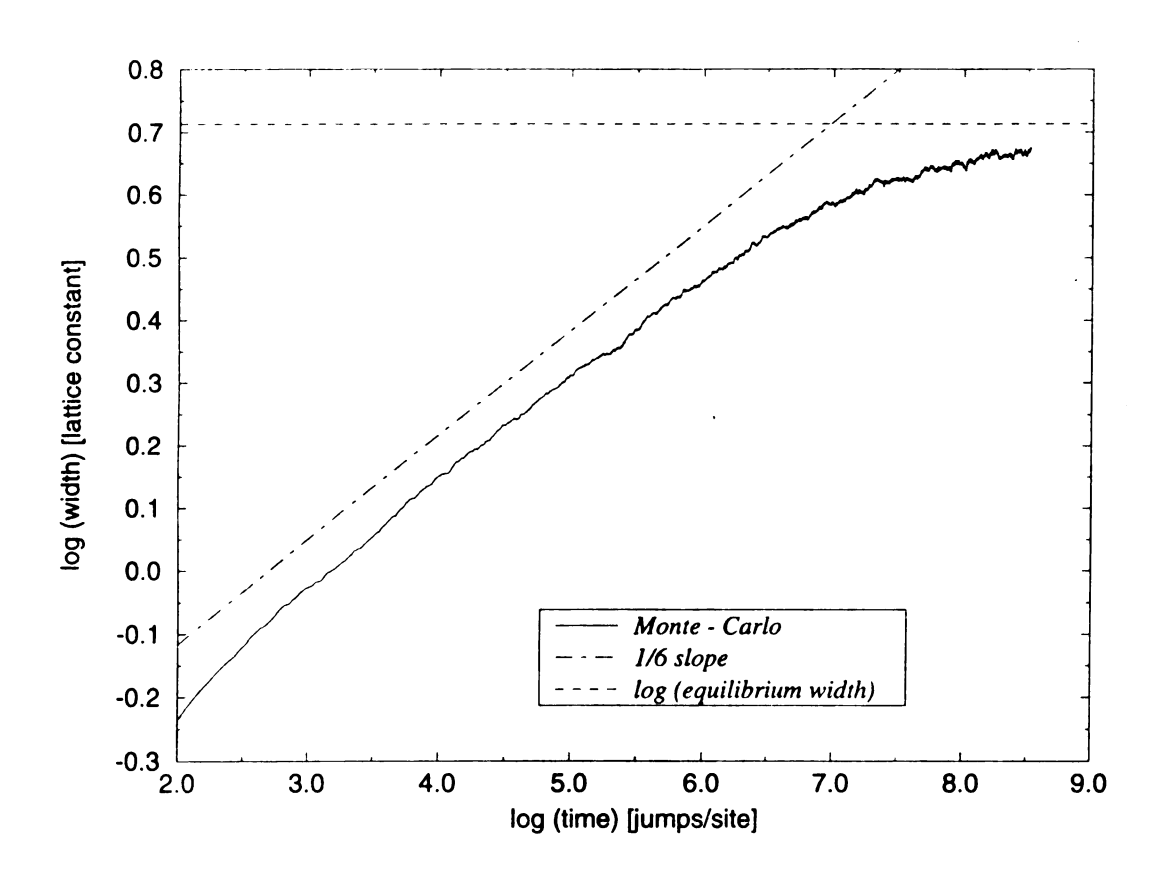


Figure 6.2 Isolated step Monte-Carlo simulation for the terrace diffusion with perfect sticking. It agrees with theoretical prediction (3.40) that $w(t) \propto t^{1/6}$ (compare also with Figure 3.4).

Sticking coefficient alpha = 0.1

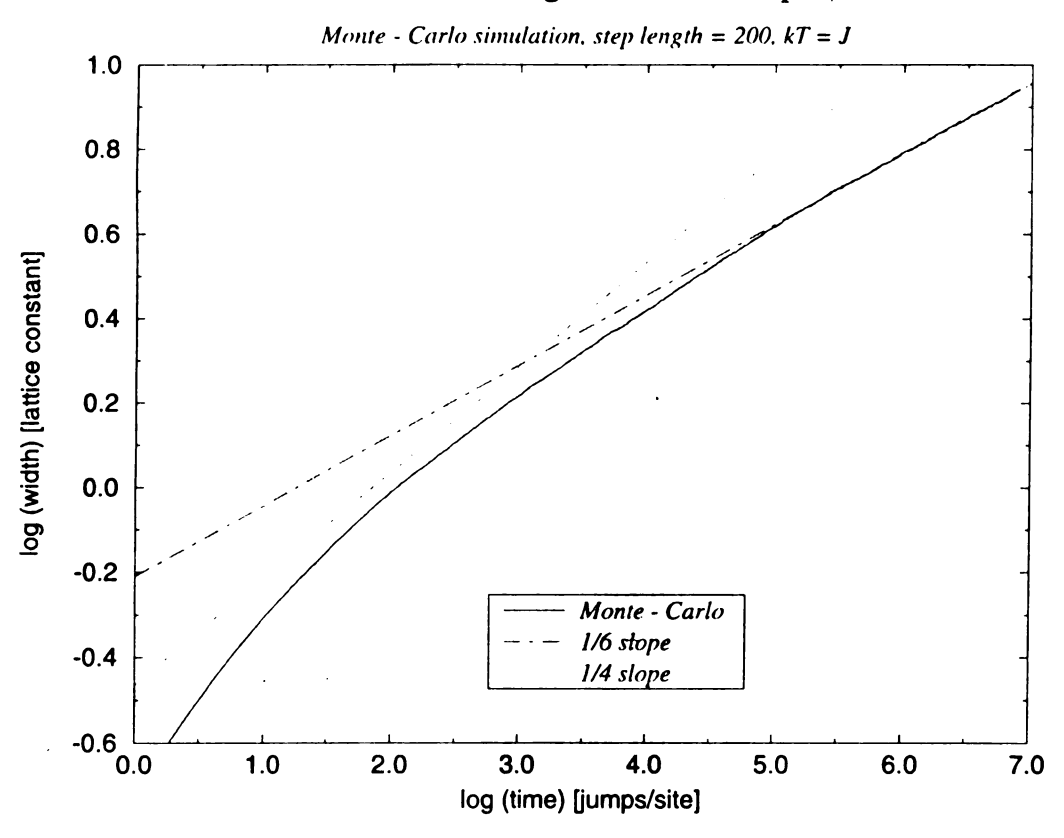


Figure 6.3 Isolated step Monte-Carlo simulation for weak sticking terrace diffusion $\alpha_L = \alpha_U = 0.1/a_{\perp}$. As predicted by (3.39), there is the tendency toward $w(t) \propto t^{1/4}$ for small times, while $w(t) \propto t^{1/6}$ for large times (compare also with Figure 3.4).

Two Steps - Monte Carlo Simulation

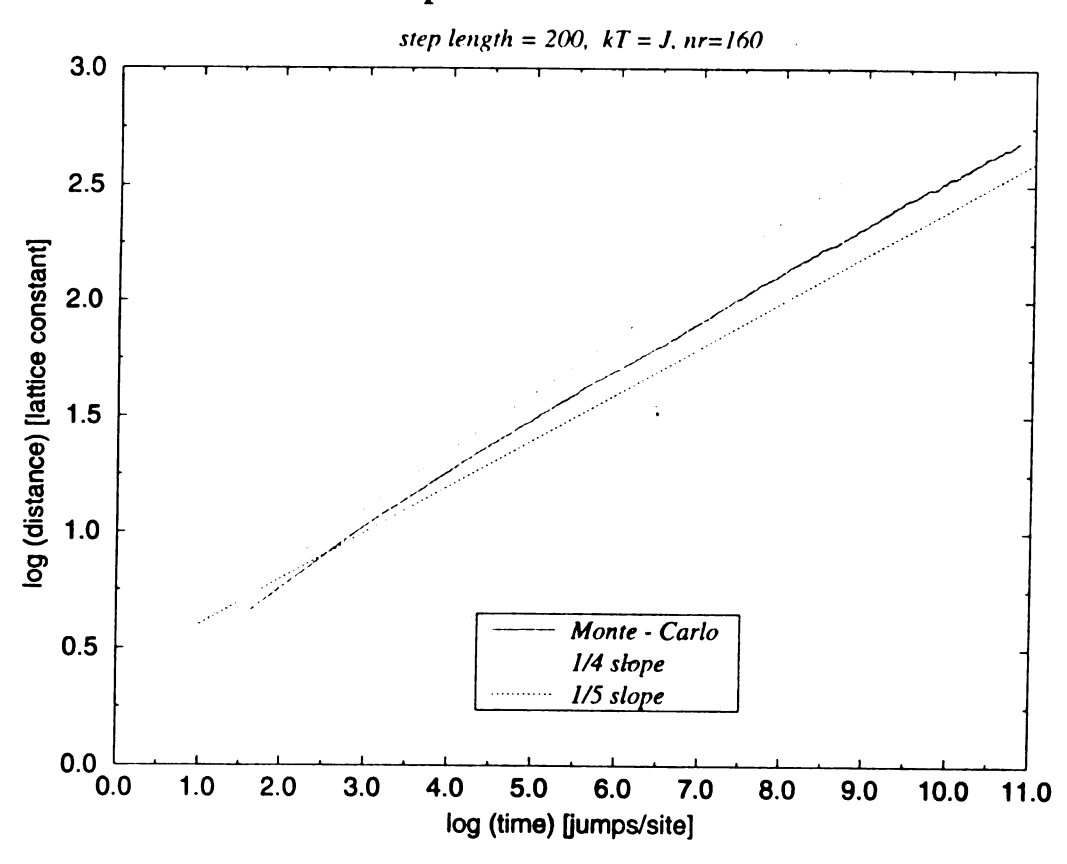


Figure 6.4 The simulation of terrace diffusion with perfect sticking. It gives $d(t) \propto t^{1/5}$ where d(t) is the distance between two steps. It agrees with theoretical prediction (5.17).

isolated step Monte-Carlo result for the terrace diffusion with perfect sticking. It agrees with theoretical prediction (3.40) that $w(t) \propto t^{1/6}$ (compare also with Figure 3.4). Figure 6.3 shows same isolated step Monte-Carlo simulation but for weak sticking terrace diffusion $\alpha_L = \alpha_U = 0.1/a_\perp$. As predicted by (3.39), there is the tendency toward $w(t) \propto t^{1/4}$ for small times, while $w(t) \propto t^{1/6}$ holds for large times (compare also with Figure 3.4). The step-train results from Chapter 5 are checked with a 2-step train with contact repulsion. The best way to do it would be to take at least 10 steps in order to avoid boundary effects. But that would even more increase already tremendously huge simulation time due to the large step size. Despite the approximation of taking only 2 steps, Figure 6.4 shows that the simulation of terrace diffusion with perfect sticking gives $d(t) \propto t^{1/5}$ where d(t) is the distance between two steps. That agrees with the theoretical prediction (5.17) (change in slope is inversely related to the change in distance between the steps).

6.3 Integration of Stochastic Equations

The solution of Langevin equations (3.9) and (5.8) are checked by doing the discrete numerical integration of those equations. The noise is randomly generated according to correlation equations (B.15). On Figure 6.5, the fluctuation width of an isolated step is obtained doing numerical integration of (3.9) for terrace diffusion case with perfect sticking. It agrees with $w(t) \propto t^{1.6}$ theoretical prediction (3.40) (compare also with Figure 3.4 and Figure 6.2). Also, on Figure 6.6, the distance between steps in 2-step train is obtained doing numerical integration of (5.8) for terrace diffusion case with perfect

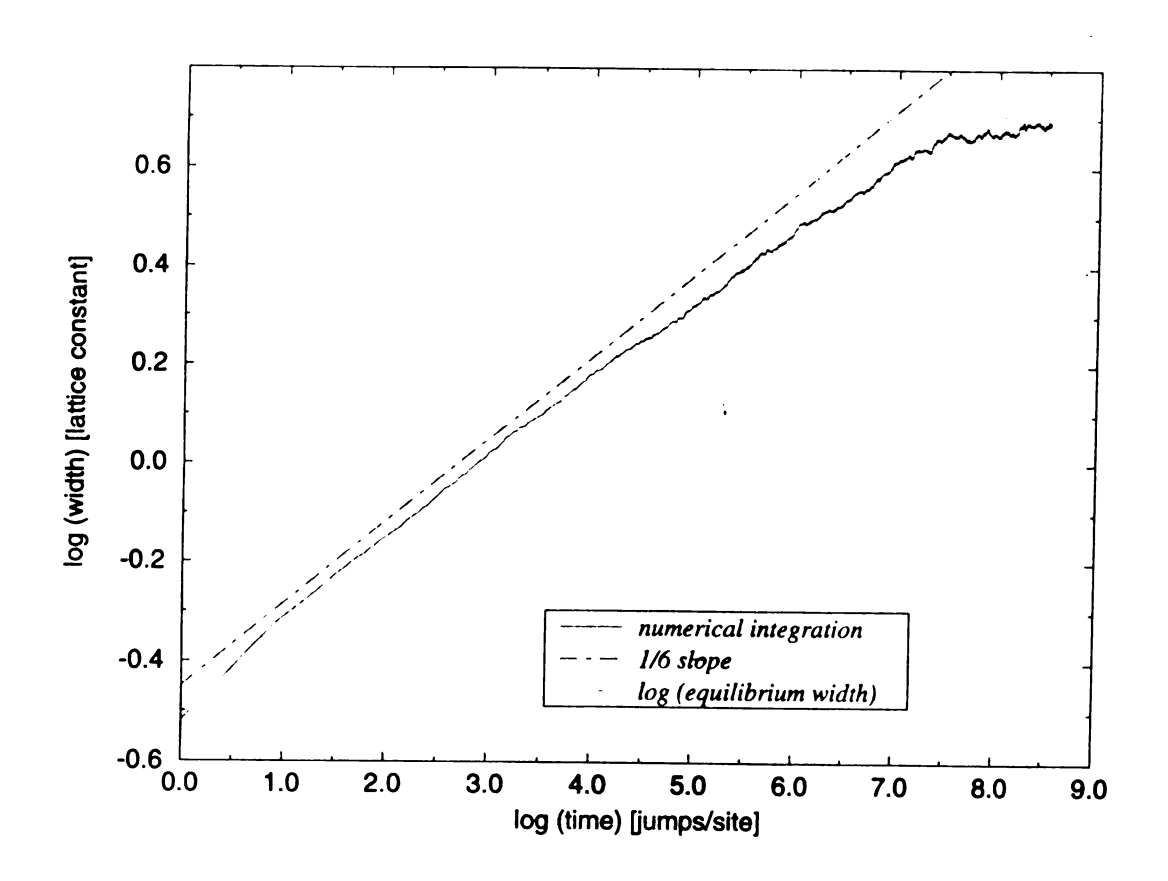


Figure 6.5 The fluctuation width of an isolated step obtained doing numerical integration of (3.9) for terrace diffusion case with perfect sticking. It agrees with $w(t) \propto t^{1/6}$ theoretical prediction (3.40) (compare also with Figure 3.4 and Figure 6.2).

Two Steps - Numerical Integration

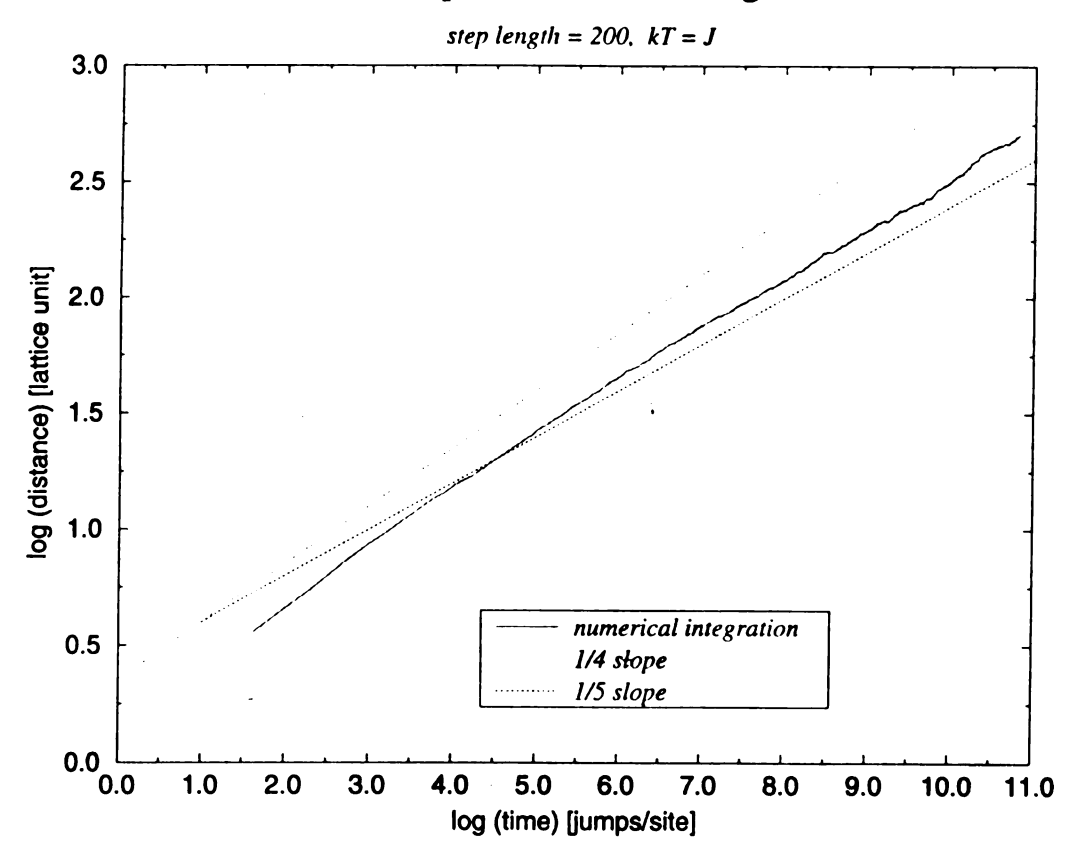


Figure 6.6 The distance between steps in 2-step train obtained doing numerical integration of (5.8) for terrace diffusion case with perfect sticking. It agrees with $d(t) \propto t^{1/5}$ theoretical prediction (5.17) (compare also with Figure 6.4).

sticking. It agrees with $d(t) \propto t^{1/5}$ theoretical prediction (5.17) (compare also with Figure 6.4).

6.4 Method for Checking Probabilities

This is an short overview of two methods used to numerically check analytically obtained probabilities p_1 and p_2 given in (C.14). The simplest method is to do a simulation of random walk on the discrete lattice. But, that approach takes a lot of simulation time (especially for large system sizes).

The other alternative method is to use (see Figure 6.7)

$$P_{i,j}(t+1) = \frac{1}{4} P_{i-1,j}(t) + \frac{1}{4} P_{i+1,j}(t) + \frac{1}{4} P_{i,j-1}(t) + \frac{1}{4} P_{i,j+1}(t)$$
 (6.2)

where $P_{i,j}(t)$ is the probability that an atom is on the discrete lattice site (i, j). Or, one can write

$$P(t+1) = MP(t) \tag{6.3}$$

where the matrix M is formed in such a way to satisfy (6.2) and all assumed boundary conditions. If P(0) is the initial distribution of the probabilities (say $P_{i_0.j_0}(0) = 1$, $P_{i_{\pi i_0.j_{\pi}j_0}}(0) = 0$ if an atom starts from site (i_0, j_0)), then

$$P(t) = M'P(0) \tag{6.4}$$

Thus, in order to find static probabilities used here, one has to run (6.3) to the times large enough for P(t) to become saturated.

On Figure 6.8, this method is performed on the terrace with the large distance between the steps (isolated step case) for perfect sticking in order to confirm l^{-2} dependence (see the comment after (C.17)).

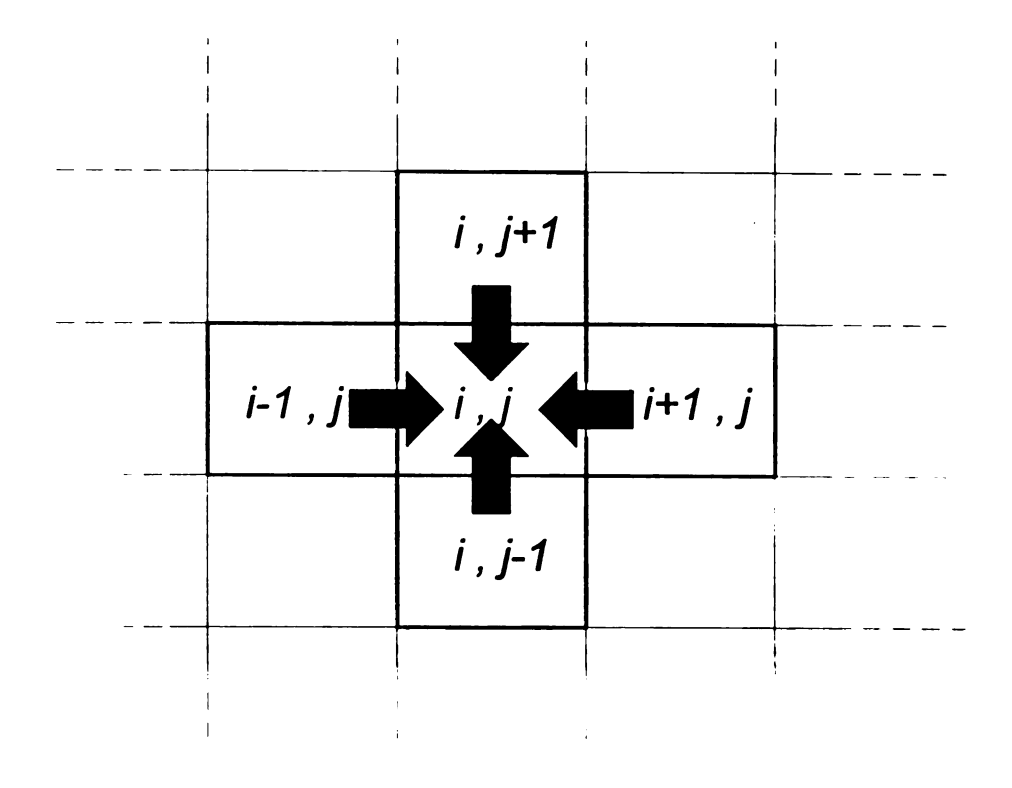


Figure 6.7 The probability that an atom is at the site (i, j) at time t + 1 is the sum of the probabilities that an atom is at one of the neighbor site at time t multiplied by 1/4 (there are four directions for atom to move).

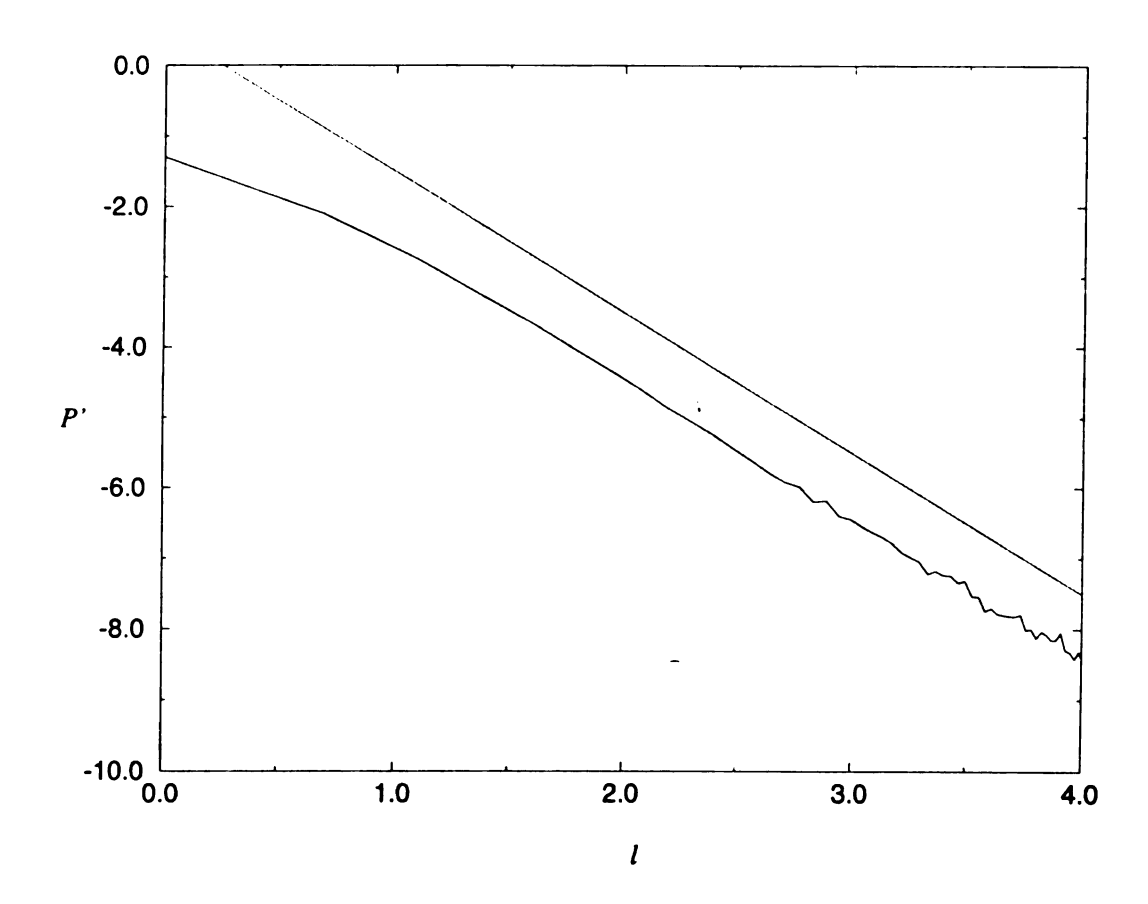


Figure 6.8 The matrix method (6.3) (bottom line) to find the diffusion kernel for isolated step in the perfect sticking case. It shows l^{-2} dependence (top line) and agrees with the analytical result (see the comment after (C.17)).

Chapter 7

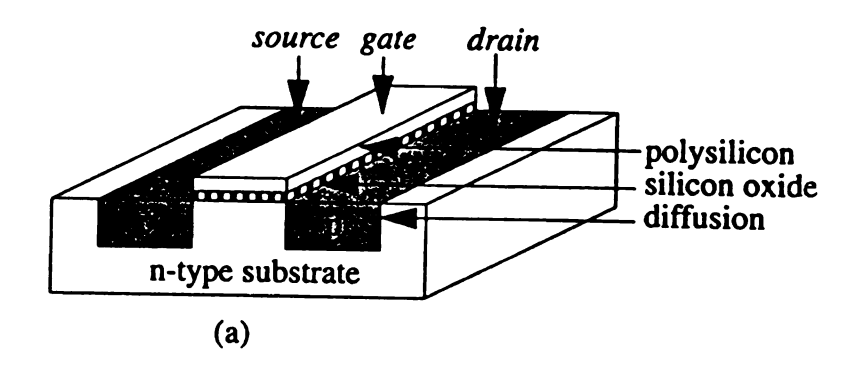
VLSI Design

7.1 Introduction

VLSI stands for Very Large Scale Integration and refers to those integrated circuits that contain more than 10⁵ transistors (in current-day technologies, circuits of 10⁸ transistors are already produced). Designing such a circuit is a difficult task and requires use of computational modeling. This chapter gives an overview of steps involved in VLSI design [51]. It starts with the description of MOS technology transistors. Then, it goes to chip design methods. Finally, the description of simulation methods is given.

7.2 MOS transistors

Design starts from transistor level cells, *logic gates*. Logic gates are usually composed of 2 to 6 transistors. They are almost always made using *MOS (Metal-Oxide-Semiconductor)* technology. Figure 7.1 shows 3-dimensional physical view of two existing types: *n-channel* (NMOS) and *p-channel* (PMOS). Figure 7.2 shows schematic symbols for these two types of transistors. The MOS transistor can be seen as a voltage-controlled switch. It is a device with three terminals. Value of voltage signal at the *gate* determines whether there is a conducting connection between the *source* and the *drain*.



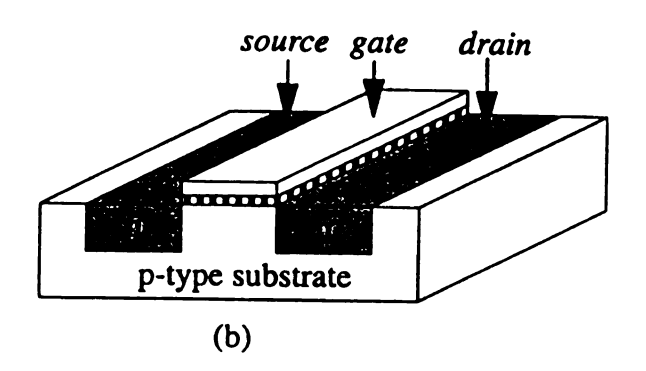


Figure 7.1 A 3-dimensional view of the (a) PMOS; and (b) NMOS.

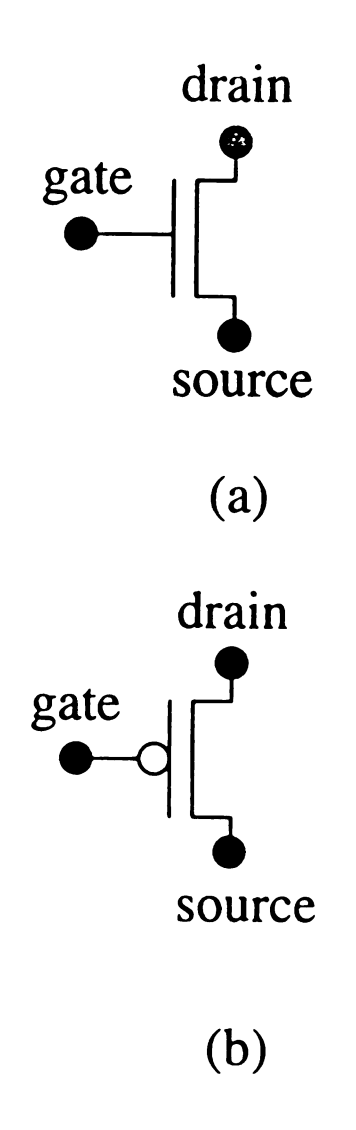


Figure 7.2 The schematic symbols for the (a) NMOS; and (b) PMOS.

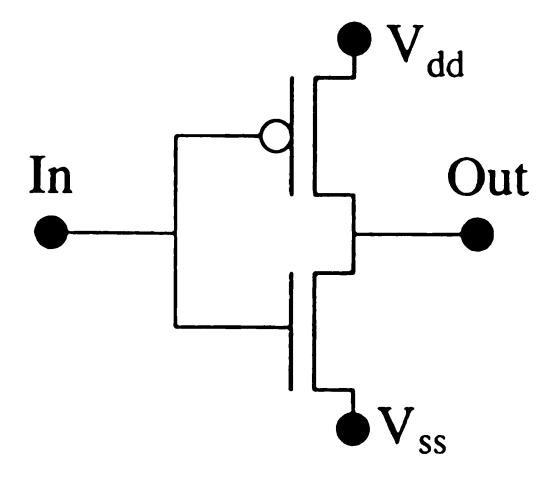


Figure 7.3 An inverter.

NMOS behaves as a closed connection when its gate signal is '1' (positive voltage), and as an open connection when its gate signal is '0' (zero voltage). PMOS has the reverse behavior. Figure 7.3 shows the simplest logic gate: *inverter*. V_{dd} is the positive supply voltage while V_{ss} is a ground. A signal '1' applied to the input In will result in a connection of Out to V_{ss} (signal '0'). Similarly, signal '0' at the input will lead to the output signal '1' as a result of the connection between the voltage supply V_{dd} and Out.

7.3 Design Steps

Suppose that one has the layout of the cells available, together with the list of interconnections to be made. From an abstract point of view, these cells are rectangles (or polygons) with terminals at their periphery to which wires can be connected. The problem is to compose the layout of the entire integrated circuit. It is often solved in two stages. First, a position in the plane is assigned to each cell, trying to minimize the area to be occupied by interconnections between these cells. This is called the *placement* problem. The next step is to generate the wiring patterns that realize the correct interconnections between these cells. This is called the *routing* problem. The goal of placement and routing is to generate the minimal chip area, while possibly satisfying some constraints. Constraints may e.g. be derived from timing requirements. As the length of a wire affects the propagation time of a signal along the wire, it may be important to keep specific wires short in order to guarantee an overall execution speed of the circuit. Layout design with timing constraints is called *timing-driven layout*.

The partitioning problem concerns the grouping of the cells in a structural description such that those cells that are tightly connected are put in the same group while the number of connections from one group to the other is kept low. This problem is not strictly a layout problem. It is encountered when some design is too large to fit in a single integrated circuit and has to be distributed among several chips. Partitioning can also help to solve the placement.

The simultaneous development of structure and layout is called *floorplanning*. In a top-down design methodology, when making a transition of a behavioral description to a structure, one also fixes the relative positions of the cells. Through floorplanning, layout information becomes available at early stages of the design. It gives early feedback on e.g. long wires in the layout and may lead to a reconsideration of the decisions on structural decomposition. The floorplanning problem is closely related to the placement problem with the difference that detailed layout information is available in placement whereas floorplanning has mainly to deal with estimations.

A cell compiler generates the layout of cells (consisting of, say, at most 100 transistors). One could follow a placement and routing approach in this case. However, such a two-stage method does not work very well here. As a transistor occupies the same area as a short wire segment, it is very difficult to estimate the area necessary for wiring at the placement stage. Most cell compilers therefore do not exploit the full freedom of being able to place and interconnect transistors arbitrarily. They target regular arrangements of

transistors, such as linear or matrix orderings, and use specific optimization techniques suitable for the particular regular arrangement.

A problem somewhat related to cell compilation is module generation. A module is normally understood to be a hardware block, the layout of which can be composed by an arrangement of cells from a small subset. These elementary cells are sometimes called microcells. They have a complexity of around 10 transistors. Given some parameters, the module generator puts the right cells at the right place and composes a module in this way.

When designing chips, the designer should have the possibility to modify the layout at the level of mask patterns. The computer tool that supports this action is called a *layout editor*. This tool is essential and any set of tools meant for full-custom design includes it. Its basic function is to allow the insertion, deletion and modification of patterns in specific layers. Most layout editors have additional functions, like the possibility of designing hierarchically and duplicating subcells, which speed up the tedious work of operating at the mask level.

Working at the mask level gives the freedom of manipulating the layout at the lowest level, but the increased freedom is as well a source of errors. In a correct design, the mask patterns should obey some rules, e.g. on minimal distances and the minimal widths, called design rules. Tools that analyze a layout to detect violations of these rules are called design-rule checkers. A somewhat related tool that also takes the mask patterns as

its inputs is the *circuit extractor* (see also Section 7.4). It constructs a circuit of transistors. Both design-rule checking and circuit extraction lean on knowledge from the field called "computational geometry".

7.4 Simulation

Depending on the accuracy required, transistors can be simulated at different levels. At the *switch level*, transistors are modeled as ideal bidirectional switches (as explained in Section 7.2) and the signals are essentially digital, although the model is often augmented to deal with different signal strengths, capacitances of nodes, etc. At the *timing level*, analog signals are considered, but the transistors have simple models (e.g. piecewise linear functions). At the circuit level, more accurate models of the transistors are used which often involve nonlinear differential equations for the currents and voltages. The equations are then solved by numerical integration. The more accurate the model, the lower the maximum size of the circuit that can be simulated in reasonable time.

The fact that an integrated circuit will be realized in a mainly two-dimensional physical medium has implications for design decisions at many levels. This is certainly true for the transistor level. The exact values of (parasitic) capacitances and resistors depend on the shapes of the patterns in the different layers of material. Therefore, it is the custom to extract the circuit from the layout data, i.e. to construct the network of transistors, resistors and capacitances taking the mask patterns as inputs. The extracted circuit can

then be simulated at the circuit or switch level especially to find out how parasitic capacitances and resistors affect the circuit behavior.

Chapter 8

Conclusion

The key physics of the model presented here is contained in the "non-local" diffusion kernels (see Equations (3.10), (4.8), and (4.9)) which occur after integrating over the atomic processes which produce step fluctuations. These kernels have been calculated for a variety of physically interesting cases and have related the parameters in those kernels to atomic energy barriers. The model used here is close in spirit to the work of Pimpinelli et al. [13], who developed a scaling analysis based on diffusion ideas. The theory of Einstein and co-workers [1,2,6,8,12,16,17,42] and Bales and Zangwill [14] is based on an "equilibrated gas" of atoms on each terrace. The concentration of this gas of atoms obeys Laplace's equation just as probability \widetilde{P} does here (see (C.2)). To make complete contact between the two methods however, one needs to treat the effect of a gas of atoms on the diffusion probabilities that have been studied here. Actually there are two effects that could be included: (1) the effect of step roughness on \widetilde{P} - it is checked numerically and found to be quite small, and (2) the effect of atom interactions on the terrace - this leads to the "tracer" diffusion problem. It is known that in the presence of interactions, Laplace's equation still holds for the calculation of \widetilde{P} , but there is a concentration dependence in the prefactors. In the small "gas" concentration limit, this analysis and that of Einstein et al. are equivalent (see Appendix D).

In addition, the link between atomic diffusion and step fluctuations on vicinal surfaces has been elucidated. It was shown how atomic diffusion leads to the limiting results (step-edge and attachment-detachment) found by the previous workers (see Sections 3.2 and 3.3). It was also shown that in terrace diffusion cases the fluctuation exponent may be non-universal (Table 4.1). It is relatively straightforward to include different types of terrace diffusion, for example as occurs due to parallel and perpendicular dimerization on Si(001), by using different diffusion kernels P_0 and P_1 on alternating terraces. A more sophisticated, but straightforward, generalization is necessary to include the possibility of transmission across a step edge, a processes which may be important at many step edges [50].

The pair correlation function between two steps $C_{k\neq 0}(x,t)$ is introduced (see (4.2)). It is identically zero for the cases of attachment-detachment and step-edge diffusion. In contrast, it is finite and quite large in the case of terrace diffusion. This means that measurement of a finite value for $C_{k\neq 0}(x,t)$ implies that terrace diffusion is important. Since G(x,t) (see (4.1)) quantifies the cumulative effect of all mass transport mechanisms, by combining the results of G(x,t) and $C_{k\neq 0}(x,t)$ it is then possible to determine the relative importance of terrace diffusion to the other types of mass transport in surface dynamics.

APPENDICES

Appendix A: Calculation of Equilibrium Width

The saturation width $w_{sat}(t)$ of step fluctuation depends on the form of the step free energy and boundary conditions. However, it does not depend on atomic mechanisms. The convenient way to derive the saturation width is by using the Fourier transform of h(x) in the expression for the free energy. The form of the Fourier transform of h(x) depends on the boundary conditions. Here, two cases will be analyzed: periodic boundaries (the case used in model presented in previous chapters) and pinned boundaries (the case in many experimental measurements when the measured part of the step is effectively pinned by the rest of the step). As shown below, the saturation width of the periodic step is by a factor $\sqrt{2}$ smaller than pinned one. Beside periodic and pinned, there can be a step with free boundaries with even greater saturation width than pinned step.

(i) periodic boundaries:

In this case, h(x) = h(x + nL) has to be satisfied. Thus, the following Fourier transform can be used

$$h(x) = \sum_{q} h_q e^{iqx}$$
 with $qL = \pm 2n\pi, n = 1,2,...$ (A.1)

where

$$h_{-q} = h_q^{\bullet} \tag{A.2}$$

has to be satisfied in order to make h(x) real. Then, the free energy (4.5) becomes

$$F = -\frac{\widetilde{\Sigma}}{2} \int_{-L/2}^{L/2} \sum_{q} \sum_{q'} h_{q} h_{q'} q q' e^{iqx} e^{iq'x} dx = \frac{\widetilde{\Sigma}L}{2} \sum_{q} |h_{q}|^{2} q^{2}$$
 (A.3)

where

$$\frac{1}{L} \int_{-L/2}^{L/2} e^{iqx} e^{iq'x} dx = \delta_{q,-q'}$$
 (A.4)

and (A.3) are used. The partition function for the system is

$$z = \prod_{q'} \int_{0}^{\infty} d\left| h_{q'} \right| e^{-\frac{\tilde{\Sigma}L}{2k_BT}q'^2 \left| h_{q'} \right|^2}.$$

Then,

$$\left\langle \left| h_{q} \right|^{2} \right\rangle = \frac{\int_{0}^{+\infty} d\left| h_{q} \right| \left| h_{q} \right|^{2} e^{-\frac{\tilde{\Sigma}L}{2k_{B}T}q^{2}\left| h_{q} \right|^{2}} \prod_{q' \neq q} d\left| h_{q'} \right| e^{-\frac{\tilde{\Sigma}L}{2k_{B}T}q'^{2}\left| h_{q'} \right|^{2}}}{\int_{0}^{+\infty} d\left| h_{q} \right| e^{-\frac{\tilde{\Sigma}L}{2k_{B}T}q'^{2}\left| h_{q} \right|^{2}} \prod_{q' \neq q} d\left| h_{q'} \right| e^{-\frac{\tilde{\Sigma}L}{2k_{B}T}q'^{2}\left| h_{q'} \right|^{2}}} = \frac{k_{B}T}{\tilde{\Sigma}Lq^{2}}.$$
(A.5)

Finally, by doing the both spatial and thermal averaging,

$$w_{sal}^{2} = \langle h^{2} \rangle - \langle h \rangle^{2} = \langle h^{2} \rangle = \frac{1}{L} \int_{1/2}^{L/2} \sum_{q} \sum_{q'} \langle h_{q} h_{q'} \rangle e^{iqx} e^{iq'x} dx = \sum_{q} \langle \left| h_{q} \right|^{2} \rangle = \frac{k_{B}TL}{12\widetilde{\Sigma}}$$
 (A.6)

where $\sum_{n=1}^{\infty} 1/n^2 = \pi^2/6$, (A.1), and (A.4) are used.

(ii) pinned boundaries

In this case, h(0) = h(L) = 0 has to be satisfied. Thus, the following Fourier transform can be used

$$h(x) = \sum_{q} h_q \sin qx$$
 with $qL = n\pi, n = 1,2,...$ (A.7)

where h_q is real. Then, free energy (3.2) becomes

$$F = \frac{\widetilde{\Sigma}}{2} \int_{0}^{L} \sum_{q} \sum_{q'} h_{q} h_{q'} q q' \cos q x \cos q' x \ dx = \frac{\widetilde{\Sigma}L}{4} \sum_{q} h_{q}^{2} q^{2}$$
 (A.8)

where

$$\frac{1}{L} \int_{0}^{L} \cos qx \cos q'x \, dx = \frac{1}{L} \int_{0}^{L} \sin qx \sin q'x \, dx = \frac{1}{2} \delta_{q,q'}$$
 (A.9)

is used. The partition function for the system is

$$z = \prod_{q'} \int_{-\infty}^{+\infty} dh_{q'} e^{-\frac{\widetilde{\Sigma}L}{4k_BT}q'^2h_{q'}^2}.$$

Then,

$$\left\langle h_{q}^{2} \right\rangle = \frac{\int_{-\infty}^{+\infty} dh_{q} h_{q}^{2} e^{-\frac{\widetilde{\Sigma}L}{4k_{B}T}q^{2}h_{q}^{2}} \prod_{q' \neq q-\infty}^{+\infty} dh_{q'} e^{\frac{\widetilde{\Sigma}L}{4k_{B}T}q^{2}h_{q'}^{2}}}{\int_{-\infty}^{+\infty} dh_{q} e^{-\frac{\widetilde{\Sigma}L}{4k_{B}T}q^{2}h_{q}^{2}} \prod_{q' \neq q-\infty}^{+\infty} dh_{q'} e^{\frac{\widetilde{\Sigma}L}{4k_{B}T}q^{2}h_{q'}^{2}}} = \frac{2k_{B}T}{\widetilde{\Sigma}Lq^{2}}.$$
(A.10)

Finally, by doing the both spatial and thermal averaging

$$w_{sat}^{2} = \langle h^{2} \rangle - \langle h \rangle^{2} = \langle h^{2} \rangle = \frac{1}{L} \int_{0}^{L} \sum_{q} \sum_{q'} \langle h_{q} h_{q'} \rangle \sin qx \sin q'x \ dx = \frac{1}{2} \sum_{q} \langle h_{q}^{2} \rangle = \frac{k_{B}TL}{6\widetilde{\Sigma}}$$
 (A.11)

where $\sum_{n=1}^{\infty} 1/n^2 = \pi^2/6$, (A.7), and (A.9) are used.

Appendix B: Solution of Langevin Equation

The linear Langevin equation (3.11) in q-space has the form

$$\frac{\partial h_q(t)}{\partial t} = -\tau_q^{-1} h_q(t) + \eta_q(t), \tag{B.1}$$

Note that by symmetry this sets $\langle h_q(t) \rangle = \langle h(x,t) \rangle = 0$ for $L \to \infty$. In order to reproduce the thermal fluctuations, the noise is assumed to satisfy the relation,

$$\langle \eta_{q_1}(t_1)\eta_{q_2}^{\bullet}(t_2)\rangle = f(q_1, q_2)\delta_{q_1, q_2}\delta(t_1 - t_2)$$
 (B.2)

The general solution of (B.1) is,

$$h_q(t) = e^{-t/\tau_q} \int_0^t e^{t'/\tau_q} \eta_q(t') dt'$$
 (B.3)

The height-height correlation function in Fourier space is then,

$$\left\langle h_{q_1}(t_1)h_{q_2}(t_2)\right\rangle = e^{-t_1+\tau_{q_1}-t_2+\tau_{q_2}} \int_{0}^{t_1} \int_{0}^{t_2} e^{t'_1+\tau_{q_1}+t'_2+\tau_{q_2}} \left\langle \eta_{q_1}(t'_1)\eta_{q_2}(t'_2)\right\rangle dt'_1 dt'_2. \tag{B.4}$$

Using (B.2), one finds (assuming $t_2 \ge t_1$)

$$\left\langle h_{q_1}(t_1)h_{q_2}(t_2)\right\rangle = \frac{f(q_1, q_2)\delta_{q_1, q_2}}{\tau_{q_1}^{-1} + \tau_{q_2}^{-1}} \left(e^{-(t_2 - t_1)/\tau_{q_2}} - e^{-t_1/\tau_{q_q} - t_2/\tau_{q_2}} \right)$$
(B.5)

The Kronecker delta function imposes $q_1 = -q_2 = q$, and since $h_{-q} = h_q$, one has

$$\langle h_q(t_1)h_q^*(t_2)\rangle = \frac{f(q)\tau_q}{2} \left(e^{-(t_2-t_1)/\tau_q} - e^{-(t_2+t_1)/\tau_q}\right)$$
 (B.6)

When $t_1 = t_2 = t$, one gets

$$\left\langle \left| h_q(t) \right|^2 \right\rangle = \frac{f(q) \tau_q}{2} \left(1 - e^{-2t/\tau_q} \right)$$
 (B.7)

Since Equation (B.7) must saturate (when $t \to \infty$) to the value of the saturation width (A.5)

$$\left\langle \left| h_q(\infty) \right|^2 \right\rangle = \frac{k_B T}{\widetilde{\Sigma} q^2 L} = \frac{f(q) \tau_q}{2}$$
 (B.8)

From Equation (B.8), then one must impose the condition $f(q) = (2k_B T)/(\tilde{\Sigma}q^2 L \tau_q)$. Fluctuation width is then (similarly to derivation of (A.6))

$$w^{2}(t) = \langle h^{2}(x,t) \rangle = \sum_{q} \frac{k_{B}T}{\widetilde{\Sigma}Lq^{2}} (1 - e^{-2t/\tau_{q}})$$
 (B.9)

On the other hand, by squaring and taking the average of each term individually in (3.17), using (B.6), and keeping in mind that $t_1 \to \infty$, one gets

$$G(t) = \sum_{q} \frac{k_B T}{\widetilde{\Sigma} L q^2} - \sum_{q} \frac{k_B T}{\widetilde{\Sigma} L q^2} e^{-t/\tau_q}$$
(B.10)

Thus, comparing (B.9) to (B.10), yields $w^2(t) = G(2t)$.

In all of the cases analyzed in Chapter 3

$$\tau_a^{-1} \approx Aq^{\gamma} \,, \tag{B.11}$$

in which case, the continuum limit of Equations (B.9) and (B.10) yields (p333-3.434(1) of [47])

$$w^{2}(t) = G(2t) \sim \frac{k_{B}T}{\pi \widetilde{\Sigma}} \Gamma(1 - \frac{1}{\gamma})(2At)^{\frac{1}{\gamma}},$$
 (B.12)

where Γ is the Gamma integral as defined for example in [34].

Analysis of linear Langevin equation (4.16) in Chapter 4 can be done similarly as (B.3),

$$v_{pq}(t) = e^{-t/\tau_{pq}} \int_{0}^{t'/\tau_{pq}} \eta_{pq}(t') dt'.$$
 (B.13)

Then,

$$< v_{p_1q_1}(t_1)v_{p_2q_2}(t_2) > =$$

$$e^{-t_1/\tau_{p_1q_1}-t_2/\tau_{p_2q_2}} \int_0^1 \int_0^2 e^{t_1'/\tau_{p_1q_1}+t_2'/\tau_{p_2q_2}} < \eta_{p_1q_1}(t_1') \eta_{p_2q_2}(t_2') > dt_1' dt_2'.$$
 (B.14)

 η is Gaussian white noise, in which case

$$<\eta_{p_1q_1}(t_1)\eta_{p_2q_2}^{\bullet}(t_2)>=f(p_1,p_2,q_1,q_2)\delta_{p_1,p_2}\delta_{q_1,q_2}\delta(t_1-t_2).$$
 (B.15)

Evaluating (B.14) using this form of the noise leads to,

$$< v_{pq}(t_1)v_{pq}^{\bullet}(t_2) > = \frac{f(p,q)\tau_{pq}}{2} (e^{(t_1-t_2)/\tau_{pq}} - e^{-(t_1+t_2)/\tau_{pq}}).$$
 (B.16)

Taking the limit $t \to \infty$ and setting $t_2 - t_1 = t$ one gets,

$$< v_{pq}(t_1)v_{pq}^{\bullet}(t_1+t)> = \frac{f(p,q)\tau_{pq}}{2}e^{-t/\tau_{pq}}.$$
 (B.17)

One can reconstruct the correlation function $C_k(x,t)$ (4.2) by inverting the Fourier transforms (4.11) and (4.15) as

$$C_k(x,t) = \frac{k_B T}{NL\widetilde{\Sigma}} \sum_{q} \frac{\cos qx \, e^{-g_0(q)t}}{q^2} \sum_{p} \cos pk \, e^{g_1(q)t\cos p} \tag{B.18}$$

where $p = 2\pi m/N$, m = 0,1,2...N-1, and $q = 2\pi m/L$, $n = \pm 1,\pm 2,...\pm L/a$. In finding Equation (B.18), one must set $f(p,q) = 2k_BT/(\widetilde{\Sigma}q^2L\tau_{pq})$. As shown Appendix A, this choice is necessary so that the formalism reproduces the equilibrium behavior (A.5).

Appendix C: Random Walk Probabilities

Consider the case of two straight parallel steps l and l at the distance l from each other. Terrace between the steps is the discrete square lattice defined by l and l axis that are parallel and perpendicular to the steps. Origin (l,l)=(0,0) is located at the distance l to the right from the step l and at the distance l to the left from the step l. Sticking coefficients for an atom on its approach from the terrace to steps l and l are l and l are l and l are probabilities that this atom will be absorbed at l by the step l and step l are spectively.

In order to find $p_1(l)$ and $p_2(l)$, one can assume that there is a source of atoms at the origin. After emerging from the source with magnitude F, atoms do random walk on the terrace until they sink on the step edges. In a static case, it is possible to define a probability density function for the distribution of the walking atoms at the terrace as $\widetilde{P}(x,y)$. By knowing $\widetilde{P}(x,y)$, $p_1(l)$ and $p_2(l)$ can be found as

$$p_1(l) = a_1 \alpha_1^l \widetilde{P}(l, -a + a_1), \quad p_2(l) = a_1 \alpha_2^l \widetilde{P}(l, d - a - a_1). \tag{C.1}$$

 $\widetilde{P}(x, y)$ must satisfy Poisson equation

$$a_{\parallel}a_{\perp}\nabla^{2}\widetilde{P}(x,y) = -F\delta(x)\delta(y)$$
. (C.2)

Beside that, it has to satisfy certain boundary conditions at the step edges. These conditions can be derived with the following simple argument. Probability that an atom, sitting on the site $(x,-a+a_{\perp})$, will stick to site (x,-a) on the step edge I is α_1^I . The

probability that it will not stick and bounce back is $1-\alpha_1'$. Thus, effectively $\widetilde{P}(x,-a) \equiv (1-\alpha_1')\widetilde{P}(x,-a+a_\perp).$ Using that and the fact that $\widetilde{P}(x,-a+a_\perp) - \widetilde{P}(x,-a) \to a_\perp \partial \widetilde{P}(x,y=-a)/\partial y, \text{ one can obtain}$

$$\frac{\partial \widetilde{P}(x, y = -a)}{\partial y} = \alpha_1 \widetilde{P}(x, y = -a)$$
 (C.3)

where notation $\alpha_1 \equiv \alpha_1^l/(1-\alpha_1^l)a_\perp$. Similarly, on the other step edge,

$$\frac{\partial \widetilde{P}(x, y = d - a)}{\partial y} = \alpha_2 \widetilde{P}(x, y = d - a)$$
 (C.4)

where $\alpha_2 \equiv \alpha_2^l/(1-\alpha_2^l)a_\perp$.

 $\widetilde{P}(x,y)$ can be found by solving Equation (C.2) with conditions (C.3) and (C.4) in the following way. Using the Fourier transform,

$$\widetilde{P}(x,y) = \frac{1}{2\pi} \int_{-\infty}^{+\infty} \widetilde{P}_{k}(x) e^{iky} dk$$
 (C.5)

and,

$$\delta(y) = \frac{1}{2\pi} \int_{-\infty}^{\infty} e^{iky} dk , \qquad (C.6)$$

one finds that,

$$\frac{d^2\widetilde{P}_k(x)}{dx^2} - k^2\widetilde{P}_k(x) = -F\delta(x). \tag{C.7}$$

One can take the solutions to this equation to be,

$$\widetilde{P}_{k}^{+}(x) = a_{k}e^{-kx} + d_{k}e^{kx} \text{ for } d - a \ge x > 0$$
 (C.8)

$$\widetilde{P}_{k}^{-}(x) = A_{k}e^{kx} + D_{k}e^{-kx} \quad \text{for} \quad -a \le x < 0$$
 (C.9)

One must ensure that the beside (C.3) and (C.4), the following boundary conditions are also satisfied,

$$\widetilde{P}_{k}^{+}(0, y) = \widetilde{P}_{k}^{-}(0, y)$$
 (C.10)

and

$$\int_{0^{-}}^{0^{+}} \frac{d^{2} \widetilde{P}_{k}(x)}{dx^{2}} dx = -F = -\frac{\partial \widetilde{P}_{k}^{+}}{\partial x} (0^{+}) + \frac{\partial \widetilde{P}_{k}^{-}}{\partial x} (0^{-})$$
 (C.11)

The first of these equations ensures continuity, while the fourth equation ensures flux conservation near the source. From the boundary conditions, one gets equations for the coefficients A_k , D_k , a_k and d_k as

$$A_k + D_k = a_k + d_k ,$$

$$A_k (k - \alpha_L) e^{-ka} = D_k (k + \alpha_L) e^{ka} ,$$

$$a_k (k - \alpha_U) e^{-k(d-a)} = d_k (k + \alpha_U) e^{k(d-a)}$$
(C.12)

and

$$k(A_{\iota}-D_{\iota}+a_{\iota}-d_{\iota})=F.$$

Solving these equations yields $\widetilde{P}_k(x)$ that through Equations (C.5) gives $\widetilde{P}(x,y)$.

After calculating $\widetilde{P}(x, y)$, by using Equation (C.1) and normalization

$$2\int_{0}^{L/2} (p_{1}(l) + p_{2}(l))dl = 1, \qquad (C.13)$$

that gives $F = a_{\perp}^{-2}$, $p_1(l)$ and $p_2(l)$ can be found as

$$p_1(l) = P(\alpha_1, \alpha_2, d, d - a, l), \quad p_2(l) = P(\alpha_1, \alpha_2, d, a, l)$$
 (C.14)

where

$$P(\alpha_1, \alpha_2, d, b, l) = \frac{\alpha_1}{2\pi} \int_{-\infty}^{+\infty} dk \frac{(k \cosh kb + \alpha_2 \sinh kb)}{(k^2 + \alpha_U \alpha_L) \sinh kd + k(\alpha_U + \alpha_L) \cosh kd} \cos kl$$
 (C.15)

with $k = \pm 2 \pi m/L$ where m = 1,...,L/a.

It is interesting to note that after manipulation with above equations, it can be obtained that

$$p_1(l) = a_\perp^2 \frac{\partial \widetilde{P}(x, y = -a)}{\partial y}, \quad p_2(l) = -a_\perp^2 \frac{\partial \widetilde{P}(x, y = d - a)}{\partial y}$$
 (C.16)

as another interesting relationship between $\widetilde{P}(x, y)$, and $p_1(l)$ and $p_2(l)$, besides (C.1).

Finally, one can obtain results in some limiting cases which are relevant to the discussion in the text.

(i) An isolated step with arbitrary sticking coefficient

Take $d \to \infty$, then $p_2 \to 0$, and (from Equation (C.14)),

$$p_1(l) = \frac{\alpha_L}{\pi} \int_0^\infty \frac{e^{-ka_1} \cos kl \ dk}{k + \alpha_L}$$
 (C.17)

There are two limiting behaviors. If $l >> 1/\alpha_L$, then $p_l(l) \sim l/l^2$, while if $l << 1/\alpha_L$, then $p_l(l) \sim constant - ln(l)$.

(ii) Both steps perfectly absorbing $\alpha_L, \alpha_U \rightarrow \infty$

Then the sum (C.15) can be evaluated (for $a_{\perp} \rightarrow 0$) and gives

$$p_1(l) \sim \frac{1}{d^2} \csc h^2 \left(\frac{\pi l}{2d}\right)$$
 (C.18)

and

$$p_2(l) \sim \frac{1}{d^2} \operatorname{sec} h^2(\frac{\pi l}{2d}).$$
 (C.19)

For *l* small compared to the step separation, one has,

$$p_1(l) \sim \frac{1}{2l^2}$$
 and $p_2(l) \sim \frac{\pi^2}{8d^2}$ for $l << d$. (C.20)

while when l is large compared to the step separation, one has,

$$p_1(l) \approx p_2(l) \sim \frac{1}{2d^2} e^{-\frac{\pi l}{d}} \quad \text{for} \quad l >> d$$
 (C.21)

(iii) Step 1 perfectly absorbing $\alpha_L \to \infty$, step 2 repelling $\alpha_U = 0$

Then

$$p_1(l) \sim \frac{1}{d^2} \operatorname{csc} h(\frac{\pi l}{2d}) \coth(\frac{\pi l}{2d})$$
 (C.22)

and,

 $p_2(l)=0.$

Appendix D: Overview of Other Models

In order to compare the results with other groups, an overview of two models (Khare and Einstein [17], and T.Ihle et al.[43]) for the dynamics of step fluctuation is given in this appendix. Both models have similar approach that is different from the one presented here in previous chapters. However, they obtain approximately same results as the one found for the terrace diffusion case in Chapter 4. Different models have different notation for the same physical quantities. To make the comparison simpler, notation used here will be assigned to all common quantities in those two models. Of course, the notation of the quantities that are unique for the model will be kept in its original form.

Khare and Einstein assume the same free energy form (4.5) for non-interacting steps as here. The surface is defined with axis x parallel to the steps and axis y perpendicular to the steps. Instead of sticking coefficients, they introduce kinetic coefficients $k_{-}(k_{+})$ for the mass exchange with the upper (lower) terrace. Instead of diffusion kernels, they define the chemical potential $\mu_{k,k+1}(x,y)$ of the terrace between steps k and k+1. The step edge moves as

$$\frac{\partial h_k(x,t)}{\partial t} = \frac{k_+}{k_B T} (\mu_{k,k+1}(x,kd_+) - \mu_k(x,t)) + \frac{k_-}{k_B T} (\mu_{k,k-1}(x,kd_-) - \mu_k(x,t))$$
 (D.1)

where $\mu_{k,k+1}(x,kd_+)$ ($\mu_{k,k-1}(x,kd_-)$) is the terrace chemical potential just right (left) of step edge k. $\mu_k(x,t)$ is the step chemical potential as defined in (4.4). On the other hand, mass conservation at the step edge leads to the equation

$$\frac{\partial h_{k}(x,t)}{\partial t} = \frac{1}{k_{B}T} \left\{ a_{\perp} D_{st} \left(\frac{\partial^{2} \mu_{k,k+1}(x,kd_{\perp})}{\partial x^{2}} + \frac{\partial^{2} \mu_{k,k-1}(x,kd_{\perp})}{\partial x^{2}} \right) - D_{su} \left(\frac{\partial \mu_{k,k+1}(x,kd_{\perp})}{\partial y} - \frac{\partial \mu_{k,k-1}(x,kd_{\perp})}{\partial x} \right) \right\} \tag{D.2}$$

where D_{st} is the diffusion constant of atoms moving only along the step edge and D_{su} is the diffusion constant of atoms on the terrace. Equating (D.1) to (D.2) gives the following boundary condition for $\mu_{k,k+1}(x,y)$

$$k_{\pm}(\mu_{k,k\pm1}(x,kd_{\pm}) - \mu_k(x,t)) = a_{\perp}D_{st}\frac{\partial^2 \mu_{k,k\pm1}(x,kd_{\pm})}{\partial x^2} \mp D_{st}\frac{\partial \mu_{k,k\pm1}(x,kd_{\pm})}{\partial y}. \tag{D.3}$$

Note that for $D_{si} = 0$ (no step edge diffusion coupled with terrace diffusion) this resembles Equations (C.3) and (C.4). Beside boundary condition (D.3), chemical potential has to satisfy

$$\nabla^2 \mu_{k,k+1}(x,y) = 0. {(D.4)}$$

After finding chemical potential $\mu_{k,k+1}(x,y)$ by solving (D.4) with boundary condition (D.3), substituting it in (D.1), and taking Fourier transform, they also obtain equations (4.48) and (4.49) with diagonal elements

$$g_0(q) = \bar{s}q^2(k_* I_a^- + k_* I_a^+) \tag{D.5}$$

and off-diagonal elements

$$g_1(q) = \widetilde{s} q^2 (k_{\perp} a_q^+ + k_{\perp} a_q^-) / (2E_q \cosh(|q|d))$$
 (D.6)

where

$$E_{q} = \left[a_{q}^{+} (1 + b_{q}^{-}) + a_{q}^{-} (1 + b_{q}^{+}) \right] + \left[a_{q}^{+} a_{q}^{-} + (1 + b_{q}^{+}) (1 + b_{q}^{-}) \right] \tanh(|q|d), \tag{D.7}$$

$$I_{q}^{\pm} = \frac{1}{E_{q}} \left\{ a_{q}^{\mp} (1 + 2b_{q}^{\pm}) + \left[a_{q}^{+} a_{q}^{-} + b_{q}^{\mp} (1 + b_{q}^{\pm}) \right] \tanh(|q|d) \right\}, \tag{D.8}$$

and

$$a_a^{\pm} \equiv D_{su} |q|/k_{\pm}, \qquad b_a^{\pm} \equiv D_{st} a_{\perp} q^2/k_{\pm}.$$
 (D.9)

In order to compare this with (4.48) and (4.49), one has to set $D_{st} = 0$, $k_{\perp}/D_{su} \rightarrow \alpha_U$, $k_{\perp}/D_{su} \rightarrow \alpha_L$ and $\alpha_{\perp}^2/\tau_{TD} \rightarrow D_{su}$. Khare and Einstein did not go further then to decouple the system and find correlation functions by summing over all modes.

T. Ihle et al. applied the similar principle, but went further to decouple the system. Similarly to terrace chemical potential (see Equation (D.4)) in the Khare and Einstein model and diffusion kernel (see Equation (C.2)) used here in Chapters 3 and 4, they introduce atom concentration c(x, y, t) on the terrace that satisfies

$$\frac{\partial c}{\partial t} = D\nabla^2 c - \frac{c}{\tau} + F + f - \nabla \vec{q} . \tag{D.10}$$

Here, steps interact and thus atom concentration on the terrace depends on time. D is the diffusion constant. Deposition of atoms on the surface is assumed and F is the rate of that deposition. Atoms can also evaporate from the surface after an average time τ . Noise f describes the fluctuation of the deposition rate while conserved noise \vec{q} is related to fluctuations of the diffusion current.

The interaction between steps is assumed to be entropic, thus step chemical potential $\mu_k(x,t)$ is given by (5.3) with (5.14). Similarly to (D.1) in Khare and Einstein's model, step edge motion is described with

$$\frac{\partial h_k}{\partial t} = \Omega \left(v_+ (c_+ - c_{eq} + \eta_+) + v_- (c_- - c_{eq} + \eta_-) \right) + \frac{\partial}{\partial s} \left(B \frac{\partial \mu}{\partial s} + \Omega \widetilde{q} \right)$$
 (D.11)

where v_+ (v_-) are the attachment coefficients for an atom on its approach from lower (upper) terrace, η_+ (η_-) are the random attachment-detachment forces, and c_+ (c_-) are the atom concentrations on a lower (upper) terrace just next to the step edge. c_{eq} is the equilibrium concentration at a step. The last term in (D.11) corresponds to fluctuation of the mass flux along the step edge. B is the transport coefficient, s is the arc length along the step and \tilde{q} is the noise related to that fluctuation. As in Khare and Einstein's model (D.3), concentration has to satisfy boundary conditions

$$\mp \vec{n} \cdot (-D\nabla c + \vec{q})_{\pm} = v_{\pm}(c - c_{eq} + \eta_{\pm}). \tag{D.12}$$

By comparing to (D.3), one sees that T.Ihle et al. do not assume coupling between terrace and step-edge diffusion.

After linearization and diagonalization by Fourier transform, system (D.10)-(D.12) gives

$$h_{wpq} = \psi_{wpq} \chi_{wpq} \tag{D.13}$$

where the Fourier transform of $h_k(x,t)$ (like any other quantity) is defined as

$$h_{wpq} = \sum_{k=-\infty}^{k=+\infty} \int_{-\infty}^{+\infty} dx \int_{-\infty}^{+\infty} dt \, h_k(x,t) e^{-i(wt+kp+qx)}. \tag{D.14}$$

 ψ is a noise resulting from the random forces introduced above, and χ is, so called, linear susceptibility of the step. The inverse of the susceptibility is

$$\chi_{wpq}^{-1} = iw + \lambda_{wpq} \tag{D.15}$$

with

$$\lambda_{wpq}^{-1} = \left(\widetilde{\Sigma}q^2 + 12\frac{C}{d^4}(1 - \cos p)\right) \times \left\{ B\Omega q^2 + \frac{Dc_{eq}^0 \Omega^2 \Lambda_{wq}}{k_B TR} \left\{ 2(\cosh(\Lambda_{wq}d) - \cos p) + \Lambda_{wq}(d_+ + d_-) \sinh(\Lambda_{wq}d) \right\} \right)$$
(D.16)

where c_{eq}^0 is the equilibrium concentration in front of an isolated straight step, C is the constant from interaction term (5.14),

$$\Lambda_{wq} = \sqrt{iw/D + q^2 + 1/x_s^2} \,, \tag{D.17}$$

$$R = (d_{+} + d_{-})\Lambda_{wq} \cosh(\Lambda_{wq} d) + (d_{+} d_{-} \Lambda_{wq}^{2} + 1) \sinh(\Lambda_{wq} d), \qquad (D.18)$$

$$d_{+} = D/\nu_{+} \tag{D.19}$$

and diffusion length

$$x_{r} = \sqrt{D\tau} . {(D.20)}$$

Susceptibility here corresponds to relaxation time (4.17) with (4.48) and (4.49). In order to compare results, one must set C=0 (step interactions are not assumed in Chapter 4), B=0 (there is no step-edge diffusion), w=0 (static case) and $x_s \to \infty$ (since $\tau \to \infty$, no evaporation) thus $\Lambda_{wq} = |q|$, $D \to a_{\perp}^2/\tau_{TD}$, and $d_{\pm} = c_{eq}^0 \Omega/\alpha_{ij}$.

BIBLIOGRAPHY

Bibliography

- 1. B. Jóos, T.L. Einstein and N.C. Bartelt, Phys. Rev. **B43**, 8153 (1991)
- 2. X.S. Wang, J.L. Goldberg, N.C. Bartelt, T.L. Einstein and E.D. Williams, Phys. Rev. Lett. 65, 2430 (1990)
- 3. B. Swartzentruber, Y.W. Mo, R. Kariotis, M.G. Lagally and M.B. Webb, Phys. Rev. Lett. 65, 1913 (1990)
- 4. J. Frohn, M. Giesen, M. Poensgen, J.F. Wolf and H. Ibach, Phys. Rev. Lett. 67, 3543 (1991)
- 5. C. Alfonso, J.M. Bermond, J.C. Heyraud and J.J. Métois, Sur. Sci. 262, 371 (1992)
- 6. E.D. Williams, R.J. Phaneuf, J. Wei, N.C. Bartelt and T.L. Einstein, Sur. Sci. 294, 219 (1993)
- 7. D.B. Abraham and P.J. Upton, Phys. Rev. **B39**, 9650 (1989)
- 8. N.C. Bartelt, J.L. Goldberg, T.L. Einstein and E.D. Williams, Surf. Sci. 273, 252 (1992)
- 9. M. Poensgen, J.F. Wolf, J. Frohn, M. Giesen and H. Ibach, Sur. Sci. 274, 430 (1992)
- 10. L. Kuipers, M.S. Hoogeman, J.W.M. Frenken, Phys. Rev. Lett. 71, 3517 (1993)
- 11. M. Giesen-Seibert, R. Jentjens, M Poensgen and H. Ibach, Phys. Rev. Lett. 71, 3521 (1993)
- 12. N.C. Bartelt, J.L. Goldberg, T.L. Einstein, E.D. Williams, J.C. Heyraud and J.J. Métois, Phys. Rev. **B48**, 15453 (1993)
- 13. A. Pimpinelli, J. Villain, D.E. Wolf, J.J. M\étois, J.C. Heyraud, I Elkinani and G. Uimin, Sur. Sci. 295, 143 (1993)
- 14. G.S. Bales and A. Zangwill, Phys. Rev. **B41**, 5500 (1990)
- 15. M. Giesen-Seibert, F. Schmitz, R. Jentjens and H. Ibach, Sur. Sci. 329, 47 (1995)
- 16. N.C. Bartelt, T.L. Einstein and E.D. Williams, Sur. Sci. 312, 411 (1994)
- 17. S. V. Khare and T. L. Einstein, Phys. Rev. **B57**, 4782 (1998)

- 18. H.P. Bonzel and W.W. Mullins, Sur. Sci. 350, 285 (1996)
- 19. B.Blagojevic and P.M.Duxbury, From atomic diffusion to step dynamics in *Dynamics* of Crystal Surfaces and Interfaces, ed. by P.M.Duxbury and T.J.Pence
- 20. B.Blagojevic and P.M.Duxbury, Atomic diffusion, step relaxation and step fluctuations, submitted to Phys. Rev. E.
- 21. W.W. Mullins, J. Appl. Phys. 30, 77 (1959)
- 22. W.W. Mullins, in "Metal Surfaces: Structure, Energetics and Kinetics", R. Vanselow and R. Howe (eds.), New York: Springer 1963
- 23. W. Selke and P.M. Duxbury, Phys. Rev. 52, 17468 (1995)
- 24. E.E. Gruber and W.W. Mullins, J. Phys. Chem. Solids 28, 875 (1967)
- 25. D. Kandel and J.D. Weeks, Phys. Rev. **B49**, 5554 (1994)
- 26. A. Rettori and J. Villain, J. Phys. (Paris) 49, 257 (1988)
- 27. F. Lançon and J. Villain, Phys. Rev. Lett. 64, 293 (1990)
- 28. P. Noziéres, in *Solids Far from Equilibrium*, Ed. C. Godréche (Cambridge University Press, Cambridge, 1991)
- 29. M. Ozdemir and A. Zangwill, Phys. Rev. **B42**, 5013 (1990)
- 30. H. Spohn, J. Phys. I (France) 3, 69 (1993)
- 31. W. Selke and T. Bieker, Surf. Sci. 281, 163 (1993)
- 32. H.P. Bonzel and E. Preuss, Sur. Sci. 336, 209 (1995)
- 33. P. Noziéres, J. Physique 48, 1605 (1987)
- 34. M. Abramowitz and I.A. Stegun, *Handbook of Mathematical Functions*, Dover (1972)
- 35. J.Blakely et. al., Atomic Steps in the Decay of 1- and 2- Dimensional Gratings in *Dynamics of Crystal Surfaces and Interfaces*, ed. by P.M.Duxbury and T.J.Pence
- 36. F. Family and T. Vicsek, J. Phys. A 18, L75-L81 (1985)
- 37. A.-L.Barabasi, H.E.Stanley, Fractal Concepts in Surface Growth, Cambridge University Press, 1995

- 38. W. W. Mullins, J. Appl. Phys. 28. 333-339 (1957).
- 39. G. Forgacs, R. Lipowsky, Th. M. Nieuwenhuizen in Vol. 15 of Phase Transitions and Critical Phenomena C. Domb and J.L. Lebowitz eds., Academic Press (1992).
- 40. M.E. Fisher, J. Stat. Phys. 34, 667 (1984)
- 41. M.P.A. Fisher, D.S. Fisher and J.D. Weeks, Phys. Rev. Lett. 48, 368 (1982)
- 42. T. L. Einstein and S. V. Khare, in *Dynamics of Crystal Surfaces and Interfaces*, ed. by P.M.Duxbury and T.J.Pence.
- 43. T. Ihle, C. Misbah. and O. Pierre-Louis, Phys. Rev. **B58**, 2289 (1998)
- 44. A. Zangwill, Physics at Surfaces, Cambridge University Press, 1988
- 45. R. L. Schwoebel, J. Appl. Phys. 40, 614 (1969)
- 46. P. J. Davis, Circulant Matrices, Wiley (1979)
- 47. I. S. Gradshteyn and I. M. Ryzhik, *Table of Integrals, Series, and Products*, Academic Press (1965)
- 48. B. Blagojevic, P. M. Duxbury, Step-step correlations, to be submitted soon.
- 49. P. M. Duxbury, B. Blagojevic, Annealing of nanostructures at low temperatures, in preparation.
- 50. N. Bartelt, private communication.
- 51. S.H.Gerez, Algorithms for VLSI Design Automation, Wiley (1999).

